

CRC Report No. A-113

THE INFLUENCE OF NO_x ON SOA AND OZONE FORMATION

Final Report

December 2022



COORDINATING RESEARCH COUNCIL, INC.

5755 NORTH POINT PARKWAY • SUITE 265 • ALPHARETTA, GA 30022

The Coordinating Research Council, Inc. (CRC) is a non-profit corporation supported by the petroleum and automotive equipment industries. CRC operates through the committees made up of technical experts from industry and government who voluntarily participate. The four main areas of research within CRC are: air pollution (atmospheric and engineering studies); aviation fuels, lubricants, and equipment performance; heavy-duty vehicle fuels, lubricants, and equipment performance (e.g., diesel trucks); and light-duty vehicle fuels, lubricants, and equipment performance (e.g., passenger cars). CRC's function is to provide the mechanism for joint research conducted by the two industries that will help in determining the optimum combination of petroleum products and automotive equipment. CRC's work is limited to research that is mutually beneficial to the two industries involved. The final results of the research conducted by, or under the auspices of, CRC are available to the public.

LEGAL NOTICE

This report was prepared by University of California, Riverside as an account of work sponsored by the Coordinating Research Council (CRC). Neither the CRC, members of the CRC, University of California, Riverside, nor any person acting on their behalf: (1) makes any warranty, express or implied, with respect to the use of any information, apparatus, method, or process disclosed in this report, or (2) assumes any liabilities with respect to use of, inability to use, or damages resulting from the use or inability to use, any information, apparatus, method, or process disclosed in this report. In formulating and approving reports, the appropriate committee of the Coordinating Research Council, Inc. has not investigated or considered patents which may apply to the subject matter. Prospective users of the report are responsible for protecting themselves against liability for infringement of patents.

Acknowledgements

Report Prepared by: Sahar Ghadimi, Weihan Peng, Qi Li, David Cocker

UC Riverside, College of Engineering, Center for Environmental Research and Technology (CE-CERT)

This work was funded by the Coordinated Research Council (CRC) through CRC Project A-113. The authors thank Shaokai Gao and Timothy Wallington for grant management support and helpful discussions.

The authors thank William Porter (UCR) for useful discussions and implementation of GEOS-CHEM work within this manuscript. The authors also give thanks to Thomas Eckel for leading the upgrade of the UCR chamber and Ryan Drover and Daniel Gonzalez for assistance in the upgrade of the chamber. We also thank Chen Le for critical development of the LabView data acquisition systems. We also thank Chen Le for the data analysis packet implemented as part of this program.

List of Tables

Table 1: Particle loss correction of pure seed test in the new UCR fixed-volume chamber.....	23
Table 2: Experiments with variable VOC injection strategies.....	28
Table 3: Experiments with variable NO _x injection strategies	29
Table 4: Experiments with continuous NO injection.....	30
Table 5 VBS parameters for <i>m</i> -xylene at three branching ratios	53
Table 6 VBS parameters for α -pinene at three branching ratios	53
Table 7: Two-product SOA yield parameters	64
Table 8. SOA yield VBS parameters at different HO ₂ /RO ₂ conditions.	76
Table 9: Experimental conditions for additional α -pinene experiments.....	78
Table 10: Naphthalene experimental conditions.....	85

List of Figures

Figure 1: NO aerosol suppression and promotion pathways. (Figure from Li <i>et al.</i> 2015)	17
Figure 2. β value variation throughout the experiment. A) Continuous NO _x injection in this study; B) Classical chamber experiments with instantaneous NO _x injection.	18
Figure 3: Schematic of the dual 90 m ³ collapsible environmental chambers	19
Figure 4: Schematic of the new 118 m ³ fixed volume environmental chamber.....	20
Figure 5: Particle number decay rate shown as a function of particle size updated on Oct 2nd, 2022.....	22
Figure 6: Uncorrected and corrected particle volume concentration shown as a function of time. Data shown is being corrected by (V1) exceed measurement range loss due to coagulation, (V12) V1 plus dilution correction, (V123) V12 plus size dependent particle wall loss.....	24
Figure 7: A) Four global branching ratios scenarios in July. B) Branching ratio profile during a day of four scenarios. (Li <i>et al.</i> , 2022)	26
Figure 8: Final SOA formation vs final HC consumption from experiments with different <i>m</i> -xylene injection methods	31
Figure 9: Final ozone formation from experiments with 35 ppb <i>m</i> -xylene injected differently	32
Figure 10. Branching ratio over the course of the experiment with different VOC injection timings.....	32
Figure 11. Branching ratio of experiment with different initial NO _x	33
Figure 12. SOA formation vs <i>m</i> -xylene consumption during the experiments with different initial NO _x concentrations	34
Figure 13. Instantaneous yield vs branching ratio	35
Figure 14. NO _x concentration throughout the experiment	36
Figure 15. SOA formation throughout the experiment	37
Figure 16: Ozone formation throughout the course of the experiment.....	37
Figure 17 Modelled branching ratios from three sets of experiments.....	38
Figure 18 SOA formation and modelled branching ratio of set #1	39

Figure 19 <i>m</i> -xylene concentration of set #1 runs	40
Figure 20 SOA yield at different branching ratios.....	40
Figure 21 modelled OH concentrations of set #1 runs.....	41
Figure 22 SOA formation and modelled branching ratio of set #2 runs	42
Figure 23 modelled OH concentration of set #2 runs	43
Figure 24 <i>m</i> -xylene concentration of set #2 runs	43
Figure 25 SOA yield at different branching ratios.....	44
Figure 26 SOA formation and modelled branching ratio of set #3 runs	45
Figure 27 <i>m</i> -xylene concentration of set #3 runs	46
Figure 28 volume fraction remaining of SOA from <i>m</i> -xylene at different branching ratios	46
Figure 29. Four global branching ratio scenarios (Provided by William Porter).....	49
Figure 30. Branching ratio profile during a day of four scenarios. (Peng <i>et al.</i> , 2022)	49
Figure 31 SOA(Mo) vs <i>m</i> -xylene consumption at different branching ratios.....	50
Figure 32 SOA yield vs Mo from <i>m</i> -xylene at different branching ratios	51
Figure 33 SOA(Mo) vs α -pinene consumption at different branching ratios.....	51
Figure 34 SOA yield vs Mo from α -pinene at different branching ratios	52
Figure 35 VBS fitted yield vs Mo from <i>m</i> -xylene	54
Figure 36 VBS fitted yield vs Mo from α -pinene.....	55
Figure 37. Final SOA yield (Y) and final SOA mass (M) from 160 classic <i>m</i> -xylene chamber experiments	58
Figure 38. Final SOA yield (Y) and final SOA mass (M) from 160 classic <i>m</i> -xylene chamber experiments colored by VOC consumption.....	59
Figure 39. Typical branching ratio profiles throughout experiments.....	60
Figure 40. Final SOA yield (Y) and final SOA mass (M) from 160 classic <i>m</i> -xylene chamber experiments colored by average branching ratio.....	60

Figure 41. SOA yield vs. Beta with similar M(189-229 ug/cm ³) or similar HC (265-303 ug/cm ³).....	61
Figure 42. Final SOA mass (M) and total VOC consumption from 160 classic <i>m</i> -xylene chamber experiments colored by branching ratio.....	62
Figure 43. Measured and SAPRC11-estimated gas-phase species comparison.....	63
Figure 44. SOA yield vs SOA mass and corresponding fitted curves from runs with controlled branching ratio (0, 0.25, 0.75, and 1).....	64
Figure 45: SOA Yield from <i>m</i> -xylene experiments with no additional NO _x	65
Figure 46. SOA formation, HO ₂ *RO ₂ , and accumulative <i>m</i> -xylene consumption of <i>m</i> -xylene experiments with different light intensities	67
Figure 47. SOA yield from <i>m</i> -xylene experiments with no additional NO _x at different light intensity (represented by k ₁)	67
Figure 48. Gas-phase chemistry simulation of <i>m</i> -xylene+H ₂ O ₂ with different NO _x offgasing rates.....	70
Figure 49. SOA formation and <i>m</i> -xylene concentration from <i>m</i> -xylene with different initial concentration of H ₂ O ₂	74
Figure 50. SOA yield from <i>m</i> -xylene experiments with no additional NO _x with different initial H ₂ O ₂	75
Figure 51. SOA formation with average HO ₂ /RO ₂	75
Figure 52. SOA yield from <i>m</i> -xylene experiments with no additional NO _x at different HO ₂ /RO ₂	76
Figure 53. A) SOA yield versus SOA mass formed under no and low NO _x conditions. B) SOA mass formed versus Delta HC consumed at low and no-NO _x conditions.	80
Figure 54. A) SOA yield versus SOA mass formed under high and 2X high NO _x conditions. B) SOA mass formed versus Delta HC consumed at under high and 2X high NO _x conditions.	81
Figure 55: RO ₂ lifetime simulated under high and 2X high NO _x conditions at A) 20 ppb, B) 40 ppb, C) 80 ppb.	82
Figure 56. Volume of the particles formed over the course of experiment at A) low and no-NO _x conditions, B) at high NO _x conditions.	82

Figure 57. SOA yield versus SOA mass formed of Continuous NO injections versus instantaneous NO I injections..... 83

Figure 58. SOA yield versus OA mass formed under no-NO_x, low NO_x, and high NO_x experiments using Naphthalene as SOA precursor..... 85

Figure 59: H:C and O:C ratios determined by HR-ToFMS for α -pinene and naphthalene..... 87

Executive Summary

The secondary organic aerosol (SOA) formation from select aromatic (*m*-xylene), poly-aromatic (naphthalene), and biogenic monoterpene (α -pinene) was explored over a variety of atmospheric chemical regimes. Experiments were carefully designed to explore a range of conditions from very low-NO_x to very high-NO_x to identify critical atmospheric pathways for SOA formation. Novel environmental chamber experiments were designed to control the branching ratio (β) of RO₂ chemistry with HO₂ and NO, where β of zero represents peroxide rich conditions where the fate of RO₂ is reaction with HO₂ and β of one represents high NO conditions where the fate of RO₂ is reaction with NO. These experiments deviate from classical SOA environmental chamber experiments by maintaining β throughout the duration of the experiment (traditional SOA NO_x environmental chamber experiments commence at $\beta = 1$ and often drop to $\beta = 0$ thru the course of the experiment). The experiments reported herein are designed to inform the atmospheric community on the sensitivity of select volatile organic compounds to NO_x levels (using β) in the atmosphere. Specifically, the SOA formation from *m*-xylene, naphthalene, and α -pinene was explored at fixed $\beta = 0, 0.3,$ and 1.0 conditions as determined by SAPRC-11 modelling of the experimental conditions and achieved thru continuous NO_x injection (except for $\beta=0$, which was achieved by adding H₂O₂ instead of NO_x to the system).

The project aims were to conduct novel environmental chamber experiments to elucidate the key roles of NO_x on SOA formation by performing experiments specifically designed to investigate the role of peroxide chemistry. Primary objectives included

- 1) the design of new experimental methods using environmental chambers to best elucidate the interplay of NO_x with select anthropogenic and biogenic precursors at atmospherically relevant (current and projected) oxidant levels;
- 2) identify SOA formation potential of select VOC precursors within these well-controlled environments;

- 3) evaluate ozone prediction under these scenarios and
- 4) provide guidance to regional air quality models on how to implement improvements to SOA predictive models.

The primary objectives were achieved through:

- 1) Design of new experimental methods using environmental chambers elucidated the interplay of NO_x with select anthropogenic and biogenic precursors at atmospherically relevant (current and projected) oxidant levels (Section 3.0). Typical atmospheric values of β , the ratio of reaction of NO with hydroperoxyl (HO₂) and peroxy (RO₂) radicals, were identified and categorized using GEOS-CHEM modelling. Four major trends/categories of daytime β were identified across the globe, all of which have a relatively constant β (between 0 and 1) throughout the daytime. Conventional environmental chamber experiments conducted over the last two decades work with a single VOC and NO_x injection and have been designated as “low NO_x” and “high NO_x”. This current work clearly demonstrates that previously conducted environmental chamber studies on SOA formation from VOCs in “low NO_x” ($\beta = 0$) experiments (unless the system contains zero NO_x) still include $\beta = 1$ environments at the start of the experiment and that VOCs in “high NO_x” ($\beta = 1$) experiments quickly work toward $\beta = 0$ environments after ozone production commences. According to GEOS-CHEM modelling, β values remain fairly constant at a value between 0 and 1 due to the continuous influx of both VOC and NO_x. This work, after extensive gas-phase modelling and experimental investigation in Sections 3.0 and 4.0, that continuous injection of low concentrations of NO are the most effective method to maintain constant β values throughout the VOC oxidation process (Section 4.0).
- 2) SOA formation potential of *m*-xylene within these well-controlled environments with fixed β were determined for a variety of NO_x conditions and adapted to GEOS-CHEM to evaluate the impact of the updated chamber experimental simulation strategies (Section 5.0). This

work has been published as Peng et al. (2022). This work directly challenges the convention used in current chemical transport models that generally use a constant secondary organic aerosol (SOA) yield to represent SOA formation from aromatic compounds under low NO_x conditions. This work demonstrates, using the experimental strategies developed as part of the CRC program, that a wide range of SOA yields (10 to 42%) from *m*-xylene under “low- NO_x ” conditions can be observed. Increasing HO_2/RO_2 ratio is observed to increase SOA yield. The $\text{RO}_2 + \text{RO}_2$ pathway, which is most important as β approaches zero, is found to have a lower SOA-forming potential compared to the $\text{RO}_2 + \text{HO}_2$ pathway and cannot be ignored under certain atmospheric conditions. On the global scale, the chemical transport model GEOS-Chem is used to identify regions characterized by lower surface HO_2/RO_2 ratios, suggesting that the $\text{RO}_2 + \text{RO}_2$ pathway is more likely to prove significant to overall SOA yields in those regions. Current models generally do not consider the $\text{RO}_2 + \text{RO}_2$ impacts on aromatic SOA formation, but preliminary sensitivity tests with updated SOA yield parameters based on such a pathway suggest that without this consideration, SOA from aromatic compounds may be overestimated in regions with lower HO_2/RO_2 ratios.

- 3) The extensive existing UCR database (over 160 experiments) for *m*-xylene – NO_x from traditional experiments (single VOC- NO_x injection, variable β) is then explored (Section 6.0) in detail using the observations from Sections 3.0-5.0 of this work. Specifically, the ability to predict SOA formation in a variable β experiment using fixed β values was explored in depth. (Section 6.0). In this Section it is determined that the variable β experiments cannot be explained as a linear combination of fixed beta experiments. This is attributed to the complexity of the multi-generational oxidation mechanism leading to SOA formation where the oxidation conditions of slower reacting multi-generational products in the variable experiments prevent simple linear combination modelling of the fixed β experiments. Further, the SOA yield for $\beta=0$ is not a simple single fixed value as discussed in the next Section.

- 4) SOA formation under very low NO_x (no NO_x added, $\beta=0$) environmental conditions is explored extensively in Section 7.0. Large variability in SOA formation has been reported between different research groups for “no- NO_x ” $\beta=0$ experiments. Further, observations in the Sections above indicate that a single, simple aerosol yield for $\beta=0$ conditions may not be sufficient to account for SOA formation in a variable β run. Therefore, a series of $\beta=0$ experiments were conducted and explored the role of light intensity, chamber wall NO_x , and HO_2/RO_2 on variability in SOA yield. H_2O_2 levels in $\beta=0$ experiments were found to influence HO_2/RO_2 ratios and accounting for them improved our predictive ability of these experiments. This led to the determination that there are multiple SOA formation regimes for β equal to zero scenarios governed by the HO_2/RO_2 mixing ratio achieved within the β zero environment. A paper is in progress for this work with expected submission quarter 1 of 2023. (Section 7.0)
- 5) SOA formation from α -pinene was explored in depth first in the design of fixed β experiments and then in SOA formation as a function of β . α -Pinene was selected to represent biogenic precursors and a similar approach to that of the anthropogenic representative *m*-xylene above was applied to α -pinene. Auto-oxidation was suggested to explain α -pinene SOA formation potentials even at higher β values. Findings included the presence of multiple SOA formation regimes at high NO_x ($\beta=1$) with SOA yield continuing to drop with further increased NO_x concentration due to shortening of RO_2 lifetime. While it has generally been observed that SOA formation from monoterpenes increase with increasing NO_x for traditional variable β experiments, it is shown in this work that at the highest levels of NO_x SOA formation begins to decrease. Similar to *m*-xylene, variable β α -pinene/ NO_x experiments could not be modelled by fixed β experiments due to the multiple SOA formation potentials observed for fixed $\beta=0$ and $\beta=1$. A paper is in progress for this work with expected submission January, 2023, which will include GEOS—CHEM simulation of the impacts of the observed SOA from α -pinene on lower tropospheric SOA formation around the globe. (Section 8.0)

6) SOA formation from naphthalene for fixed β conditions was additionally quantified (Section 9.0) as well as a comparison of the O:C composition of α -pinene and naphthalene derived SOA (Section 10.0). SOA formation was observed to be highest for naphthalene at $\beta=0.3$, then $\beta=0$, and then $\beta=1.0$. This observation is unique to naphthalene in this work and is attributed to the ability of the HO₂ and RO₂ radicals to recycle more efficiently with some NO present but without so much NO available to significantly suppress SOA formation via RO₂ + NO reaction similar to that observed for *m*-xylene. The recycle of OH provides for additional oxidation of multi-generational products leading to the larger SOA formation. Oxygen to carbon content (O:C) for naphthalene (0.69-0.89) SOA was observed to be higher than that of *m*-xylene and α -pinene. The observed O:C is quite high for naphthalene indicating that the SOA products must have been produced thru a number of oxidation steps and is consistent with SOA formation highest at $\beta=0.3$, which produces the highest level of OH in the system.

Due to major delays in the program due to COVID related laboratory shutdowns and subsequent development and improvement of the environmental chamber during the shutdown, experiments were conducted in both the UCR dual 90 m³ collapsible environmental chambers and the new 118 m³ fixed volume environmental chamber. Additionally, due to a Windows automatic update that obsoleted the data acquisition systems of the lab, this work in part updated and rebuilt the entire data operating system of the lab including major upgrades in control and management of the data inversion algorithms. Additional time was spent during the project upgrading the facility to the new 118 m³ fixed volume chamber with superior particle wall loss characteristics (more than order of magnitude improvement) and extreme low background (over three orders of magnitude lower background for PM formation) and long experimental lifetimes (improved from about 10 hours to >60 hours).

Table of Contents

Disclaimer	2
Acknowledgements.....	3
List of Tables	4
List of Figures	5
Executive Summary	9
Table of Contents	14
1.0 Introduction.....	15
2.0 Experimental conditions	18
3.0 Experimental Design: Types of Chamber Experiments.....	25
3.1 Varied VOC injection methods	31
3.2 Varied initial NO _x concentrations	33
3.3 Continuous NO injection:	36
4.0 Experiment design: Experimental control of β	38
5.0 Further investigation into branching ratios – blending experiment with model observations of β	48
6.0 Use of historical UCR chamber data to further explore SOA as a function of β	55
7.0 Variation in SOA formation potential of <i>m</i> -xylene in low (no NO _x added) conditions.....	65
8.0 A deeper look into NO _x chemistry in the α -pinene system	77
9.0 A deeper look into NO _x chemistry of Naphthalene system	84
10.0 The elemental composition of SOA formed from α -pinene versus naphthalene.....	86
11.0 Conclusions and Future Work.....	88
12.0 References.....	90

1.0 Introduction

Roughly 20 to 90% of the submicron ambient aerosols are organic aerosols (OA), which mainly consists of secondary organic aerosols (SOA). SOA is formed through the condensation of photooxidation products from gas-phase precursors (Jimenez *et al.*, 2009). Traditional environmental chamber studies inject both the test VOC and NO_x (when present) prior to the start of the reaction. This leads to experiments that move from NO_x rich conditions to peroxide rich conditions. SOA formation potential of test VOCs from such experiments are a combination of the NO_x rich and the peroxide rich conditions.

Biogenic volatile organic compounds (BVOCs), such as monoterpenes (C₁₀H₁₆), and sesquiterpenes (C₁₅H₂₄), are one of the most important contributors to atmospheric emissions due to their high emissions rates, reactivity, and relatively high SOA yield. The BVOCs in the atmosphere are mainly oxidized by hydroxyl radicals (OH), ozone (O₃) or nitrate (NO₃), leading to the formation of SOAs (Guenther *et al.*, 1995). α -Pinene and β -pinene are two major contributors to primary biogenic hydrocarbon emission in the atmosphere (Zhang *et al.*, 1992). α -Pinene is the most abundant emitted monoterpene and mainly found in the resins of pine trees. The total global monoterpene emissions are roughly 127 TgC yr⁻¹ annually, which α -pinene accounts for roughly 50 TgC yr⁻¹ (Pye *et al.*, 2010; Guenther *et al.*, 1995). The aerosol carbon yields are 18.3% and 13.8% for the reactions between α -pinene with hydroxyl radical (\cdot OH) and ozone (O₃), respectively, while it is found that NO suppressed the aerosol carbon yield (Kavouras *et al.*, 1999).

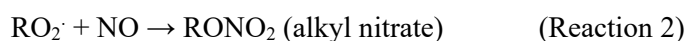
Aromatic volatile organic compounds, such as benzene, toluene, and xylenes, are most commonly associated with fuel evaporation and with combustion by-products although a number of other sources also exist (e.g., solvent evaporation). *m*-xylene oxidation in the presence of NO_x and sunlight has been studied extensively in the UCR chambers for a variety of atmospheric conditions (e.g., Li *et al.*, 2016abc; Li *et al.*, 2017) making it an ideal molecule to be used for development of new environmental chamber studies in this work. Moreover, another major sources of semi-volatile gas-phase emissions are anthropogenic polycyclic aromatic hydrocarbons (PAHs), such as Naphthalene, with form due to incomplete combustion

emissions. The California Air Resources Board (CARB) 2010 California Toxic Inventory (CARB, 2013) estimated the total emissions of Naphthalene to be ~ 910.7 tons yr^{-1} in California (Chia-Li *et al.*, 2018).

The SOA formation potentials are represented by SOA yields (Y) which is defined by the produced aerosol mass (M_o) per hydrocarbon (ΔHC) consumed. SOA yield highly depends on the atmospheric conditions. Nitrogen oxides (NO_x) level is one of the key factors that impacts SOA yield (Ng *et al.*, 2007). The NO_x level alters the direction of peroxy-radical (RO_2^\cdot) reaction pathways which highly affects the distribution of oxidation products leading to the different SOA yields. Under low- NO_x conditions, RO_2^\cdot tend to react more with HO_2^\cdot to afford low volatile products. These products mainly contain OH, OOH (Reaction 1) functional groups that allows in new particle formation via hydrogen bonding interactions (Deng *et al.*, 2020). For example, Reaction 1 is the dominant pathway for RO_2^\cdot radicals under low- NO_x conditions which leads to formation of low volatile hydroperoxides which participates in new particle formation (Deng *et al.*, 2020).



Contrary, under high- NO_x conditions, RO_2^\cdot radicals (obtained from α -pinene reaction with $\cdot\text{OH}$ and O_2) reacts with NO resulting in the formation of organic nitrates (Reaction 2) and/or alkoxy radicals (Reaction 3). The products are more volatile compared to the products formed from (Reaction 1).



However, only considering low- NO_x or high- NO_x conditions in SOA yield study underestimate the complex photooxidation conditions in which many gas phase species are involved. Likewise, Li *et al.* stated that at sub-ppb NO levels, $\cdot\text{OH}$ formation was enhanced resulting in increasing HO_2^\cdot , RO_2^\cdot formation, leading to higher SOA formation (from aromatic precursors). The NO_x condition was maintained at sub-ppb level via continuous NO injection. Also, high initial NO concentration and NO free condition resulted lower the SOA formation (Li *et al.*, 2015). This arises from both NO suppression and promotion pathways to SOA formation (**Figure 1**) (Li *et al.*, 2015).

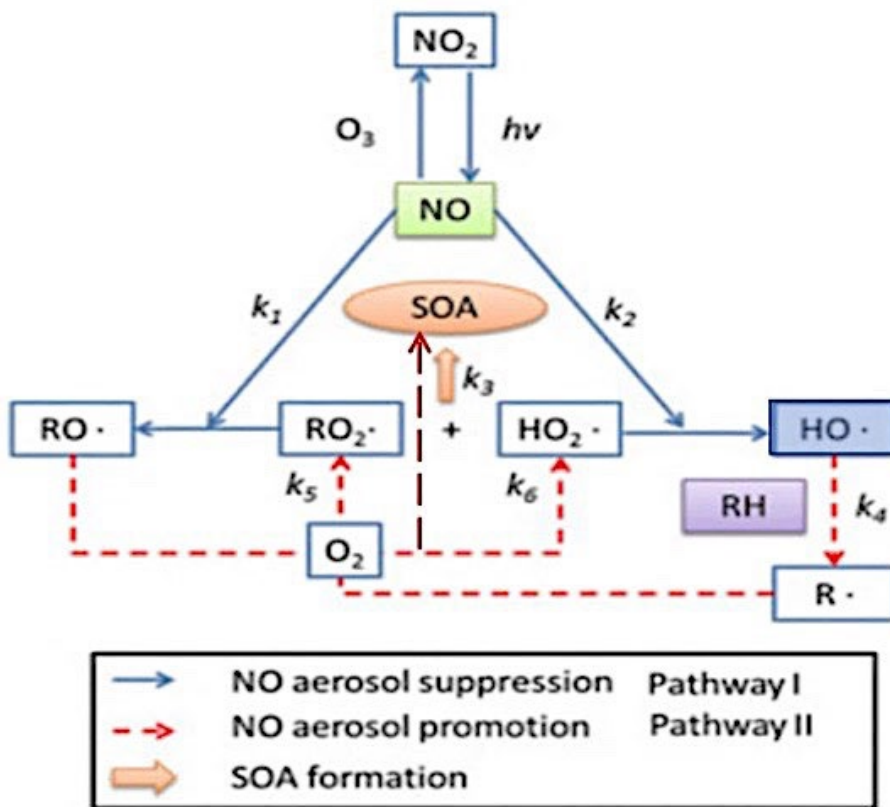


Figure 1: NO aerosol suppression and promotion pathways. (Figure from Li *et al.* 2015)

The competition of $RO_2\cdot$ reaction in either NO or $HO_2\cdot$ pathways are defined by “branching ratio” (β) which is the ratio of $NO + RO_2\cdot$ reaction rate over the total $RO_2\cdot$ decay rate (in both NO and $HO_2\cdot$ pathways) (Equation 1) (Pye *et al.*, 2010; Farina *et al.*, 2010). Thus, it is important to explore the correlation between SOA formation and the branching ratios. Where $k (RO_2\cdot + NO)$ and $k (RO_2\cdot + HO_2\cdot)$ are rate constants for reactions of proxy radical with NO and $HO_2\cdot$, respectively.

$$\beta = \frac{k_{RO_2+NO}[NO]}{k_{RO_2+NO}[NO] + k_{RO_2+HO_2}[HO_2]} \quad (\text{Equation 1})$$

The branching ratio in classical experiments will be decreasing throughout the experiment substantially (**Figure 2A**). The term “classic experiments” refers to the experiments with initial injection of precursor, NO, and H_2O_2 . In classical experiments, most of the gas phase species concentration including VOC, NO, NO_2 , O_3 , etc., are not constant throughout the experiment. For instance, the high initial NO concentration

decreases to below detection limit (0.2 ppb) at the end of the experiment. However, in real atmosphere condition, NO and NO₂ are continuously emitted into the ambient by variety of sources, especially in urban areas with heavy traffics. Thus, continuous NO injection into the chamber (**Figure 2B**) could better mimic the real atmospheric conditions. In this study, the SOA yield has been evaluated using different SOA precursors such as α -pinene, and Naphthalene under different NO_x level, which has been added continuously to maintain a constant branching ratio (β) during the photochemical process in a 118 m³ fixed-volume environmental chamber at UCR/CE-CERT. Additionally, the effect of continuous VOC injection on gas phase species and the SOA yield will be evaluated. The outcomes of this novel study are critical for development of more “accurate” atmospheric SOA models.

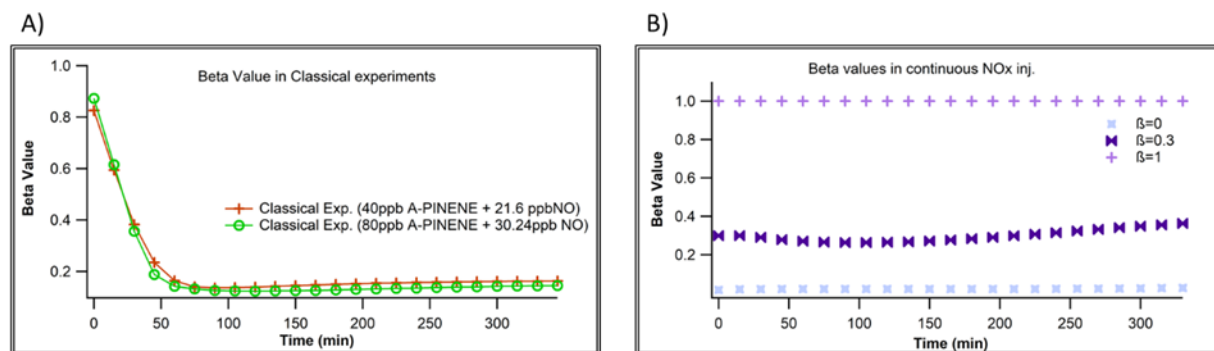
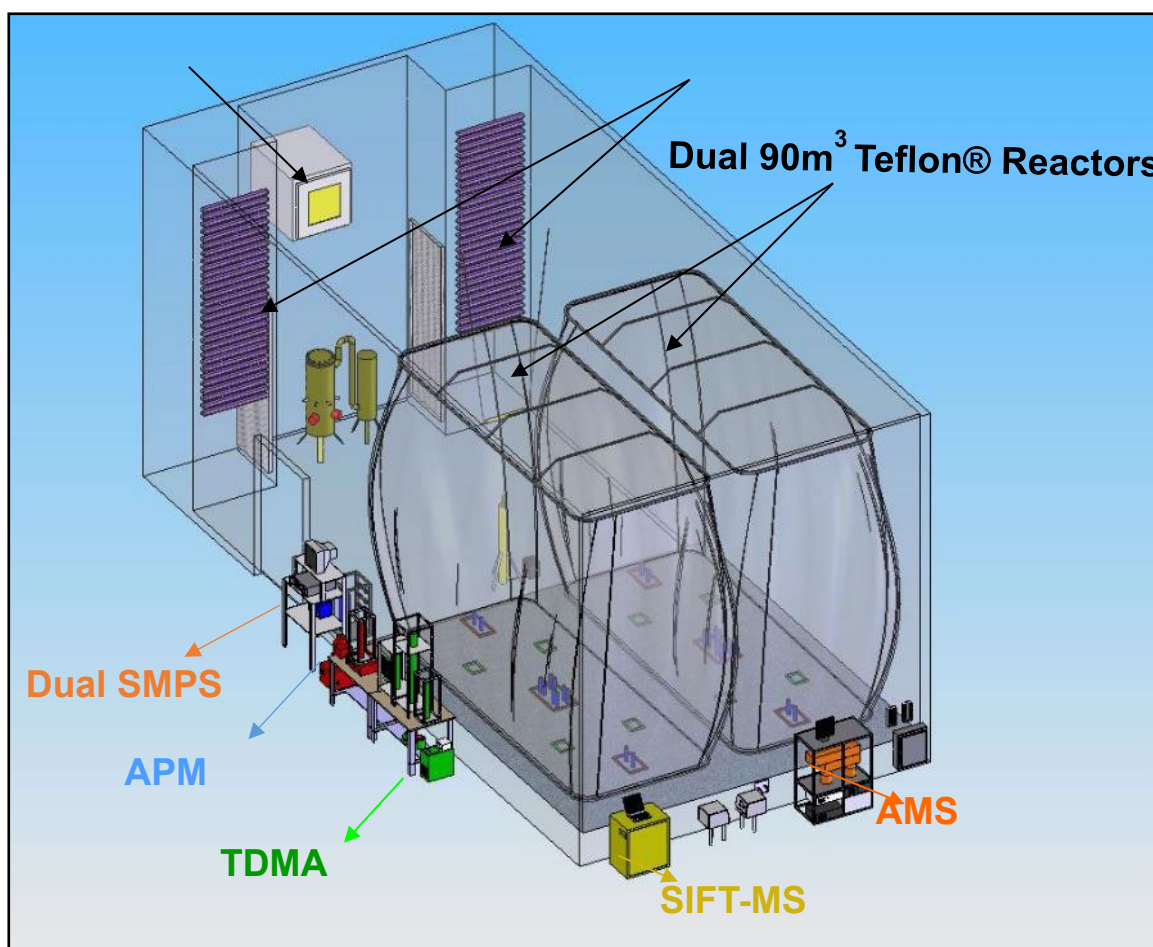


Figure 2. β value variation throughout the experiment. A) Classical chamber experiments with instantaneous NO_x injection; B) Continuous NO_x injection in this study.

2.0 Experimental conditions

Two chamber systems are included in this project, including the UCR collapsible dual chambers (UCR chamber facility at start of project, **Figure 3**) and the UCR fixed-volume chamber (current enhanced UCR chamber facility, **Figure 4**). The characterization and features of the UCR collapsible dual chambers have been previously described in detail (Carter *et al.*, 2005). Briefly, the UCR collapsible chambers consist of two 90 m³ collapsible Teflon reactors (2 mil (0.0508 mm) FEP film) kept at a positive pressure differential (3.73–4.98 Pa) to the enclosure where the reactors are located to minimize contamination and eliminate

dilution during experiments. The enclosure is relative humidity controlled ($<0.1\%$), temperature controlled (300 ± 1 K), and continuously flushed with dry purified air (dew point < -40 °C). Prior to and between experiments, reactors were collapsed to a volume < 20 m³ for cleaning. The cycle of filling-purging the reactors was repeated until particle number concentrations were < 5 cm⁻³ and NO_x mixing ratios were < 1 ppb. The reactors were then flushed with dry purified air and filled up to 90 m³ overnight. The filling-purging of the reactors is controlled by an “elevator” program in LabView.



UCR CE-CERT Chamber Reactors (Clayton Stothers)

Figure 3: Schematic of the dual 90 m³ collapsible environmental chambers

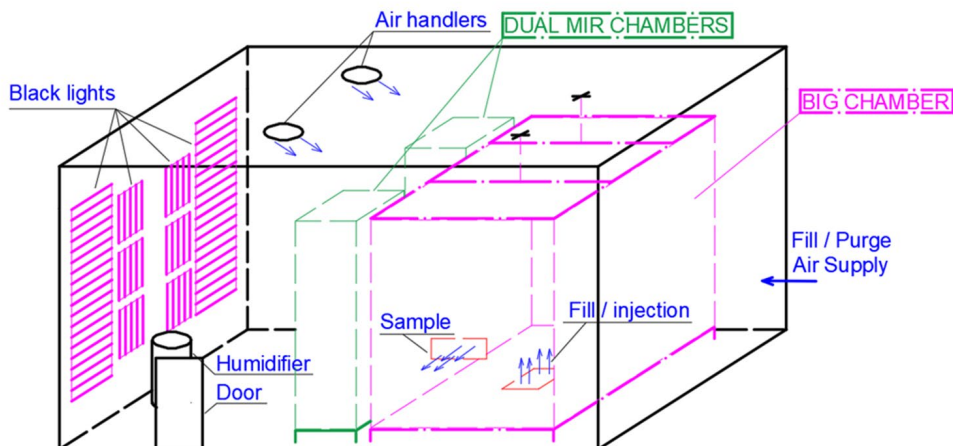


Figure 4: Schematic of the new 118 m³ fixed volume environmental chamber

The recently upgraded UCR fixed-volume chamber system keeps the enclosure features of the UCR collapsible dual chamber system. The two 90 m³ collapsible reactors were replaced with one ~118m³ fixed-volume Teflon reactor using the same FEP film. In addition to the size and change to fixed-volume, the reactor is electrically insulated from the walls, ground, and ceiling to keep “electroneutral”. Three soft x-ray PhotoIonizers were installed to discharge the reactor thoroughly before each experiment to ensure consistency. Adjustable make-up clean air can be applied to offset the sampling uptake. Particle wall loss rate is measured to be lower in this new reactor by over an order of magnitude.

NO and NO₂ mixing ratios were monitored by a Thermo Environmental Instruments Model 42C chemiluminescence NO_x analyzer. O₃ mixing ratios were monitored by a Dasibi Environmental Corp. Model 1003-AH O₃ analyzer. An Agilent 6890 gas chromatograph with flame ionization detector (GC-FID) was used to measure the VOC levels during the experiments.

Multiple instruments were used for particle-phase monitoring. Homemade scanning mobility particle sizer (SMPS) with a TSI 3081 differential mobility analyzer (DMA), is used to measure the particle number concentration. Particle effective density was directly measured by an Aerosol Particle Mass Analyzer

(APM, Kanomax) with a SMPS built in house (Malloy *et al.*, 2009). Chemical composition of SOA was measured using HR-ToF-AMS (DeCarlo *et al.*, 2006) and analyzed to obtain O:C and H:C ratios by applying the method of Canagaratna *et al.* (2015). Data processing was performed using the ToF-AMS Analysis Toolkit 1.57 and PIKA 1.16 on Igor Pro 6.36.

Particle wall loss corrections previously followed the first-order deposition method described in Cocker *et al.* (2001) for experiments in UCR collapsible dual chamber. Particles lost to the wall are assumed to no longer actively participate in further condensation of oxidation products to the aerosol phase. Vapor wall loss correction and particle coagulation were assumed to be negligible. After evaluation of relative particle wall loss and differences in particle wall loss dependence between the UCR chamber, the methods for data analysis have been updated. The updated particle wall loss method, coagulation correction, and vapor wall loss dependence are discussed in detail in the experimental protocol section.

Due to the significantly reduced particle wall loss achieved by keeping reactor “neutral” (upgraded UCR system), the particle loss caused by coagulation (exceeding detection range) and dilution became notable. The new correction method was built containing both of them and the size dependent particle wall loss. The coagulation code was developed by Chen Le based on the formula in Atmospheric Chemistry and Physics: From Air Pollution to Climate Change (Seinfeld and Pandis, 2016). At each SMPS scan interval, the exceed-range particle loss (dV_1) is calculated using the last uncorrected particle number concentration for each size bin, representing the coagulation happened during this interval (typically 2-4 mins). A total exceed-range particle loss (ΔV_1) is formed by summing up the values throughout the experiment. Another new contributor that is considered for the new UCR fixed-volume chamber is the effects from dilution, which was “0” in the previous UCR collapsible chamber due to its positive pressure differential control. The dilution ratio in the new fixed-volume chamber is calculated based on the tracer (e.g. PFH or PFB) mixing ratio change. The particle “loss” (ΔV_2) caused by dilution at a given time t is calculated by equation:

$$\Delta V_2(t) = V_t \left(\frac{[Trc]_I}{[Trc]_t} - 1 \right),$$

where V_t represents the uncorrected volume concentration at t according to SMPS data, $[\text{Trc}]_I$ and $[\text{Trc}]_t$ represents the initial mixing ratio and mixing ratio at t of the tracer, respectively. It should be noted that $\Delta V_2(t)$ already represents the “total loss” of particles due to dilution at t .

Particle wall deposition, the last contributor to the total particle loss, is decided to be size-dependent for the new UCR fixed-volume chamber. Shown in **Figure 5**, the particle number decay rate (β , day^{-1}) for each size bin was calculated using a function developed based on monodispersed seed deposition tests (Chen Le, paper in preparation).

$$\log_{10}(\beta) = 1.5387 \times \log_{10}(D_{pi})^3 - 8.5969 \times \log_{10}(D_{pi})^2 + 14.7529 \times \log_{10}(D_{pi}) - 7.9181$$

where D_{pi} is the particle size in nm.

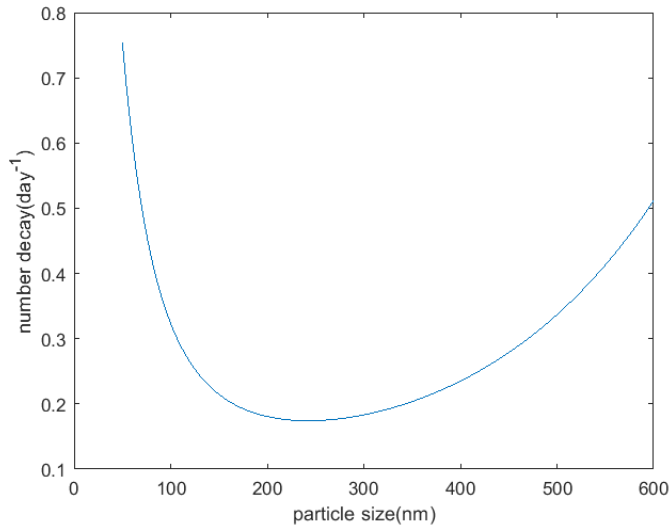


Figure 5: Particle number decay rate shown as a function of particle size updated on Oct 2nd, 2022

The particle wall deposition loss (ΔV_3) is integrated from corrected number concentration calculated by a first order kinetics described in Cocker *et al.* (2001). The total particle loss at t is then the sum of

$\Delta V_1(t)$, $\Delta V_2(t)$ and $\Delta V_3(t)$. This correction fit for β is still being iterated and optimized at this time. The most up to date correction will be reflected in papers in preparation.

New Particle Wall Loss Correction Approach: Seed only particle loss tests were carried out in the new UCR fixed volume chamber to validate the new particle loss correction method. Particle data analysis using the updated particle loss correction method introduced above shows 100% recovery of the initial particle loading (**Figure 6**). **Table 1** shows that dilution and particle wall deposition contributed the majority of the total particle loss in this case. Although exceed measurement loss due to coagulation is negligible here, it may cause a notable loss with larger particle size at higher number concentration and/or a narrow detection range.

Table 1: Particle loss correction of pure seed test in the new UCR fixed-volume chamber. Unit: $\mu\text{m}^3 \text{cm}^{-3}$.

Initial volume	Corrected end volume	Uncorrected end volume	Exceed range loss ΔV_1	Dilution loss ΔV_2	Particle deposition loss ΔV_3
37.97(± 0.66)	40.66 (± 0.80)	30.61(± 0.74)	0.02 (± 0.00)	4.06 (± 0.14)	5.39(± 0.04)
Fraction to total particle loss			0.2%	42.9%	57.0%

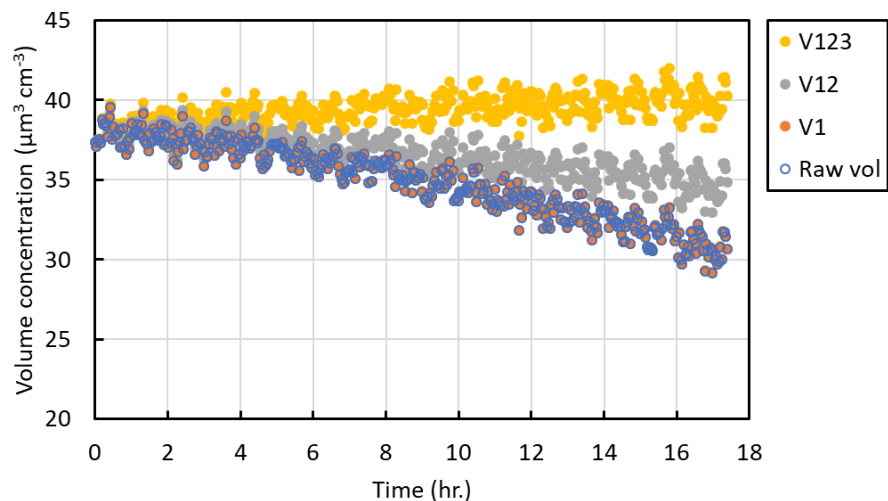


Figure 6: Uncorrected and corrected particle volume concentration shown as a function of time. Data shown is being corrected by (V1) exceed measurement range loss due to coagulation, (V12) V1 plus dilution correction, (V123) V12 plus size dependent particle wall loss.

The new UCR fixed-volume chamber was also characterized with a series of repeated oxidation experiments of *m*-xylene. The final SOA mass yield of the selected experiments were similar between the old and new UCR chambers after data being corrected using the two particle loss correction methods, respectively. However, the SOA mass yield was corrected by 100-300% for particle loss in the UCR old chamber while in the new chamber the correction was much smaller: 2-4% of raw final volume concentration. It is noted that, in the processing of particle loss correction, the data from the UCR old chamber did not include coagulation effects or vapor wall loss, among which the former one can cause an overestimation of the SOA formation while missing the latter one can cause an underestimation of the SOA formation. The exploration of the real offset of the data requires reprocessing of the previous data using coagulation engaged correction method and future investigation on vapor wall loss dependence on the physical and chemical properties of VOC. Vapor wall loss was not estimated as part of this study.

SOA yields are calculated for both groups based on a ratio of VOC reacted and wall-loss corrected calculation of SOA formed.

$$\text{SOA mass yield} = \frac{\text{SOA mass formation}}{\text{Hydrocarbon reacted mass}}$$

SOA mass formation is the difference between the measured and wall-deposition-corrected aerosol mass concentration at a given time and the aerosol concentration prior to the beginning of oxidation.

3.0 Experimental Design: Types of Chamber Experiments

Three different β values (high, medium, low) were defined in this work to mimic three different atmospheric NO_x levels. These values were chosen based on GEOS-CHEM (Porter *et al.*, 2021) (**Figure 7**). The real-time concentrations of radical species such as HO_2 and NO are required for the branching ratios calculation which can be predicted by the gas phase reaction model on SAPRC11 (Carter *et al.*, 2013). Global branching ratios in different areas were simulated from a global 3-D model of atmospheric chemistry driven by meteorological input from the Goddard Earth Observing System (GEOS-Chem) based on NO and HO_2 concentrations and classified into four different circumstances: 1) Long, 2) Short, 3) High, 4) Low.

‘Long’ illustrates the highest branching ratio and maintains at high level (**0.6-0.9**) from 5am to 8pm during a day, mainly located at highly populated areas including North America, Europe and East China. ‘Short’ and ‘high’ represent similar medium level of branching ratio (**0.4-0.6**); however, ‘short’ only upholds the level from 6 am to 7 pm and ‘high’ maintains during the whole day. ‘Short’ represents ocean areas in the Northern Hemisphere and Continents in the Southern Hemisphere, while ‘high’ represents areas close to the North Pole. ‘Low’ represents the lowest branching ratio and maintains at (**0-0.25**) from 5 am to 8 pm, locating at ocean area in the Southern Hemisphere.

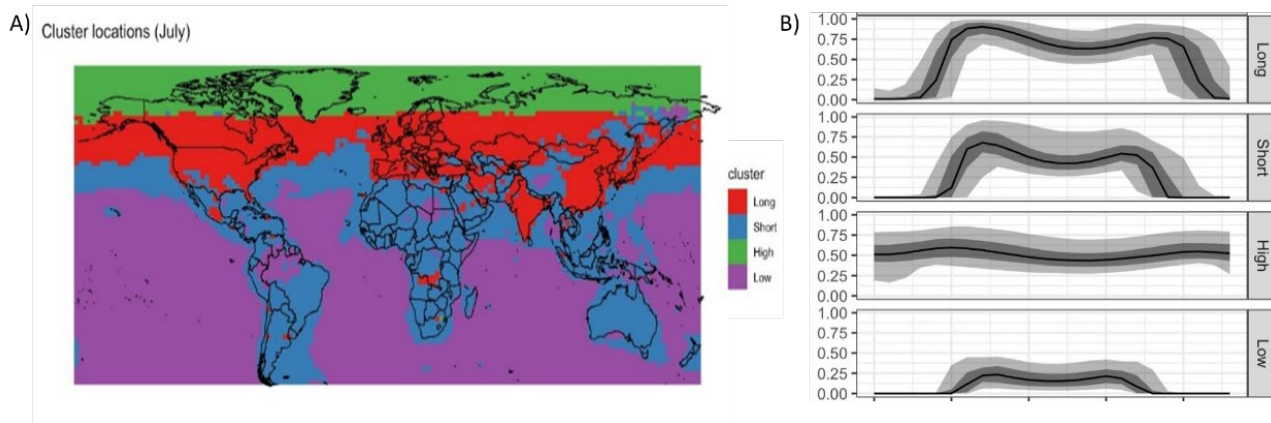


Figure 7: A) Four global branching ratios scenarios in July. B) Branching ratio profile during a day of four scenarios. (Li *et al.*, 2022)

A number of environmental chamber experimental methods were studied as part of this program. The first goal was to determine an optimum non-traditional experimental scheme to best elucidate the roles of NO_x on SOA formation. This work commenced with *m*-xylene as the test VOC due to its relatively higher SO yield, the importance of aromatic hydrocarbons in an urban environment, and the large UCR database of prior experiments to draw upon to interpret the results. The goal of these experiments were to challenge the traditional chamber experiment where all chemicals and oxidants are added to the chamber at the beginning of the reaction and then allowed to proceed following the chemistry dictated solely by the initial injections into the chamber.

Three basic strategies were ultimately adopted for this study

1. Multiple VOC injection: These experiments follow traditional SOA chamber experiments but split the VOC injection into discrete multiple injections over the course of the reaction to achieve the same amount of VOC consumption as in the traditional experiments (**Table 2**).

2. Multiple NO_x injection: These experiments follow traditional SOA chamber experiments but split the NO_x injection into discrete multiple injections over the course of the reaction to achieve the same amount of total NO_x present as in the traditional experiments (**Table 3**).
3. Continuous NO_x injection: These experiments follow traditional SOA chamber experiments but except that NO_x is slowly but continuously injected into the environmental chamber (**Table 4**).

SOA yield, defined as the ratio of the amount of SOA formed to the amount of *m*-xylene consumed, was calculated and branching ratio β was estimated from SAPRC11 from these three sets of experiments.

Table 2: Experiments with variable VOC injection strategies

Type	Run	Side	Surrogate	H2O2	NO	NO _x	<i>m</i> -xylene	delta <i>m</i> -xylene		Mo	Yield	Ozone
			ppmC	ppm	ppb	ppb	ppb	ppb	ug/m3	ug/m3		ppb
Classic	2346	B	1.1	1.0	13.14	24.86	36.64	32.16	138.02	28.25	20.47%	162
	2346	A	1.1	1.0	13.45	24.91	49.98	44.35	190.32	40.86	21.47%	188
	2347	A	1.1	1.0	14.82	25.54	98.67	90.56	388.62	84.26	21.68%	198
One time after lights	2348	B	1.1	1.0	15.95	25.11	37.23	33.26	142.71	26.66	18.68%	206
	2348	A	1.1	10	15.61	24.96	54.67	48.54	208.28	40.61	19.50%	197
	2351	A	1.1	1.0	15.87	25.62	70.27	51.99	223.11	78.40	35.14%	156
	2358	B	1.1	1.0	15.60	26.08	134.09	108.82	466.98	129.25	27.68%	133
Hourly injection after lights	2351	B	1.1	1.0	16.16	25.79	35.22	28.02	120.23	26.38	21.94%	203
	2363	B	1.1	1.0	17.31	26.48	43.85	38.32	164.46	42.66	25.94%	188
	2363	A	1.1	1.0	16.86	26.30	69.27	55.89	239.85	53.75	22.41%	174
	2323	A	1.1	1.0	17.19	25.82	115.89	70.74	303.55	66.00	21.74%	160
	2358	A	1.1	1.0	15.14	25.74	120.33	89.32	383.27	104.10	27.16%	156

Table 3: Experiments with variable NO_x injection strategies

<i>Run ID</i>		<i>Time</i>	<i>Surrogate</i>	<i>H2O2</i>	<i>Init. NO</i>	<i>Init. NO_x</i>	<i>Init. m-xylene</i>		<i>Δ m-xylene</i>	<i>SOA</i>	<i>Yield</i>	<i>Ozone</i>
#	<i>Side</i>	<i>min</i>	<i>ppmC</i>	<i>ppm</i>	<i>ppb</i>	<i>ppb</i>	<i>ppm</i>	<i>ug/m3</i>	<i>ug/m3</i>	<i>ug/m3</i>		<i>ppb</i>
2364	A	585	1.1	1	103.06	151.14	0.10	103.70	444.99	86.93	19.54%	513.6
2364	B	585	1.1	1	103.02	151.40	0.03	32.17	133.75	20.60	15.40%	565.8
2362	A	453	1.1	1	29.59	48.02	0.11	112.81	429.47	90.64	21.11%	223.9
2357	B	604	1.1	1	29.12	46.51	0.04	37.42	155.60	29.77	19.13%	297.0
2347	A	605	1.1	1	14.86	25.55	0.10	98.67	388.62	93.34	24.02%	158.6
2346	B	464	1.1	1	13.41	24.91	0.04	36.64	138.02	28.25	20.47%	157.0
2346	A	455	1.1	1	13.14	24.86	0.05	49.98	190.32	40.86	21.47%	189.7
2361	A	659	1.1	1	8.13	12.67	0.10	102.20	378.69	95.75	25.29%	75.7
2361	B	679	1.1	1	8.22	12.75	0.03	32.80	129.58	50.38	38.88%	115.4
2360	A	595	1.1	1	0.00	0.00	0.09	93.18	283.46	101.68	35.87%	9.2
2344	A	536	1.1	1	0.00	0.00	0.05	52.65	167.74	40.74	24.29%	15.3
2360	B	616	1.1	1	0.00	0.00	0.05	49.34	168.53	81.07	48.11%	9.3
2321	A	456	1.1	1	0.00	0.00	0.03	30.71	112.40	29.01	25.81%	6.7

Table 4: Experiments with continuous NO injection

<i>Run ID</i>		<i>Surrogate</i>	<i>H2O2</i>	<i>NO rate</i>	<i>Init. NO</i>	<i>Init. NO_x</i>	<i>Init. m-xylene</i>		<i>Δ m-xylene</i>	<i>SOA</i>	<i>Yield</i>	<i>Ozone</i>
#	<i>Side</i>	<i>ppmC</i>	<i>ppm</i>	<i>ppb/hr</i>	<i>ppb</i>	<i>ppb</i>	<i>ppm</i>	<i>ug/m3</i>	<i>ug/m3</i>	<i>ug/m3</i>		<i>ppb</i>
2372	<i>A</i>	0	1	3	0	0	0.086	370.75	370.75	97.6	26.32%	250.0
1863*	<i>B</i>	0	1	0	50	50	0.072	308.96	308.96	47.2	15.28%	260.6
1867*	<i>B</i>	0	1	0	22.8	51.4	0.078	334.71	334.71	49.4	14.76%	240.9

3.1 Varied VOC injection methods

As is shown in **Figure 8**, when varying *m*-xylene injection methods and maintaining the total concentration similar, no apparent difference were seen on SOA yield. It was also shown in ozone and branching ratio graph that no clear difference from experiments with VOC injected in different methods but same total concentration. The calculated branching ratio, β , as a function of experimental time. It is clearly seen that

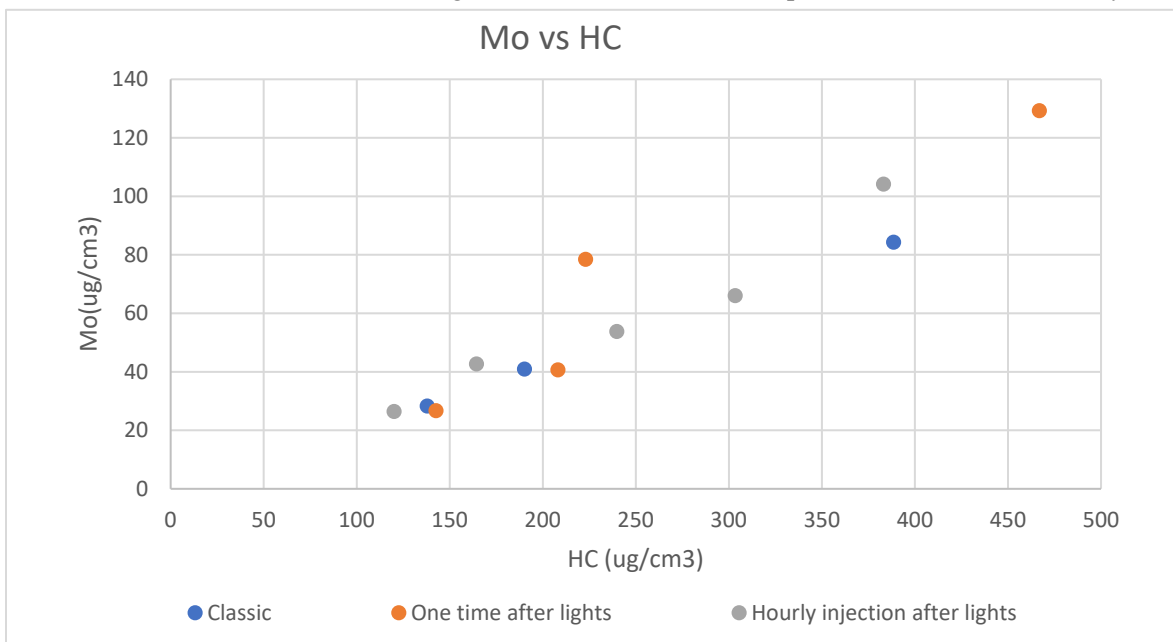


Figure 8: Final SOA formation vs final HC consumption from experiments with different *m*-xylene injection methods

β varies widely thru the course of the experiment meaning that the VOC oxidizes thru vary different NO_x regimes moving from NO_x rich to peroxide rich chemical regimes.

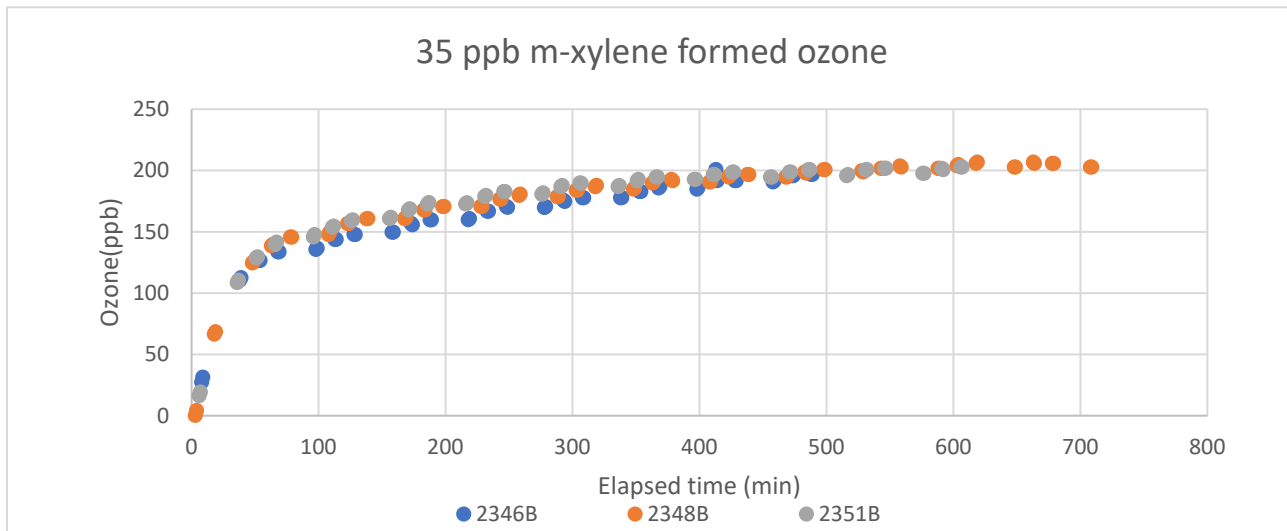


Figure 9: Final ozone formation from experiments with 35 ppb *m*-xylene injected differently

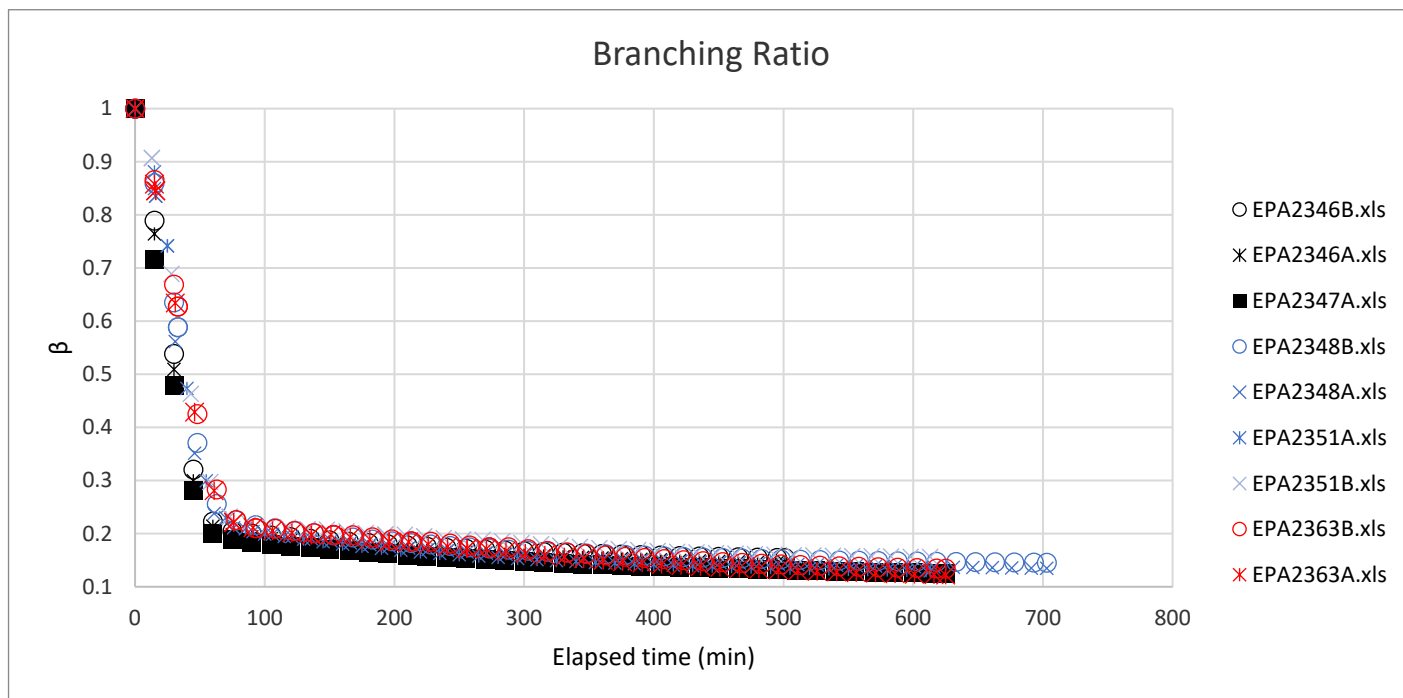


Figure 10. Branching ratio over the course of the experiment with different VOC injection timings

3.2 Varied initial NO_x concentrations

Figure 11 shows the branching ratio during the experiment when the initial NO_x concentrations are varied from 0-150 ppb. SOA yield was labelled with the final yields (**Figure 11**) and it increased as initial NO_x concentration decreased when the total *m*-xylene concentration was kept constant, which matches previous

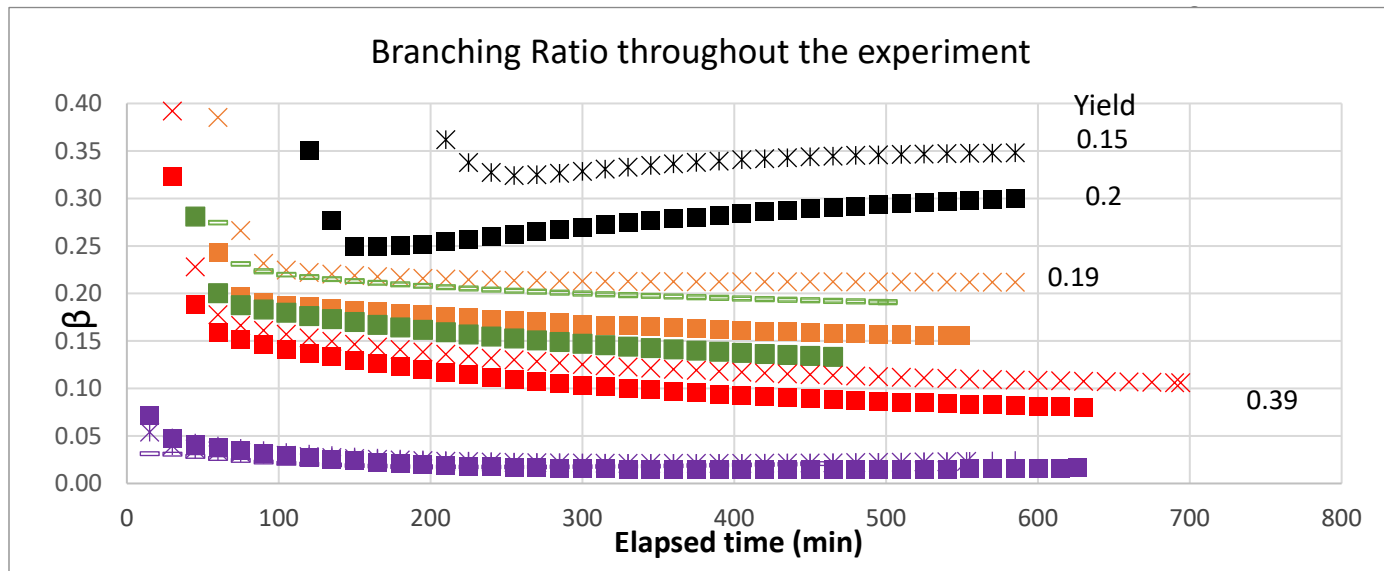


Figure 11. Branching ratio of experiment with different initial NO_x

conclusion that higher HC/NO ratio leads to higher SOA yield. A clear trend could be seen from branching ratio and SOA yield. Experiments with lower branching ratio had larger SOA yield.

Figure 12 shows the SOA formation and *m*-xylene consumption during the experiment. SOA did not start forming enough to be detected by instruments until a portion of *m*-xylene was consumed. Thus, the yield was re-calculated by offsetting this portion of *m*-xylene. The slope of these fitted curves can be regarded as

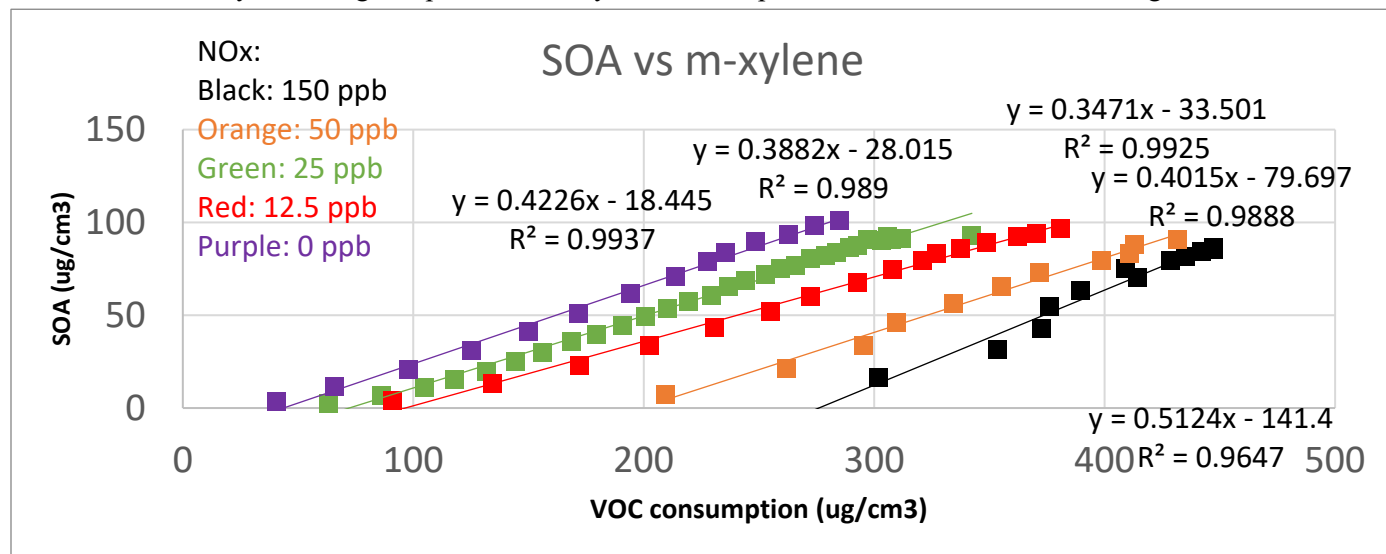


Figure 12. SOA formation vs *m*-xylene consumption during the experiments with different initial NO_x concentrations

an indicator of the new yield.

Figure 13 shows the relationship between instantaneous yield and average branching ratio for every 40 minutes. An exponential fit was applied to these data points.

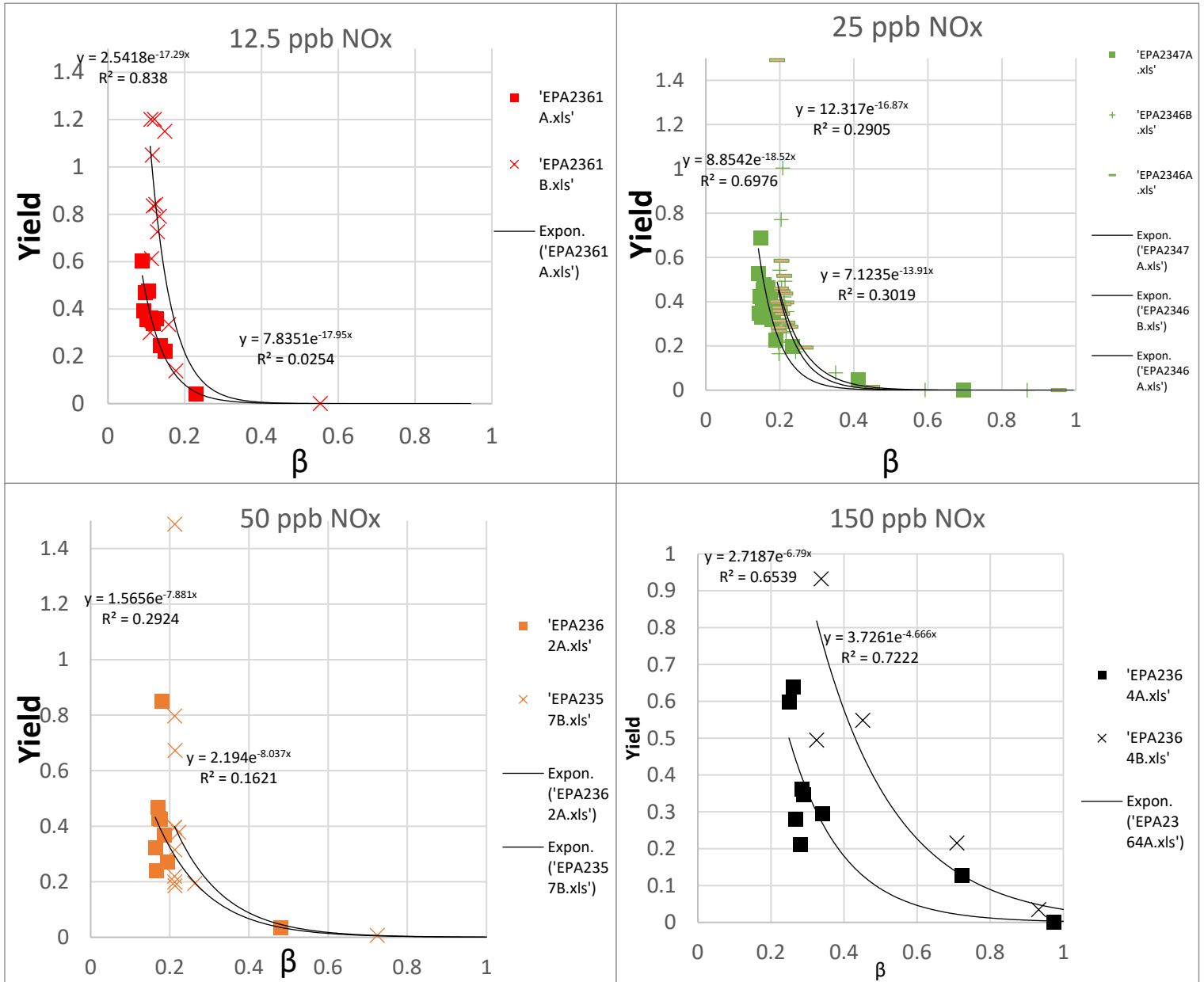


Figure 13. Instantaneous yield vs branching ratio

3.3 Continuous NO injection:

In **Figure 14**, NO_x concentration increased continuously throughout the experiment when NO was injected continuously and the total amount of injected NO_x was around 50 ppb. The SOA and ozone output was compared with previous classic experiments with similar initial concentrations of SOA precursor, oxidation

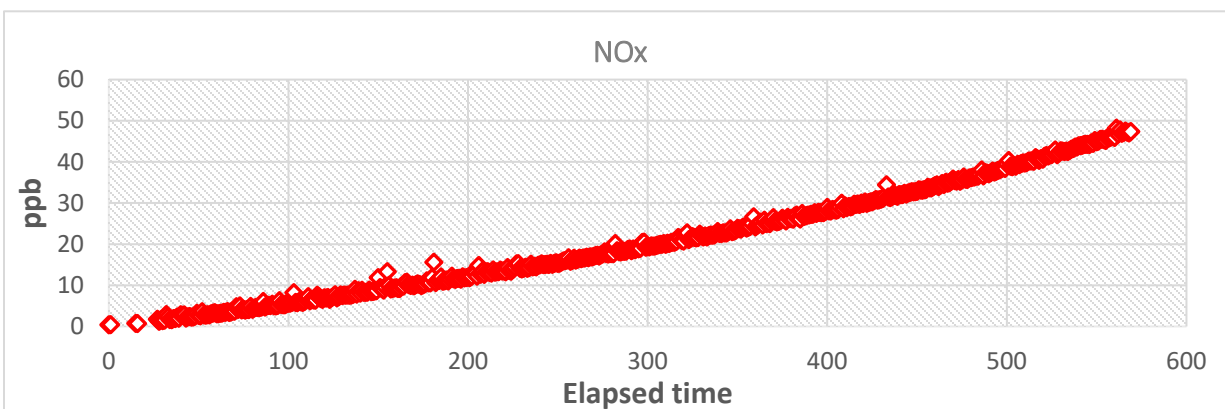


Figure 14. NO_x concentration throughout the experiment

conditions as well as total NO_x concentrations.

Figure 15 shows the SOA formation along with NO_x concentration throughout the whole experiment. As it is shown in this graph, final SOA formation and yield increased when NO was injected continuously. The ozone graph shows that ozone formation rate was different but finalized at the similar level from continuous NO injection experiment.

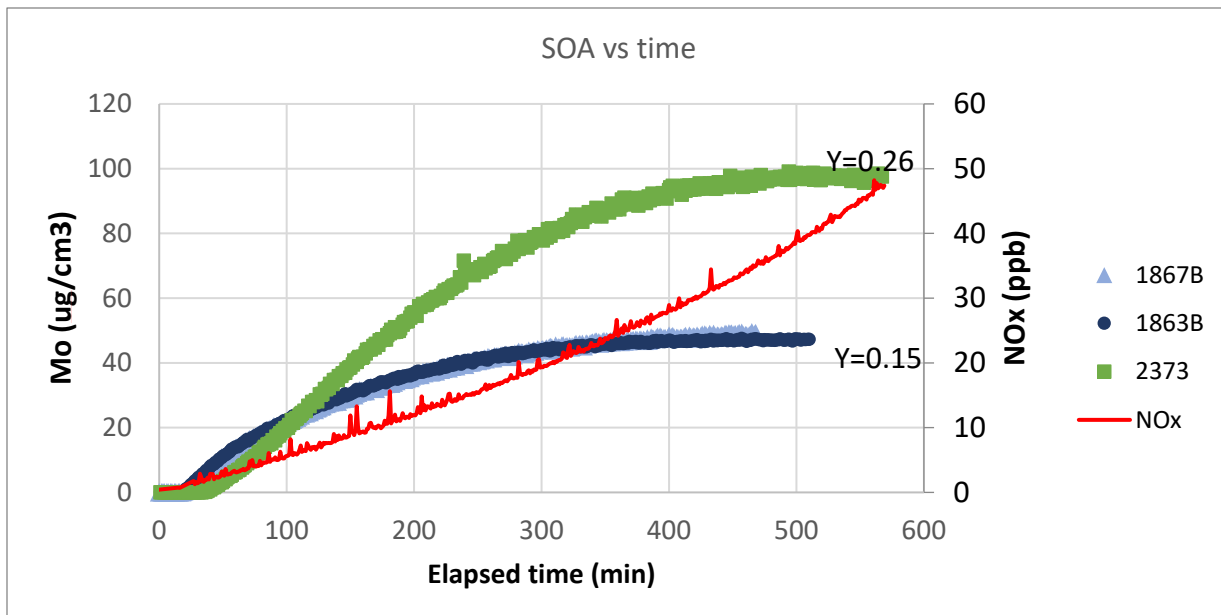


Figure 15. SOA formation throughout the experiment

Figure 16 shows the ozone formation for the continuous NO_x experiment (2373) and the instantaneous NO_x injection experiments (1863B and 1867B). Ozone formation rates are observed to be considerably different with ozone rapidly increasing for the experiment with NO_x injected

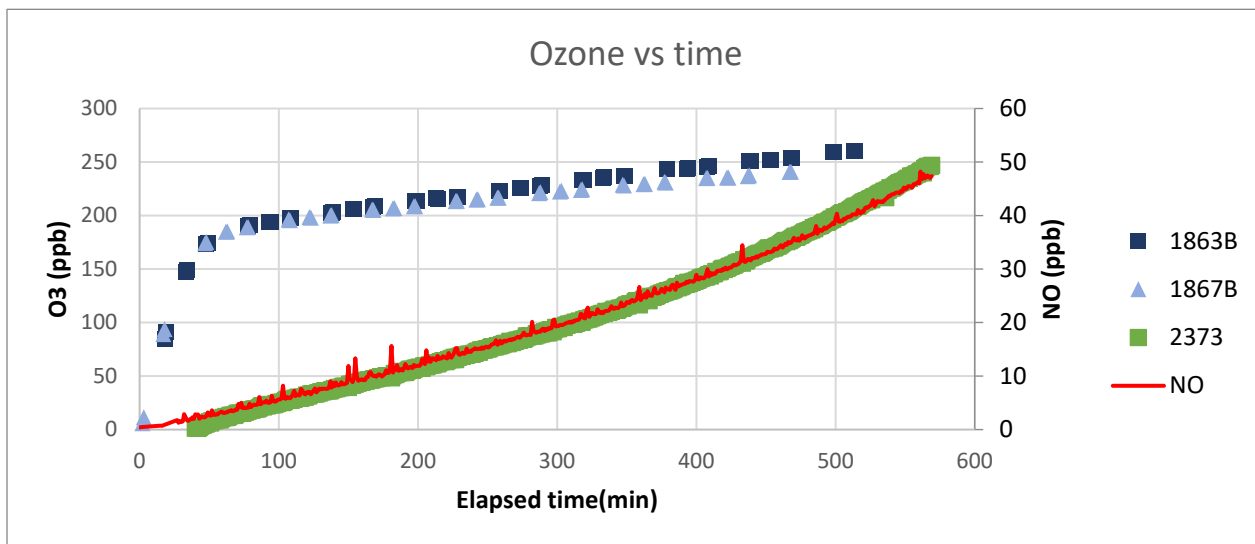


Figure 16: Ozone formation throughout the course of the experiment

only at the start of the experiment versus the slow, continuous increase of ozone observed for the experiment with NO_x continuously injected thru the duration of the experiment.

4.0 Experiment design: Experimental control of β

To further explore the effect of NO_x on SOA formation it was determined that the ideal approach would be to control the NO_x branching ratio and explore the SOA formation from these experiments. To achieve a fixed β experimental scenario, the continuous NO injection method described above was utilized combined with SAPRC-11 modelling (instead of one-time injection at beginning for traditional chamber experiments). We varied the NO injection rate and H₂O₂ (OH and HO₂ radical source) concentration to achieve desired branching ratios. Some experiments were designed for fixed β throughout while other experiments were designed to alter the β at various stages of the experiment. Sample experiment design sets with different branching ratio are shown in **Figure 17**.

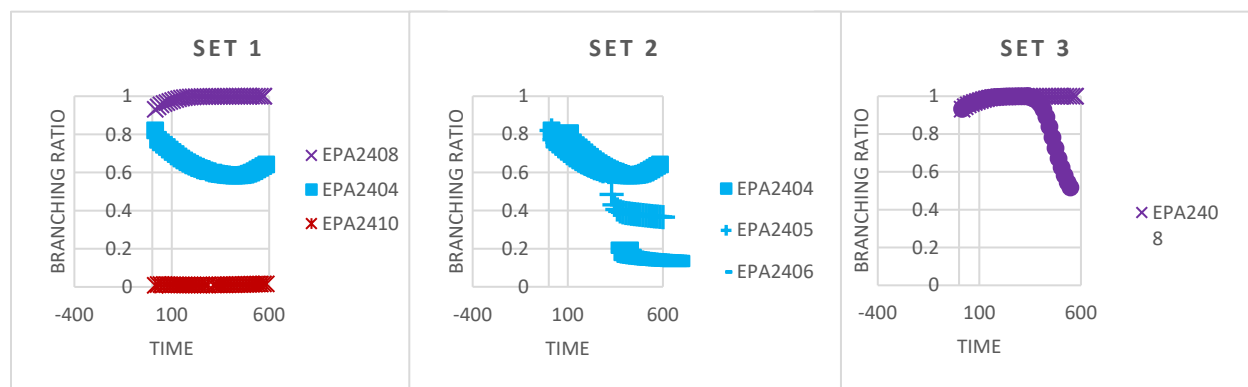


Figure 17 Modelled branching ratios from three sets of experiments

Set 1: The branching ratio was controlled at 0, 0.6 and 1 for this set of experiments. Large difference was observed between runs with $\beta=0$ and $\beta=1$. 100% more SOA formation was seen when the branching ratio is 0 compared to the run with $\beta=1$, indicating SOA formation in chamber was favored when the reaction is forced to RO_2+HO_2 pathway. This observation is corresponding to previous chamber study finding: less SOA formation was formed from aromatic hydrocarbons in higher initial NO_x condition. However, Initial NO_x condition is a less representative term compared to branching ratio since it fails to represent the real-time NO_x condition. Similar SOA formation was seen for runs with $\beta=0$ and $\beta=0.6$ where slightly different (20%) initial m-xylene was injected. We also investigated SOA yield, shown in **Figure 18** below. SOA

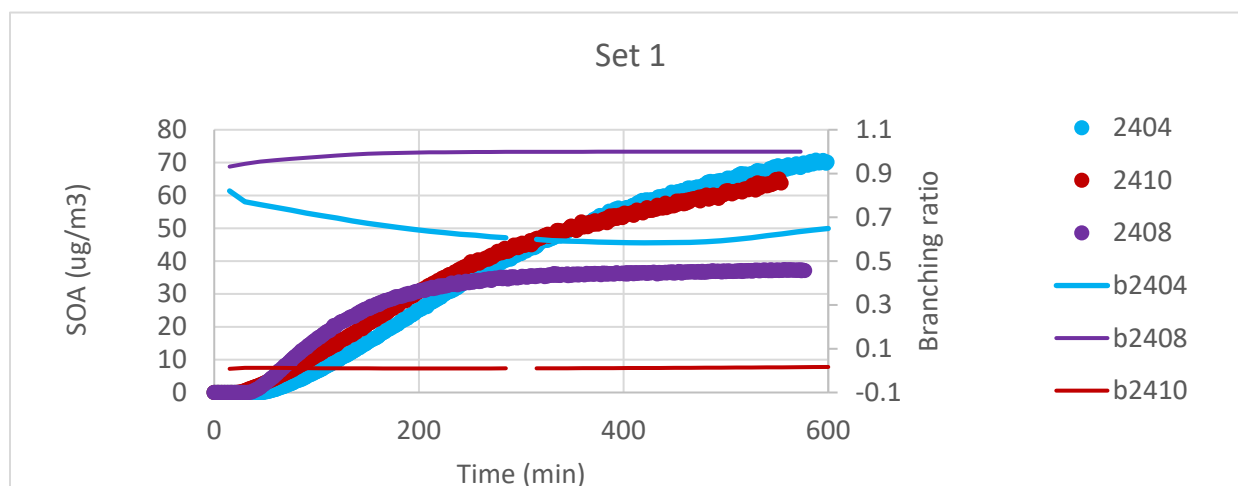


Figure 18 SOA formation and modelled branching ratio of set #1

yield decreased as branching ratio increased, indicating that SOA yield might be slowed down or inhibited as RO_2 moves more to RO_2+NO . The decay of m-xylene (**Figure 19**) is shown with m-xylene being consumed faster when branching ratio is higher. **Thus, the increase of branching ratio increased the decay rate of SOA precursor but decreased the SOA yield (Figure 20).** However, OH radical level

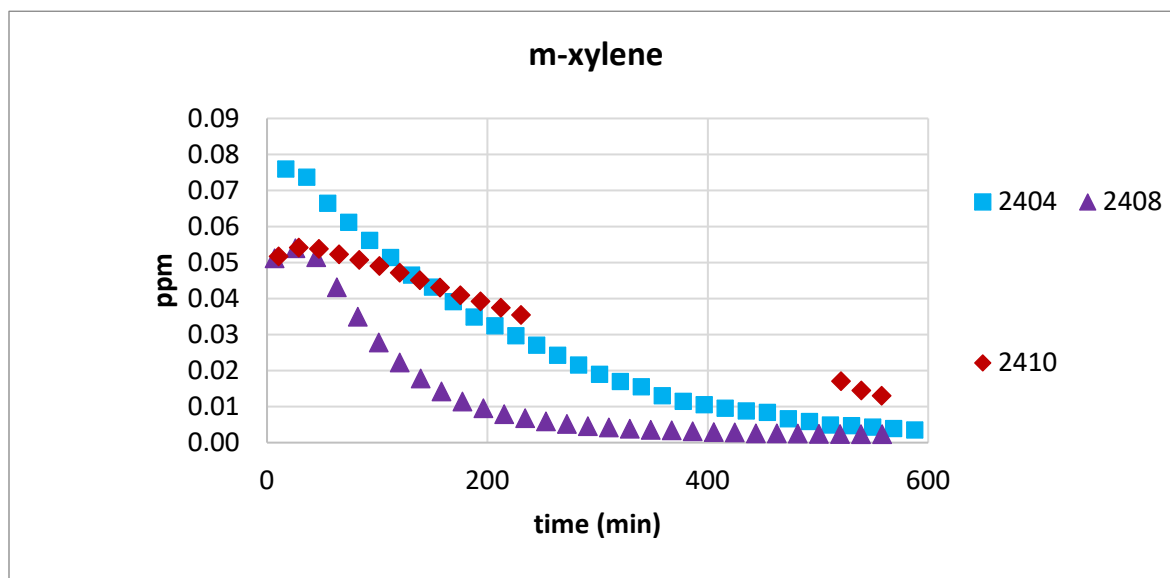


Figure 19 *m*-xylene concentration of set #1 runs

(Figure 21) also affects SOA formation because it directly participates in the photo-oxidation of *m*-xylene.

When focusing OH concentrations and SOA yield, run ($\beta=0.6$) had similar OH levels with run ($\beta=0$) while its SOA yield is only 50% of the other one, indicating branching ratio has more important effects on SOA

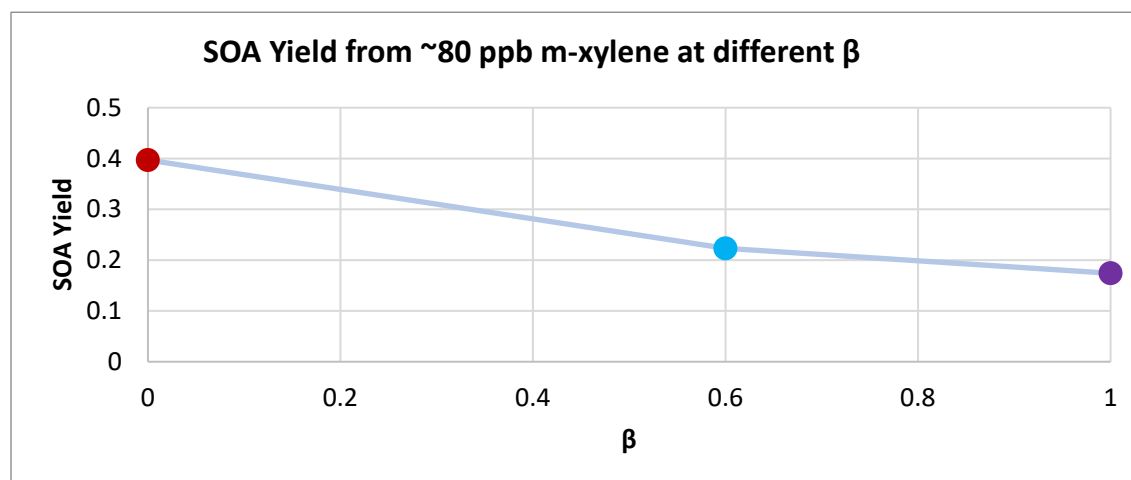


Figure 20 SOA yield at different branching ratios

yield than OH radical.

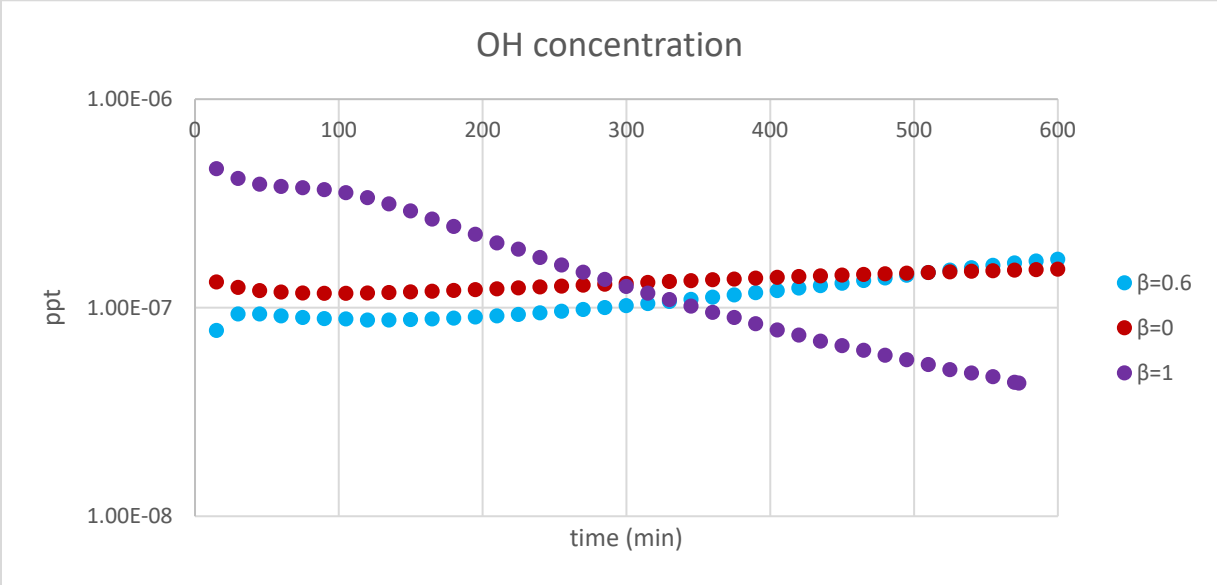


Figure 21 modelled OH concentrations of set #1 runs

Set 2: In this set of experiments, branching ratio was maintained constantly at about 0.6 at the first 300 minutes and then changed to 0.15 or 0.4 or kept constant in the second 300 minutes (Figure 22). We saw

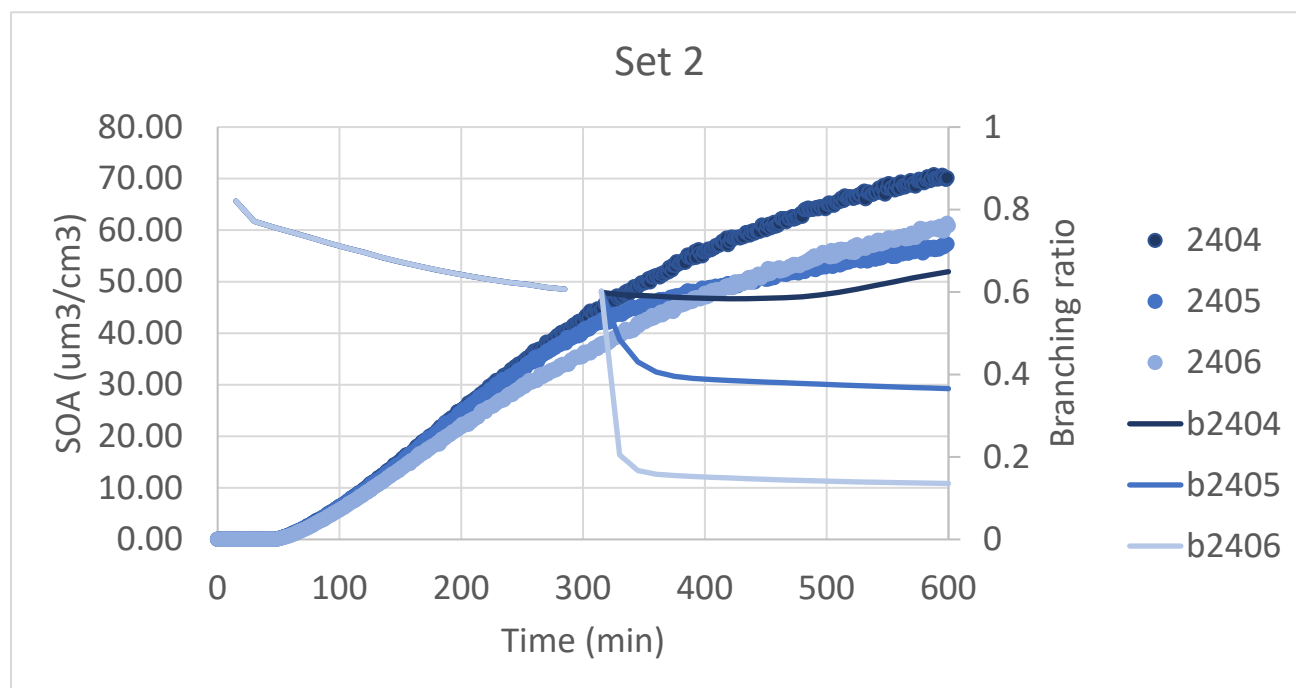


Figure 22 SOA formation and modelled branching ratio of set #2 runs

similar SOA formation from these three experiments even though the branching ratio (**Figure 22**) and OH level (**Figure 23**) were different for the second half of the experiment. About 25% *m*-xylene was left when branching ratio was changed during experiment. No obvious difference on the decay rate of unconsumed *m*-xylene was seen (**Figure 24**) and final SOA yield decreased slightly with the increase of β (**Figure 25**). This could be caused by that the amount 25% *m*-xylene was not large enough to make a difference on final SOA formation.

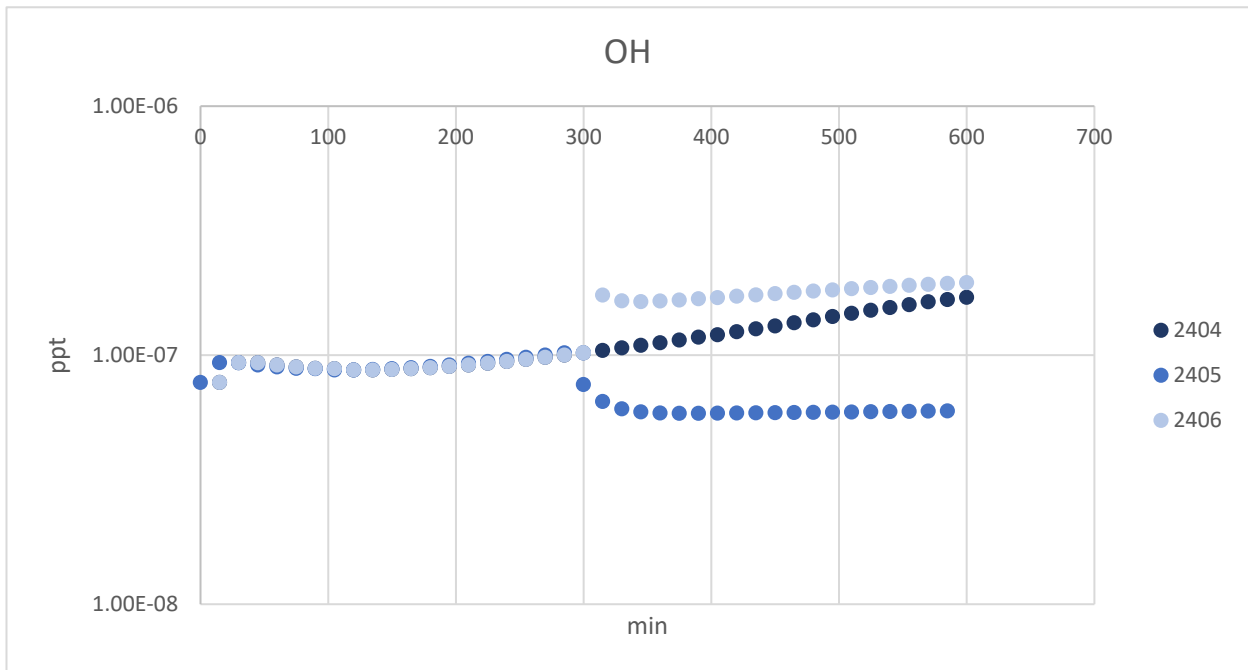


Figure 23 modelled OH concentration of set #2 runs

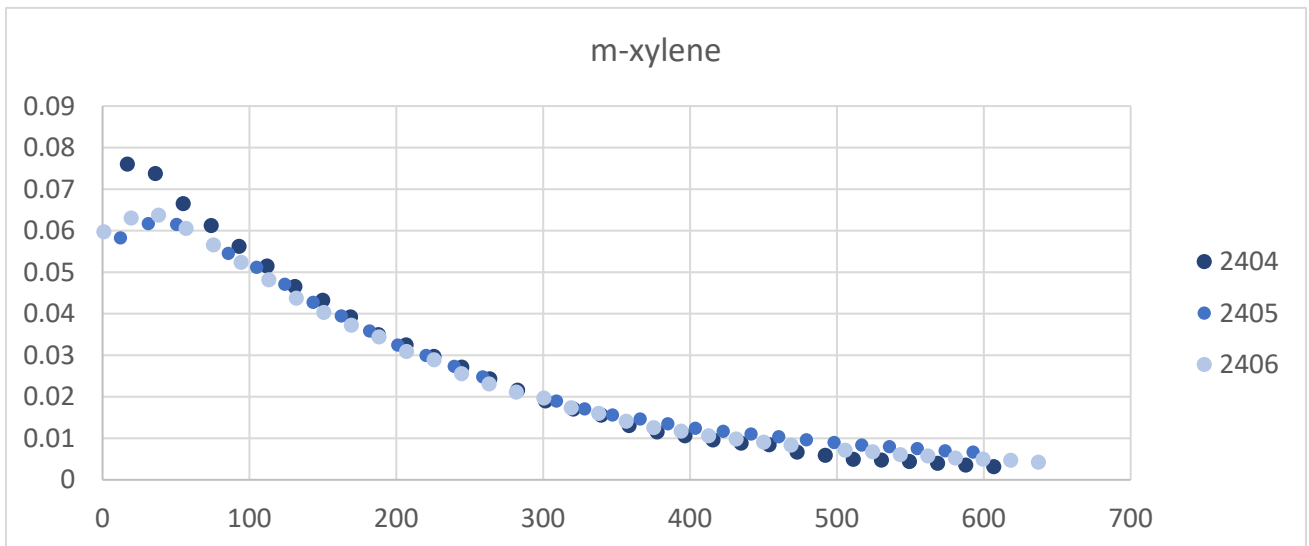


Figure 24 m-xylene concentration of set #2 runs

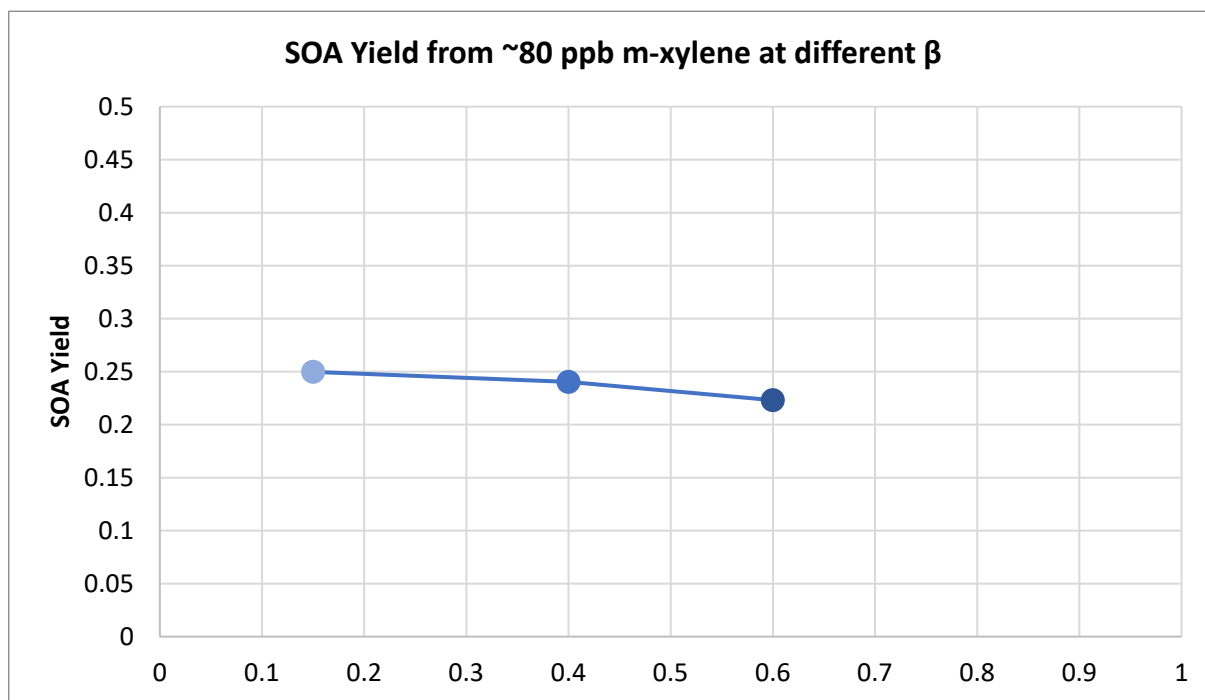


Figure 25 SOA yield at different branching ratios

Set 3: In this set, branching ratio (**Figure 26**) was changed from 1 to lower and an increase on SOA mass was observed when dropping. However, less than 10% *m*-xylene was left when changing branching ratio

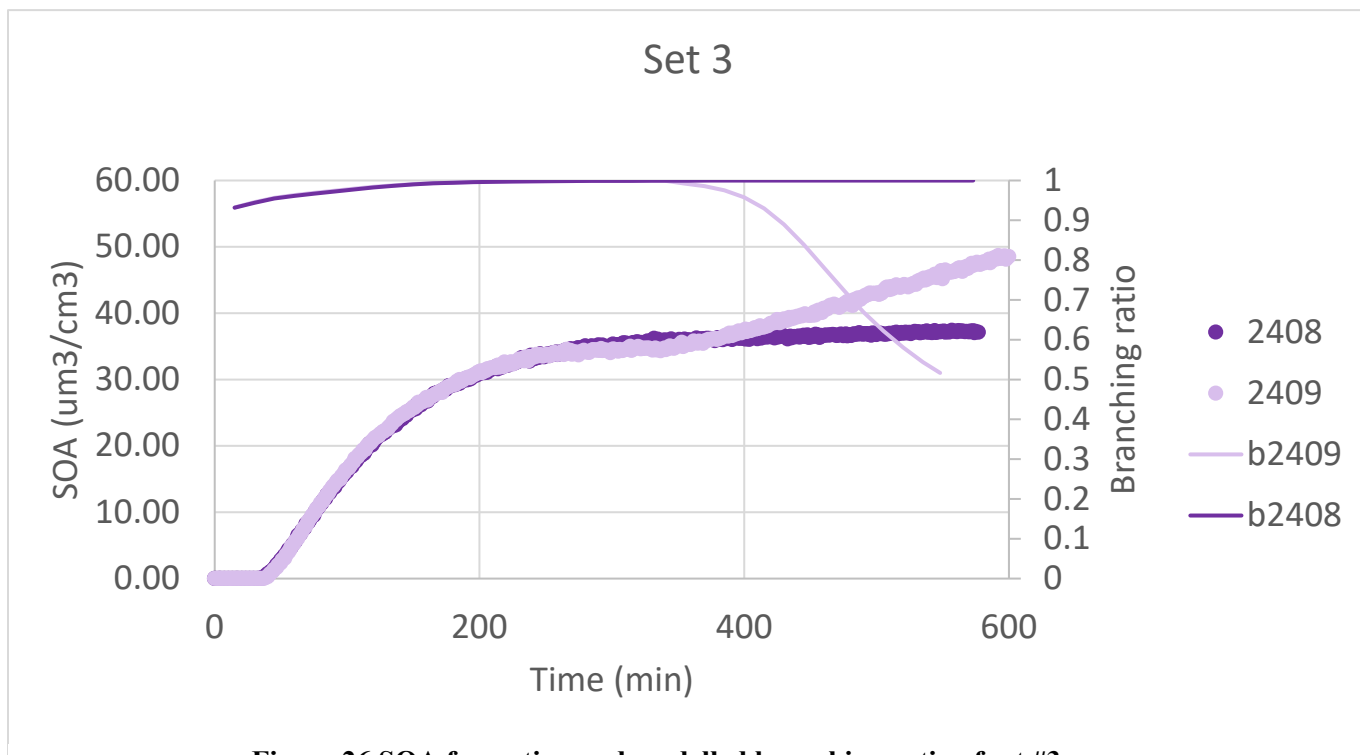


Figure 26 SOA formation and modelled branching ratio of set #3 runs

due to the fast reaction rate of *m*-xylene when β is equal to 1 (**Figure 27**). The higher SOA mass could be formed by the oxidation of *m*-xylene product. A difference in the volatility of the SOA (**Figure 28**) generated SOA was seen in the second half of the experiment. The volatility decreased with lower branching ratio, indicating different composition of SOA.

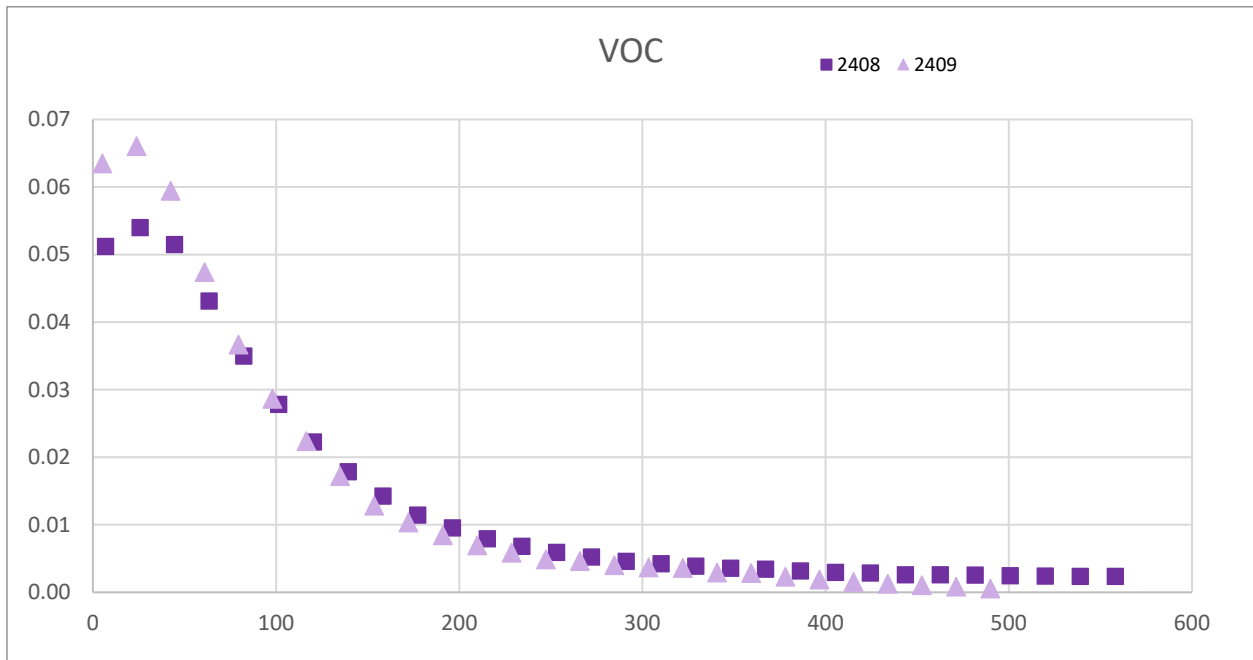


Figure 27 *m*-xylene concentration of set #3 runs

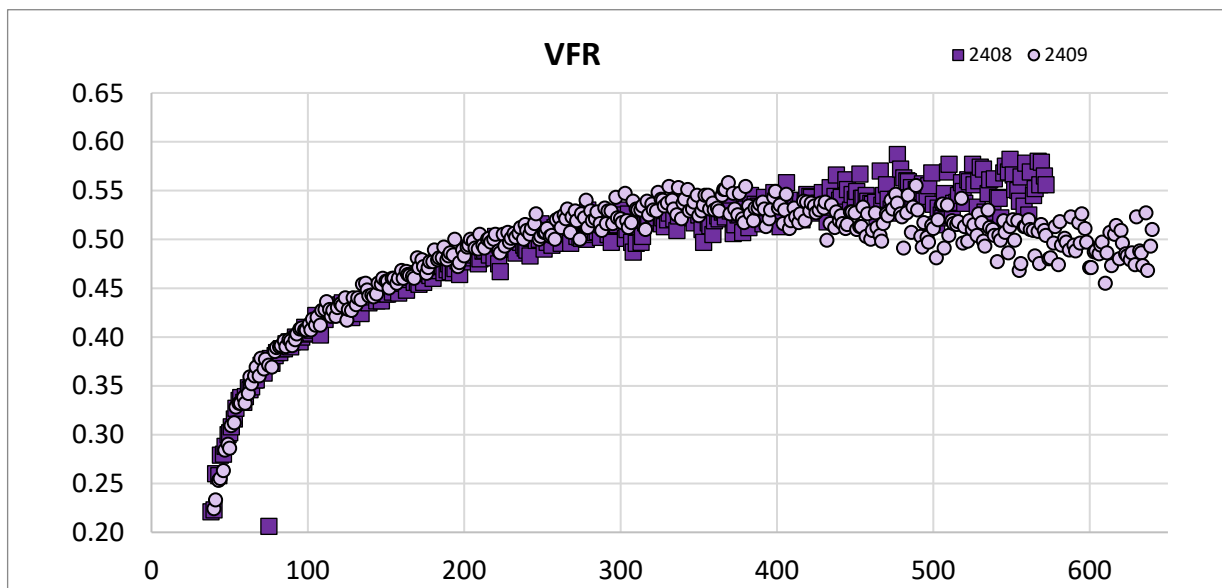


Figure 28 volume fraction remaining of SOA from *m*-xylene at different branching ratios

Based off results shown above, the decay rate of SOA precursor (*m*-xylene) increased and SOA formation potential decreased as the branching ratio increased. The decrease of branching ratio does not necessary increase final SOA formation in chamber unless same amount of *m*-xylene is consumed, which potentially takes longer time since *m*-xylene reacts slower at lower branching ratio. OH radical also affects the oxidation of *m*-xylene, so it needs to be maintained at constant level when using different branching ratios to eliminate its effect. In addition, branching ratio needs to be varied at different times (different *m*-xylene concentration) to investigate its effects on SOA precursor consumption and yield. Mass loading effects should also be considered in the future experiments by using different amounts of initial SOA precursor. Last but not least, *m*-xylene oxidation products are also SOA precursors and they should be studied in chamber to study the secondary products and the mechanism of aromatic photo-oxidation.

5.0 Further investigation into branching ratios – blending experiment with model observations of β

Having optimized approaches to evaluate changes in SOA formation under various NO_x regimes, the next step was to look at GEOS-CHEM to identify the most relevant β values to study. Global branching ratio was simulated from a global 3-D model of atmospheric chemistry driven by meteorological input from the Goddard Earth Observing System (GEOS-Chem) based on NO and HO₂ concentrations. It was categorized into four scenarios: ‘long’, ‘short’, ‘high’ and ‘low’. ‘Long’ represents highest branching ratio and maintains at high level (0.6-0.9) from 5am to 8pm during a day, mostly locating at highly populated area including North America, Europe and East China. ‘Short’ and ‘high’ represent similar medium level branching ratio (0.4-0.6) while ‘short’ maintains the level from 6am to 7 pm and ‘high’ maintains during 24 hours of a day. ‘Short’ represents ocean areas in the Northern Hemisphere and Continents in the Southern Hemisphere and ‘high’ represents area close to the North Pole. ‘Low’ represents lowest branching ratio and maintains at 0-0.25 from 5 am to 8 pm, locating at ocean area in the Southern Hemisphere.

Cluster locations (July)

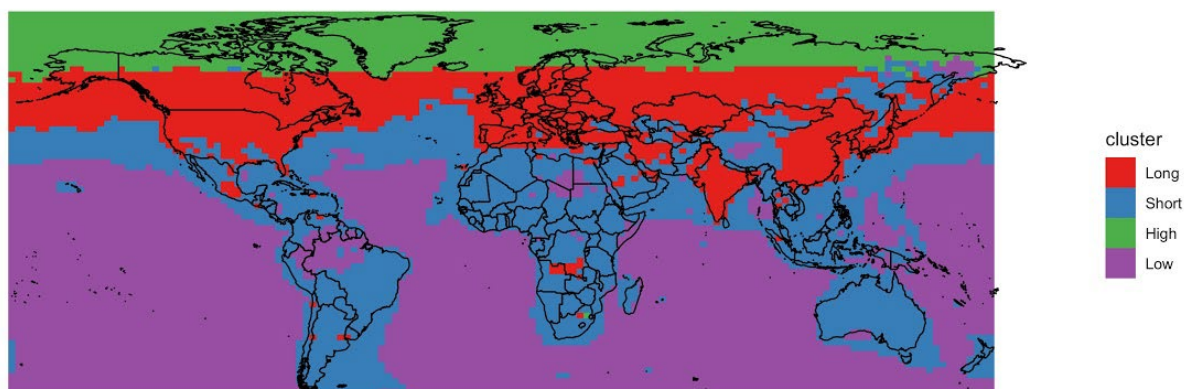


Figure 29. Four global branching ratio scenarios (Provided by William Porter)

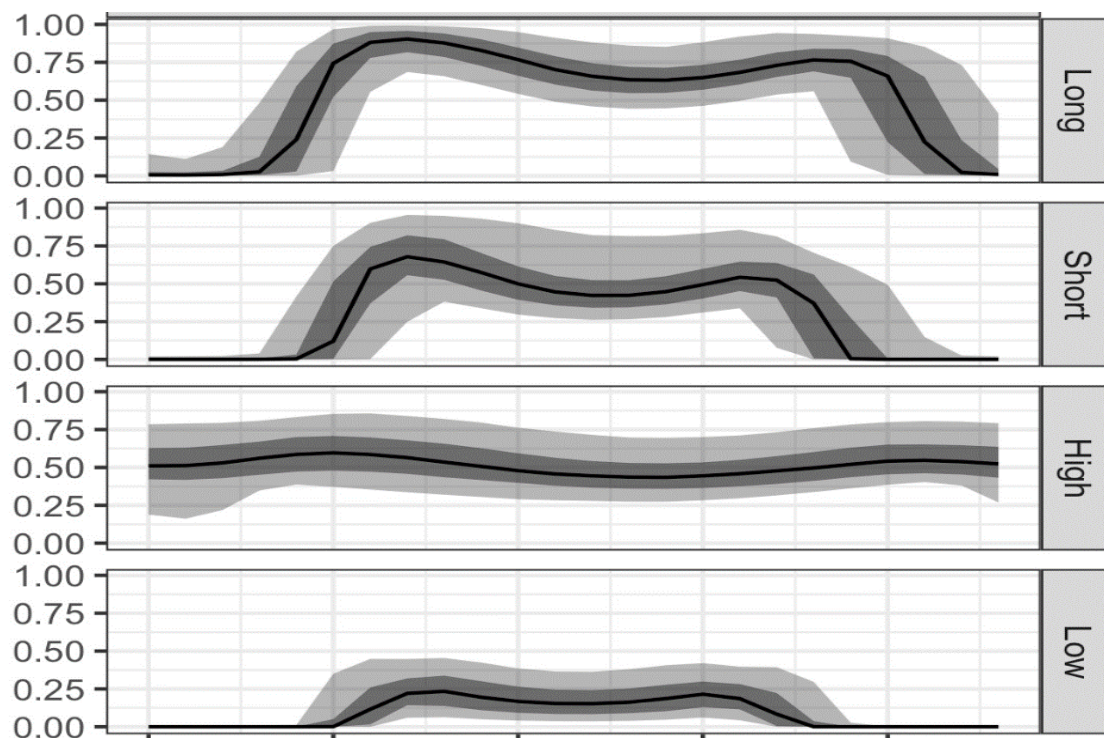


Figure 30. Branching ratio profile during a day of four scenarios. (Peng *et al.*, 2022)

Next, fixed β experiments were conducted to best simulate the long, short, high, and low scenarios emerging from GEOS-CHEM for *m*-xylene and α -pinene. SOA (Mo) was calculated using wall-loss corrected particle volume and measured particle density. The plotted the real-time Mo versus

consumed *m*-xylene (Figure 31) and α -pinene (Figure 33) as well as yield (Y) versus Mo (*m*-xylene, Figure 32 and α -pinene, Figure 34). Different branching ratios were colored differently: long (red), high (green), short (blue) and low (purple). The slope of “Mo vs HC” represents the amount of SOA formation from the specific amount of precursor consumption, which is also defined as instantaneous yield (Y_i). For *m*-xylene experiment, SOA formation is the highest at lowest branching ratio at the beginning of experiment; medium branching ratio forms highest SOA as more *m*-xylene was consumed. As *m*-xylene was further consumed, SOA formation of highest branching ratio became the highest. For α -pinene, similar trend was observed at lower HC consumption; however, highest SOA formation occurs at medium branching ratio as more α -pinene is consumed. SOA formation and yield data was used to calculate VBS parameters and VBS fitted curve (Y vs Mo) will be discussed in the following session.

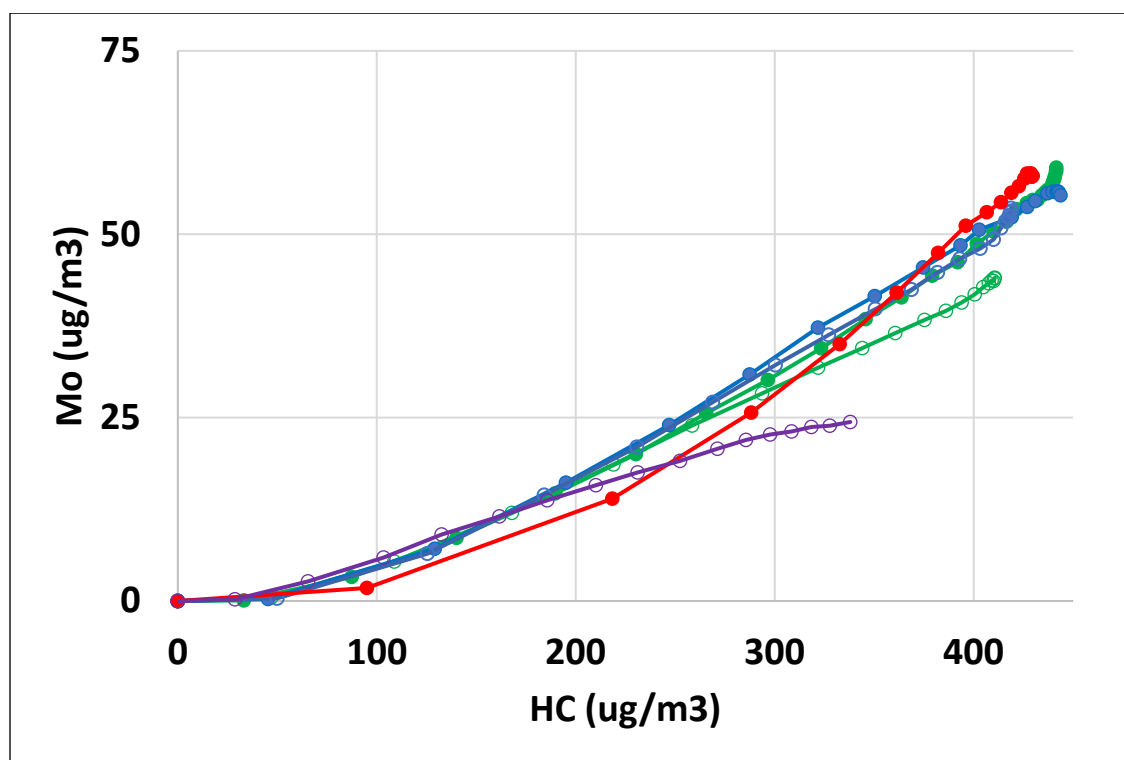


Figure 31 SOA(Mo) vs *m*-xylene consumption at different branching ratios

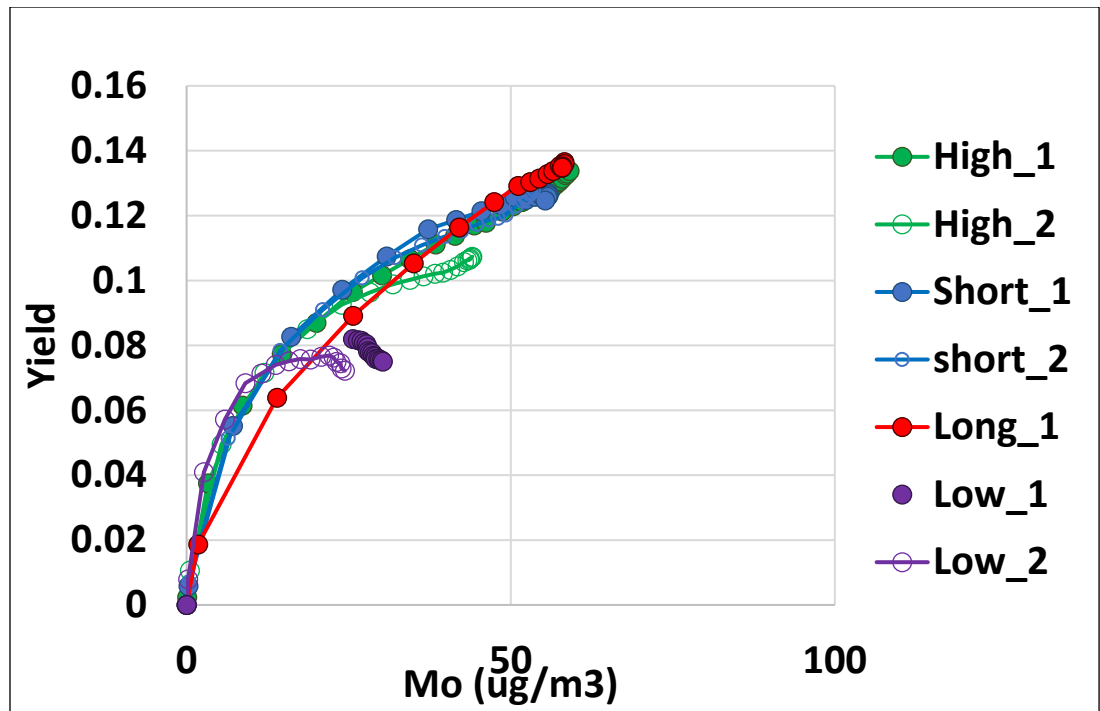


Figure 32 SOA yield vs Mo from *m*-xylene at different branching ratios

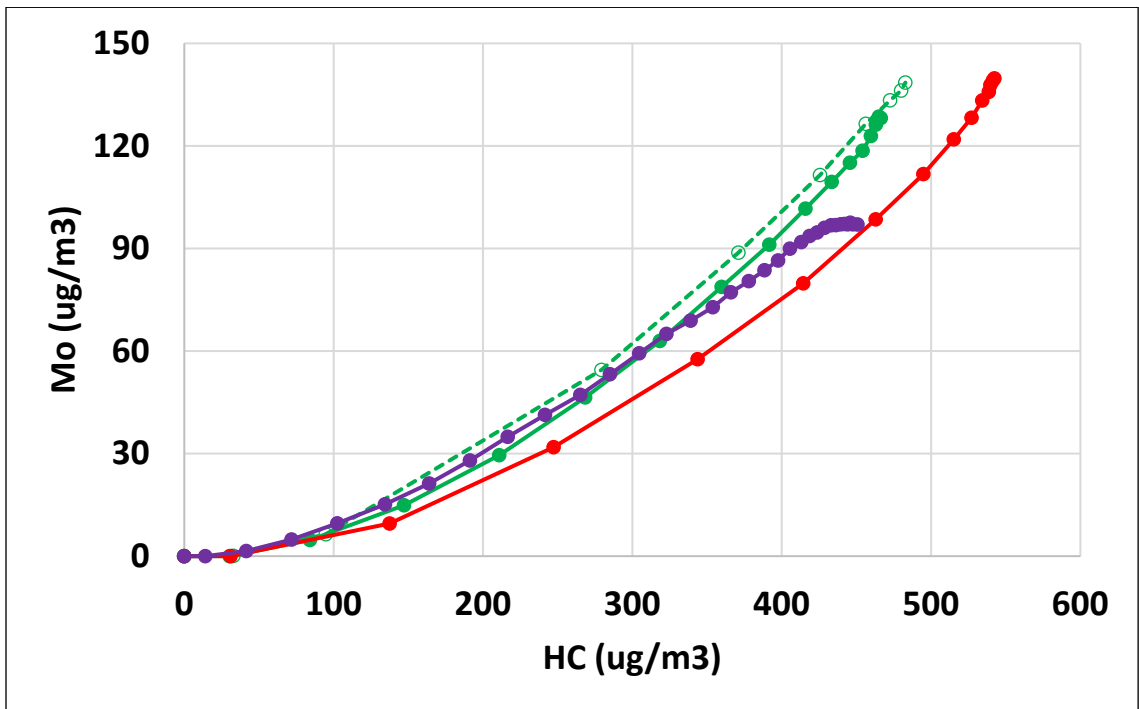


Figure 33 SOA(Mo) vs α -pinene consumption at different branching ratios

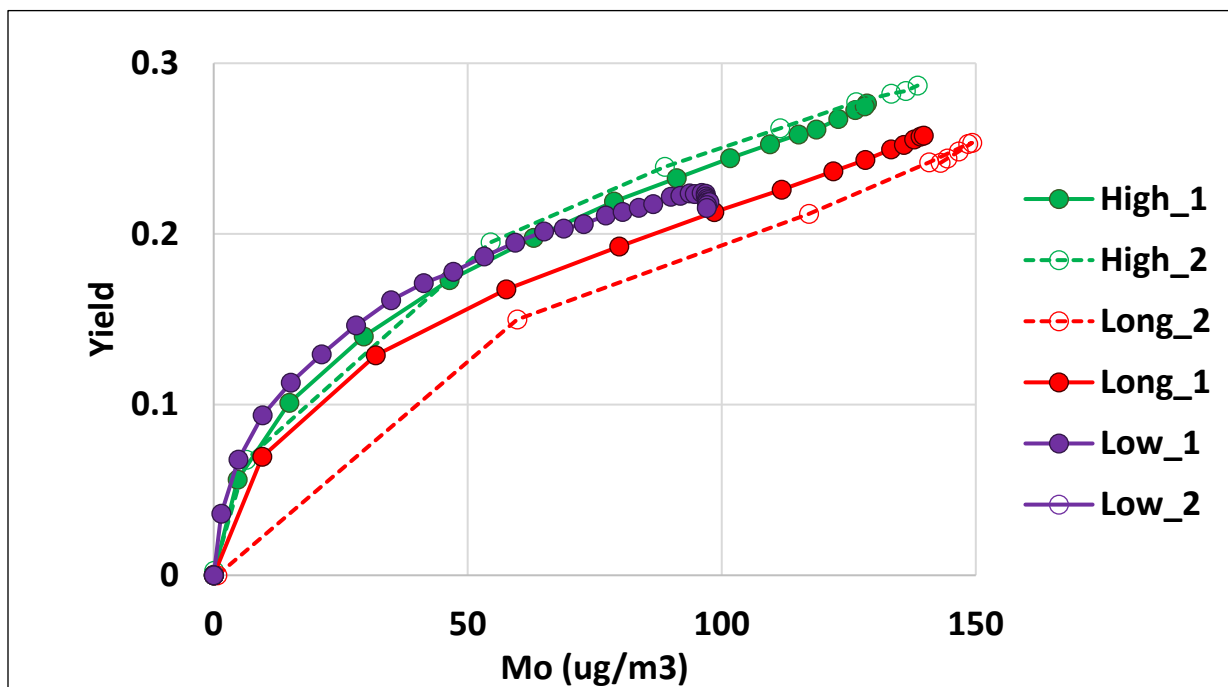


Figure 34 SOA yield vs Mo from α -pinene at different branching ratios

The Volatility Basis Set (Donahue *et al.*, 2006) is used for SOA prediction using GEOS-CHEM. Therefore, VBS (assuming four products c^* : 0.1, 1, 10, 100 $\mu\text{g}/\text{m}^3$) parameters were calculated (Table 5 & 6) for both *m*-xylene and α -pinene. The fitted Y vs Mo curves using the VBS parameters are shown in Figure 35 and Figure 36 for *m*-xylene and α -pinene, respectively.

SOA yield from *m*-xylene presents a different trends at different Mo. When Mo is lower, SOA yield increases as branching ratio decreases; however, an opposite trend was observed when Mo is higher. This is in the opposite to previous studies where higher SOA yield was consistently observed at lower NO_x conditions, while this is based on tradition experiments only considering initial NO_x conditions of every experiments. However, our experiments simulate branching ratio by consistently injecting NO_x which is more related to real atmosphere. For α -pinene, medium

branching ratio has the highest SOA yield while the yield from highest and lowest branching ratio is similar and lower than that of medium branching ratio.

Table 5 VBS parameters for *m*-xylene at three branching ratios

β	C^* ($\mu\text{g}/\text{m}^3$)			
	0.1	1	10	100
high	0.000	0.031	0.041	0.172
long	0.000	0.025	0.000	0.291
low	0.000	0.048	0.046	0.000

Table 6 VBS parameters for α -pinene at three branching ratios

β	C^* ($\mu\text{g}/\text{m}^3$)			
	0.1	1	10	100
high	0.000	0.048	0.000	0.401
long	0.000	0.018	0.021	0.359
low	0.035	0.000	0.000	0.373

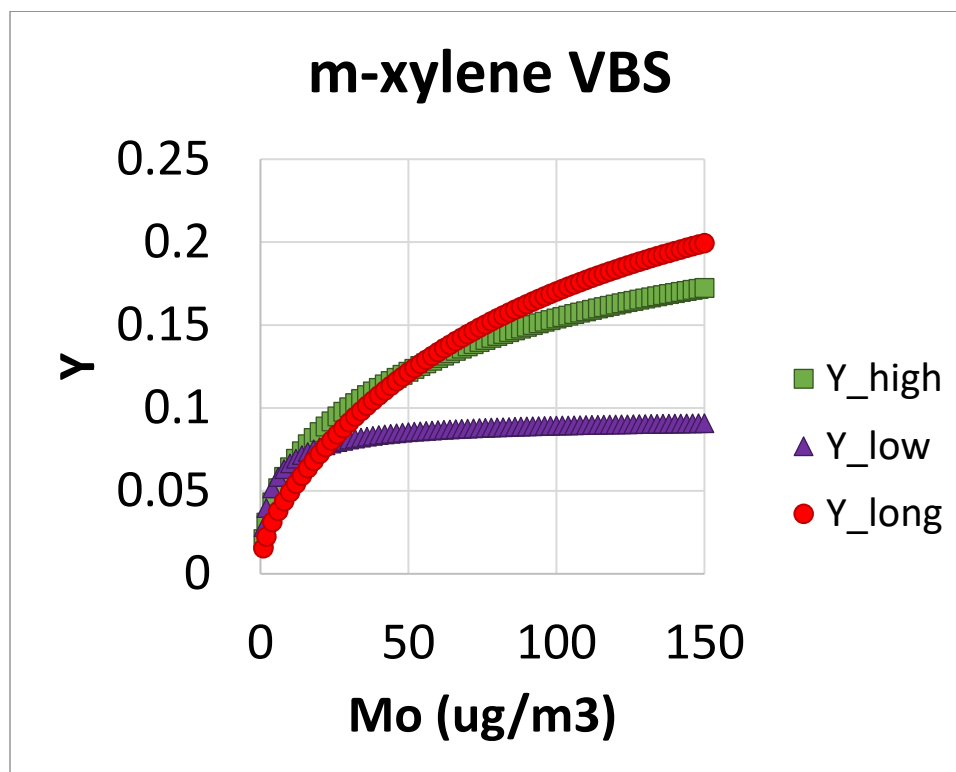


Figure 35 VBS fitted yield vs Mo from *m*-xylene

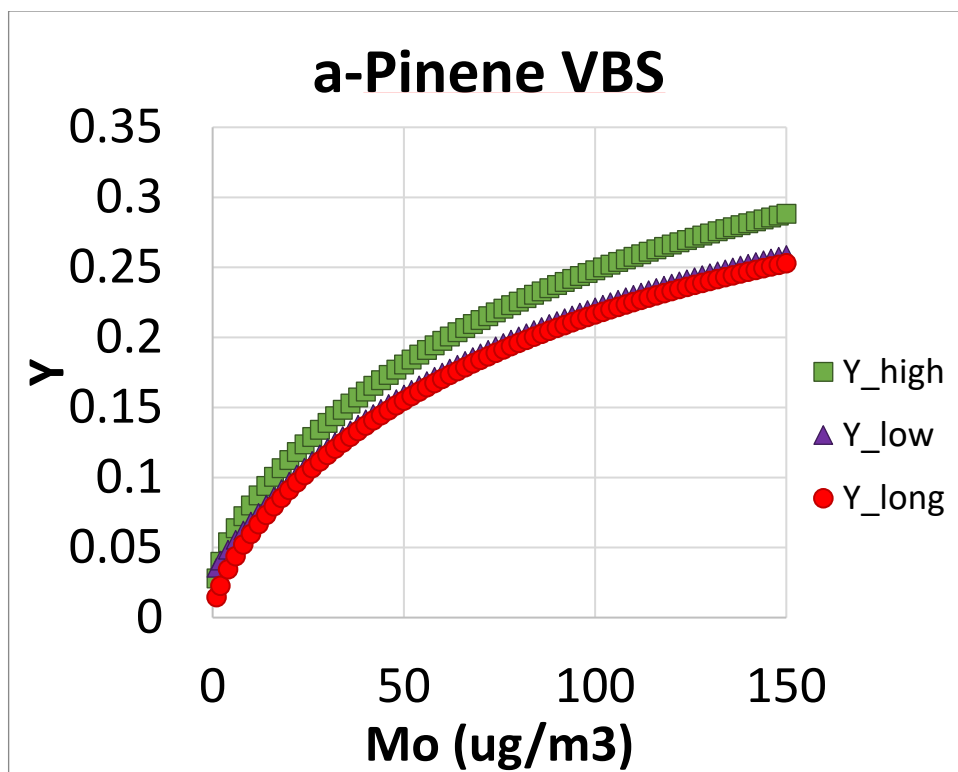


Figure 36 VBS fitted yield vs Mo from α -pinene

Summary: Current chemical transport models generally use a constant secondary organic aerosol (SOA) yield to represent SOA formation from aromatic compounds under low NO_x conditions. However, a wide range of SOA yields (10% to 42%) from *m*-xylene under low NO_x conditions is observed in this study. The chamber HO_2/RO_2 ratio is identified as a key factor explaining SOA yield variability: higher SOA yields are observed for runs with a higher HO_2/RO_2 ratio. The RO_2+RO_2 pathway, which can be increasingly significant under low NO_x conditions, shows a lower SOA forming potential compared to the RO_2+HO_2 pathway, reducing overall yields when other more efficient formation pathways are limited. While the traditional low- NO_x chamber experiments are commonly used to represent the RO_2+HO_2 pathway, this study find that the impacts of the RO_2+RO_2 pathway cannot be ignored in certain conditions. We provide guidance

on how to best control for these two pathways in conducting chamber experiments to best obtain SOA yield curves and quantify the contributions from each pathway. On the global scale, the chemical transport model GEOS-Chem is used to identify regions characterized by lower surface HO₂/RO₂ ratios, suggesting that the RO₂+RO₂ pathway is more likely to prove significant to overall SOA yields in those regions. Current models generally do not consider the RO₂+RO₂ impacts on aromatic SOA formation, but preliminary sensitivity tests with updated SOA yield parameters based on such pathway suggest that without this consideration some types of SOA may be overestimated in regions with lower HO₂/RO₂ ratios.

The work of the section above has been published in further detail in Peng et al., 2022.

6.0 Use of historical UCR chamber data to further explore

SOA as a function of β

Historical UCR chamber data on SOA formation from *m*-xylene was used to explore the correlation between average branching ratio of classic chamber experiments and SOA formation. As part of this project we data mined more than 160 previous chamber runs at UCR/CECERT and found a clear dependence of SOA yield on branching ratio.

Figure 37 shows final SOA yield (Y) and final SOA mass (M) from 160 classic *m*-xylene chamber experiments with varied initial VOC, H₂O₂ and NO_x conditions. No obvious trend was observed in **Figure 37** because more than one factors are dominating the relationship between SOA yield and final SOA mass, such as VOC consumption and branching ratio. When applying a third variable, VOC consumption in **Figure 38**, we observed that different slope corresponds to different color, or VOC consumption. This is as expected because Y vs. M is basically M/VOC vs. M and the slope in **Figure 38** should be 1/VOC. However, for the runs with similar VOC consumption (purple points), the range of final SOA mass is 0 to 100 and the yield is 0 to 0.25. It is necessary to understand what drives this large variance. We estimated

branching ratio of RO₂+NO reaction throughout experiment using SAPRC11 mechanism for each experiment (**Figure 39**). In **Figure 40**, we applied the average branching ratio from the beginning of experiment to the time point when 80% of final mass were formed to avoid the dilution effect brought by the PM plateau period when both PM and branching ratio staying constant. We observed that runs with larger branching ratio have lower SOA mass and yield and runs with lower branching ratio have higher SOA mass and yield. This trend is more obvious when looking into the runs with similar VOC consumptions: both SOA mass and yield increased as branching ratio decreased. **Figure 40** shows the negative correlation between SOA yield and average branching ratio when VOC consumption or SOA formation were similar. A comparison of final SOA formation and total VOC consumption is shown in **Figure 41**. Runs with lower branching ratios (purple points) are on the top, followed by runs with medium branching ratio. Runs with largest branching are at the bottom. The investigation of 160 classic *m*-xylene chamber experiments shows a clear negative dependence of SOA formation on branching ratio. However, simple averaging branching ratio throughout classic chamber experiments might cause large uncertainties when deriving the relationship with yield and branching ratio due to that the branching ratio changes drastically (**Figure 42**, e.g. from 1 to 0.2) throughout the experiment. Thus, it was determined that it was important control branching ratio constantly for each run.

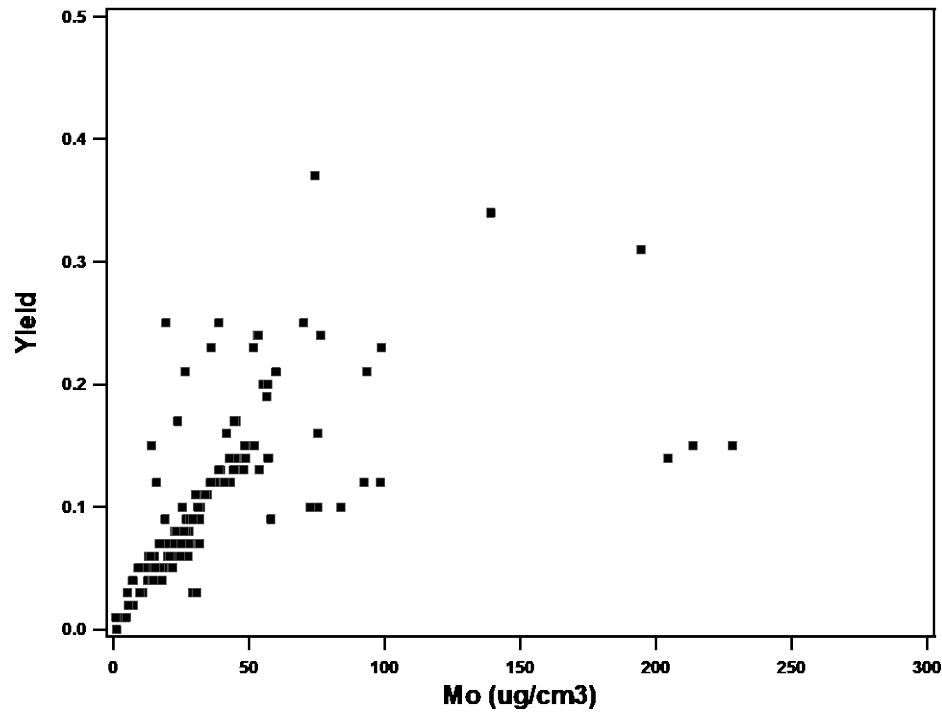


Figure 37. Final SOA yield (Y) and final SOA mass (M) from 160 classic *m*-xylene chamber experiments

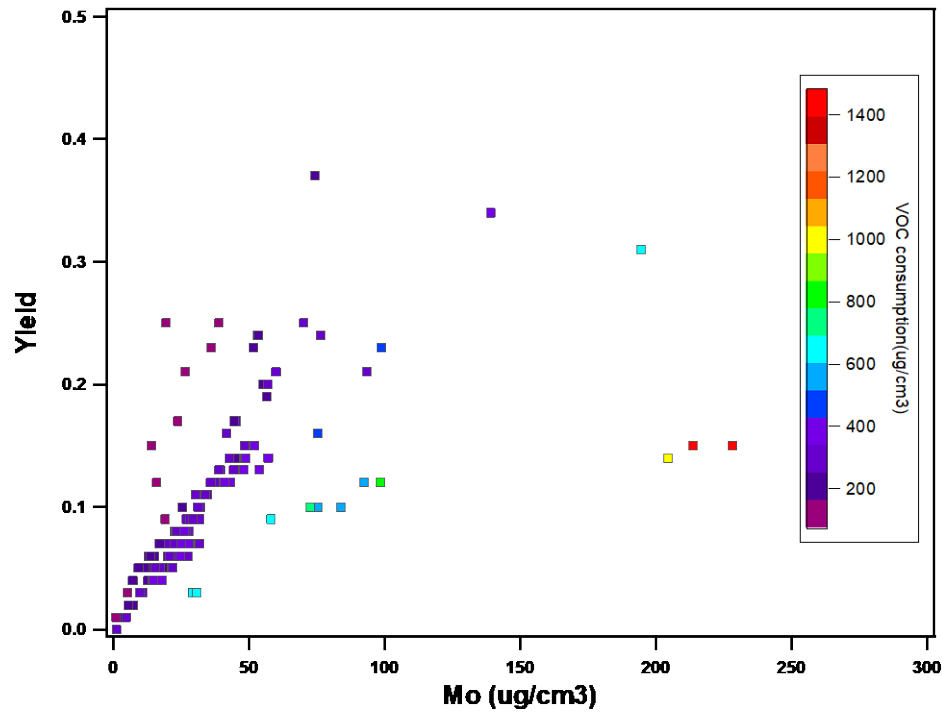


Figure 38. Final SOA yield (Y) and final SOA mass (M) from 160 classic *m*-xylene chamber experiments colored by VOC consumption.

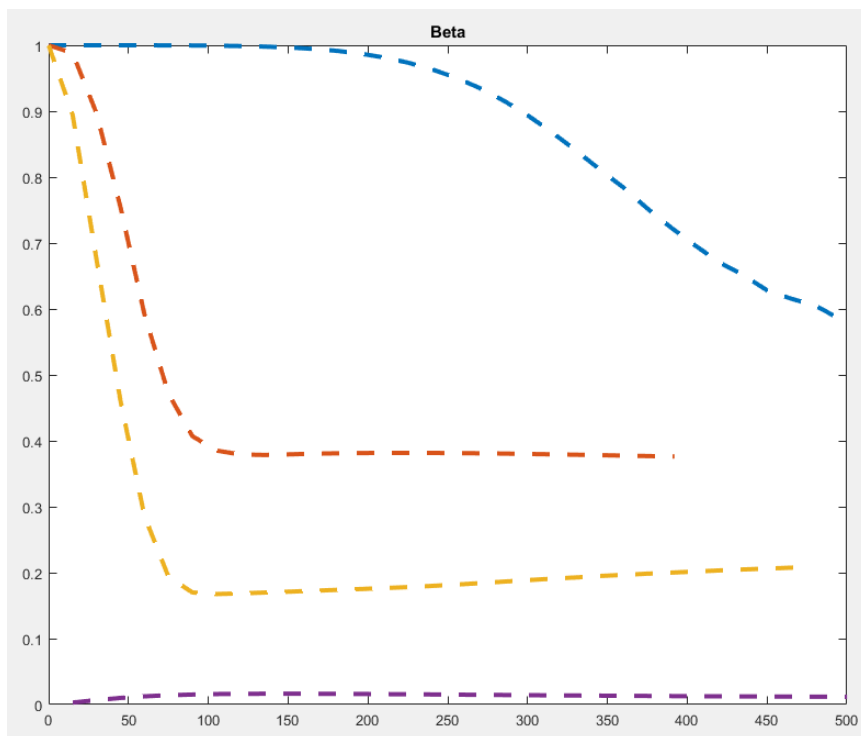


Figure 39. Typical branching ratio profiles throughout experiments.

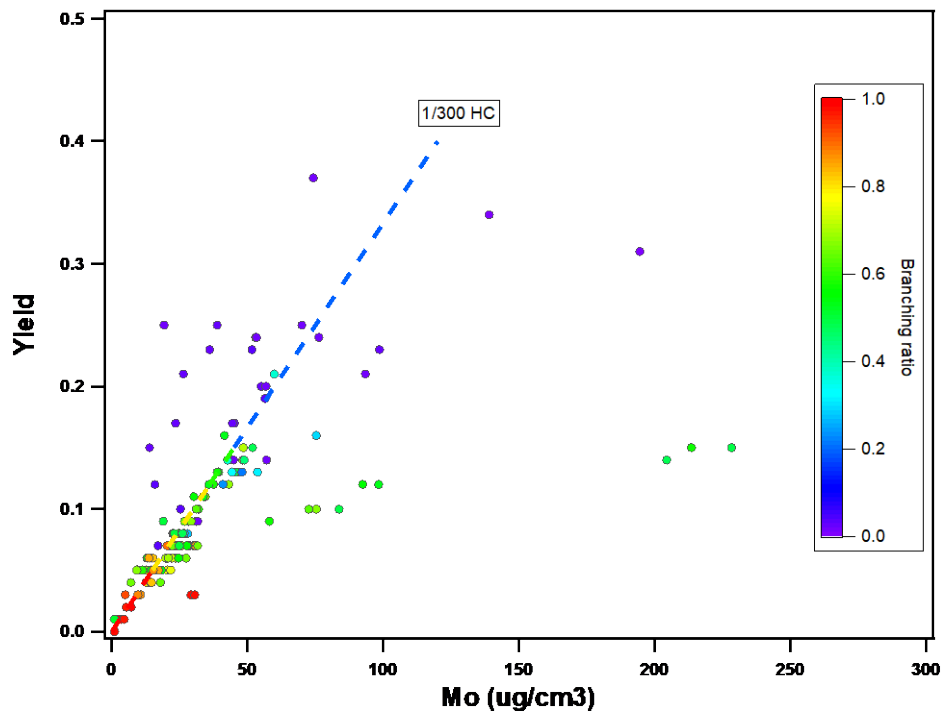


Figure 40. Final SOA yield (Y) and final SOA mass (M) from 160 classic *m*-xylene chamber experiments colored by average branching ratio.

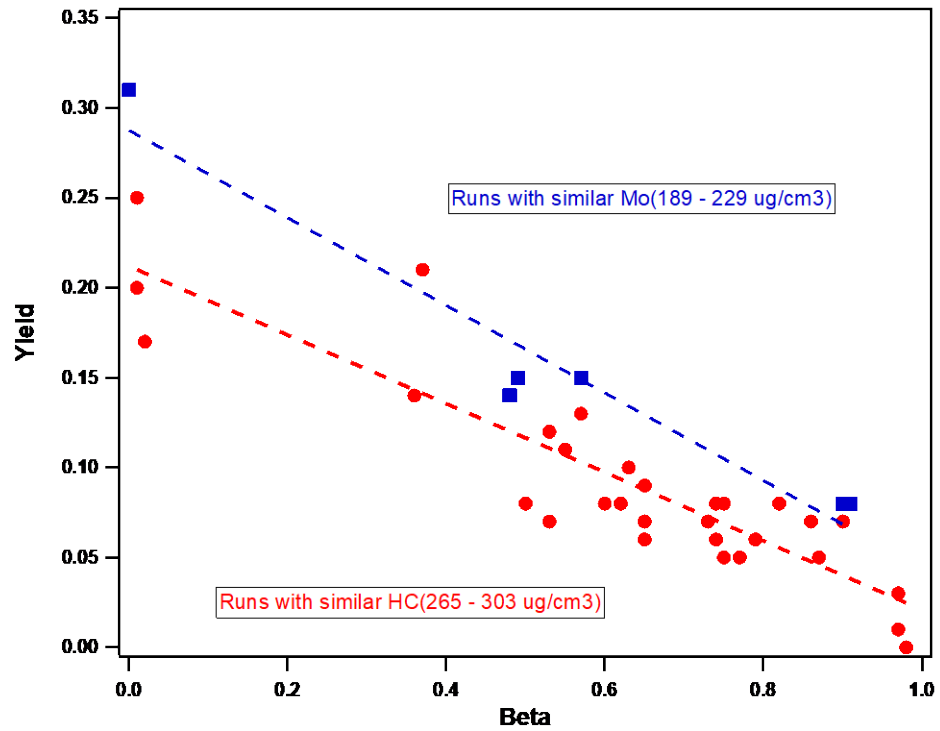


Figure 41. SOA yield vs. Beta with similar M(189-229 ug/cm³) or similar HC (265-303 ug/cm³)

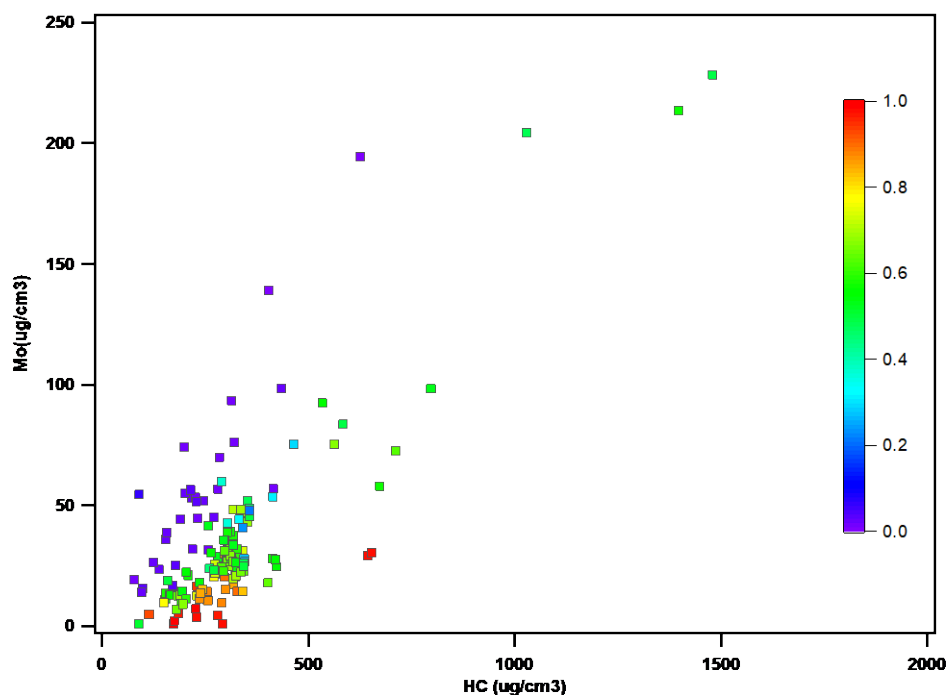


Figure 42. Final SOA mass (M) and total VOC consumption from 160 classic *m*-xylene chamber experiments colored by branching ratio.

We continuously injected NO to maintain the branching ratio at certain levels. **Figure 43** shows the branching ratio were controlled much better of four scenarios (branching ratio = 0, 0.25, 0.75 or 1) than classic chamber experiments. The comparison of measured and SAPRC11-estimated gas species including VOC, O₃, and NO_x indicates that SAPRC11 chemistry mechanism captured the gas-phase chemistry in chamber and the great confidence of branching ratio. When branching ratio was controlled at 0 and 0.25 (**Figure 44**), SOA yield from *m*-xylene were relatively constant, indicating non- or weak- dependence on absorbing materials. This is consistent with what was found previously for “low-NO_x” scenario. When branching ratio was 0.75 and 1, similar SOA yield trend was observed for these two NO_x conditions. However, currently SOA formation at branching ratio of 0.75 from *m*-xylene in GEOS-Chem model are extrapolated from two sets of SOA parameters (high- and low- NO_x conditions. Our finding that SOA yield are very similar or same at branching ratio 0.75 and 1 indicates that current method of extrapolation might

not be correct. **Table 7** shows the two-product SOA yield parameters at high- and low- NO_x conditions or branching ratio = 1 and 0 from what are used in current GEOS-Chem model and our findings.

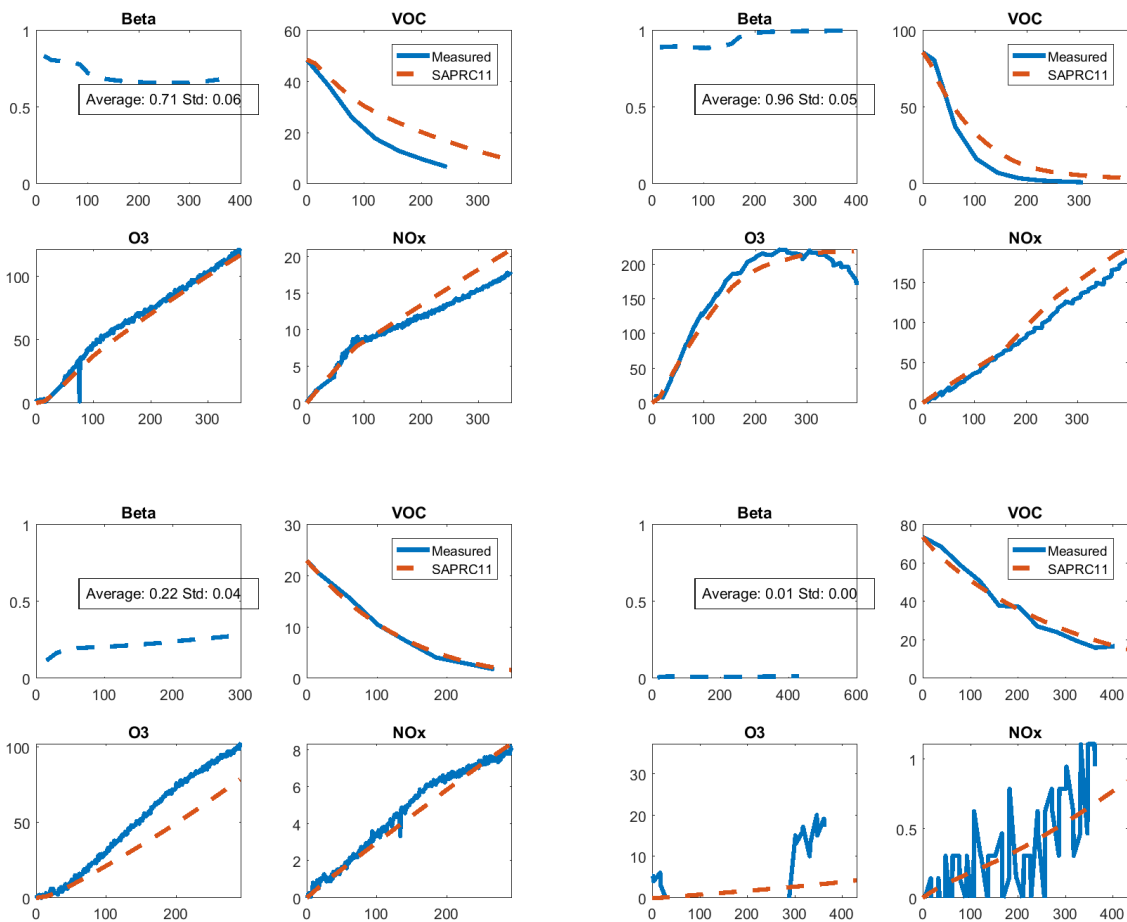


Figure 43. Measured and SAPRC11-estimated gas-phase species comparison.

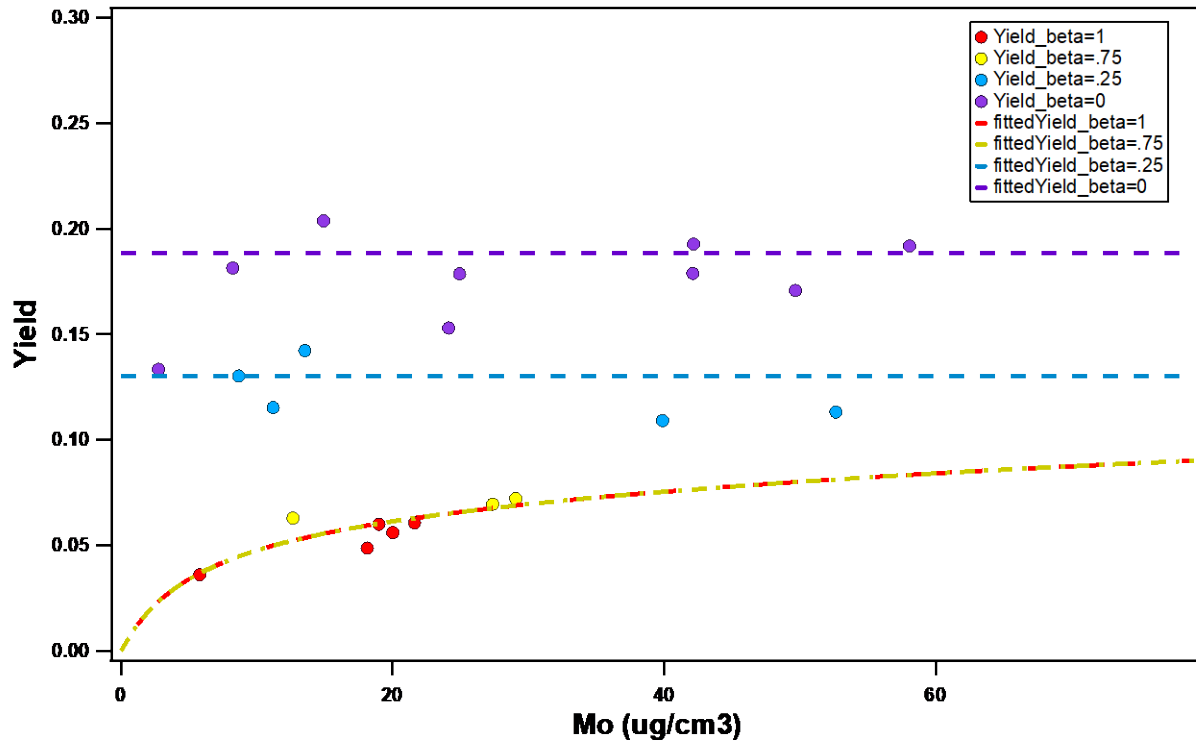


Figure 44. SOA yield vs SOA mass and corresponding fitted curves from runs with controlled branching ratio (0, 0.25, 0.75, and 1)

Table 7: Two-product SOA yield parameters

		a1	k1	a2	k2
Ng et. al., 2007	Low NO	0.3			
	High NO	0.031	0.761	0.09	0.029
This study	beta=0	0.1885			
	beta=1	0.079	0.0075	0.065	0.184

7.0 Variation in SOA formation potential of *m*-xylene in low (no NO_x added) conditions

Large variability in SOA formation (Yield: 10% to 42%) has been historically observed in “low” (no NO_x added) experiments in the UCR chamber (**Figure 45**). No clear single yield curve can be directly obtained, and current parameters can only represent a small fraction of the experiments reported here. Therefore, we investigated the effects on SOA formation from light intensity, NO_x off-gassing from chamber wall, the concentration of H₂O₂ and the radical chemistry behind it.

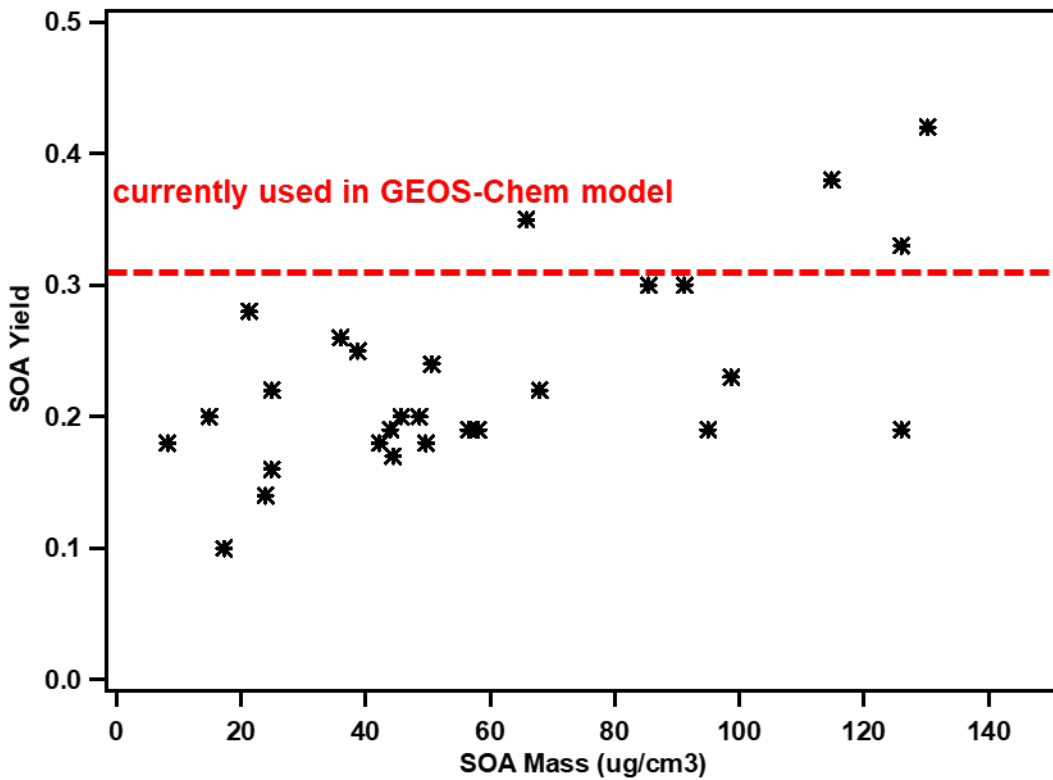


Figure 45: SOA Yield from *m*-xylene experiments with no additional NO_x

Light intensity:

Three light scenarios were used in this study. With similar initial *m*-xylene and H₂O₂ conditions but k_1 of 0.125, 0.150 and 0.401 min⁻¹ (k_1 is measure of the NO₂ photolysis rate), SOA formation rate and *m*-xylene consumption rate increase as k_1 increases (**Figure 46**) except that *m*-xylene consumption rate was the fast for the run with $k_1=0.15$ min⁻¹ due to its largest initial *m*-xylene concentration. The product of HO₂ and RO₂ for these three k_1 scenarios were plotted in **Figure 46**, which increases as k_1 increases. The similar dependence of HO₂*RO₂ on k_1 and SOA formation rate on k_1 indicates the correlation between SOA formation rate and HO₂*RO₂: SOA forms faster when HO₂*RO₂ is higher. This supports that HO₂+RO₂ reaction is the major pathway for *m*-xylene SOA formation in the absence of NO_x^{1,2}.

The similar total SOA formation and *m*-xylene consumption indicates the similar SOA formation potential with different light intensities studied here. When applying k_1 to all *m*-xylene experiments in this study and no obvious dependence on k_1 was observed (**Figure 47**).

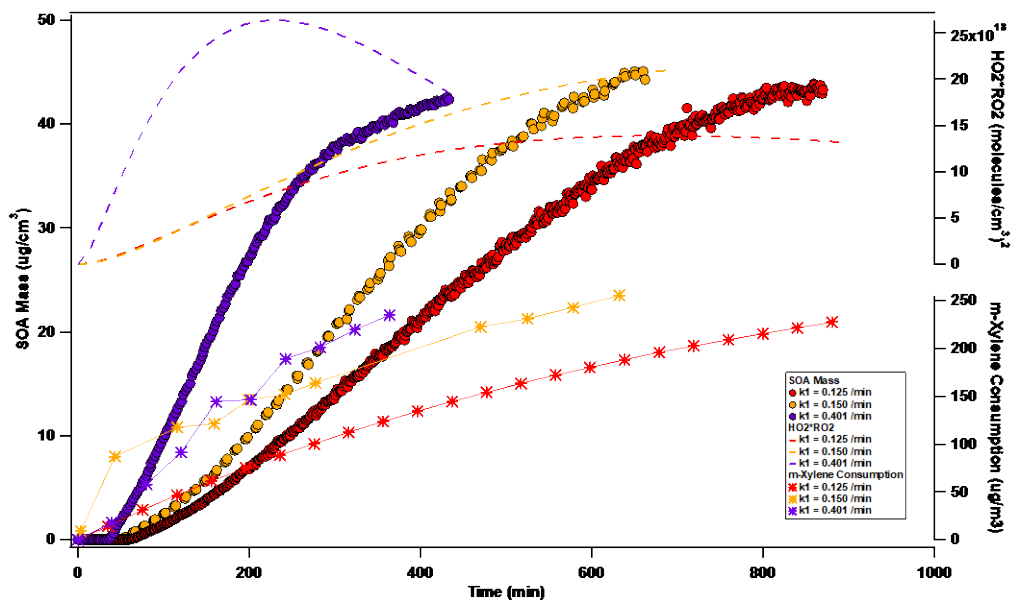


Figure 46. SOA formation, HO₂*RO₂, and accumulative *m*-xylene consumption of *m*-xylene experiments with different light intensities

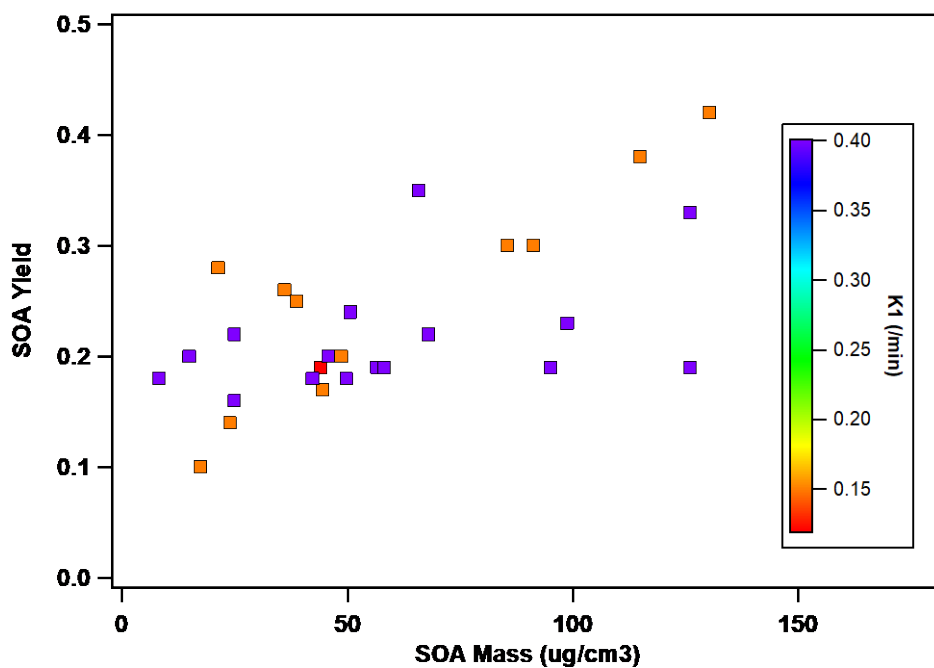


Figure 47. SOA yield from *m*-xylene experiments with no additional NO_x at different light intensity (represented by k₁)

Wall off-gassing:

While this study focuses on the *m*-xylene SOA formation in the absence of NO_x, it is almost impossible to achieve absolute no NO_x condition in Teflon environmental chamber due to wall effects³. The wall effects need to be considered when using SAPRC11 mechanism to simulate gas-phase chemistry in chamber. NO_x off-gassing rate from our chamber reactors was determined by determining the magnitude of NO_x off-gassing rate so that the model correctly predicts ozone yield from a series of chamber characterization experiments as described by Carter et al³. A range of 0.8 ppt/min to 7 ppt/min of NO_x off-gassing rate was observed for this chamber and its impact to gas-phase chemistry was investigated (**Figure 48**) with initial *m*-xylene and H₂O₂ of 80 ppb and 2 ppm. As an important NO_x source in the no additional *m*-xylene experiments, NO_x off-gassing is more important than high NO experiments since the average NO concentration is 0.9 to 12 ppt from wall off-gassing and ignorable in high NO experiments. *m*-Xylene profiles with three off-gassing rates are almost identical. The average branching ratio of RO₂+NO compared with HO₂+RO₂ increases from 0.002 to 0.03, indicating a very small portion of *m*-xylene forms SOA through HO₂+NO pathway. Using SOA parameters for HO₂+NO and HO₂+RO₂ obtained from Ng *et al.* shows the branching ratio increase caused by NO_x off-gassing rate increase only shows slight SOA formation change from 80ppb *m*-xylene. The product of average HO₂ and RO₂ in chamber decreased by 12% when changing from the lower bound to upper bound of the NO_x off-gassing. Gas-phase chemistry shows the effects of NO_x off-gassing on SOA formation from *m*-xylene in the absence of NO_x; however, NO_x off-gassing cannot explain the large variance on the SOA yield (10% to 42%) within the experiments

conducted here.

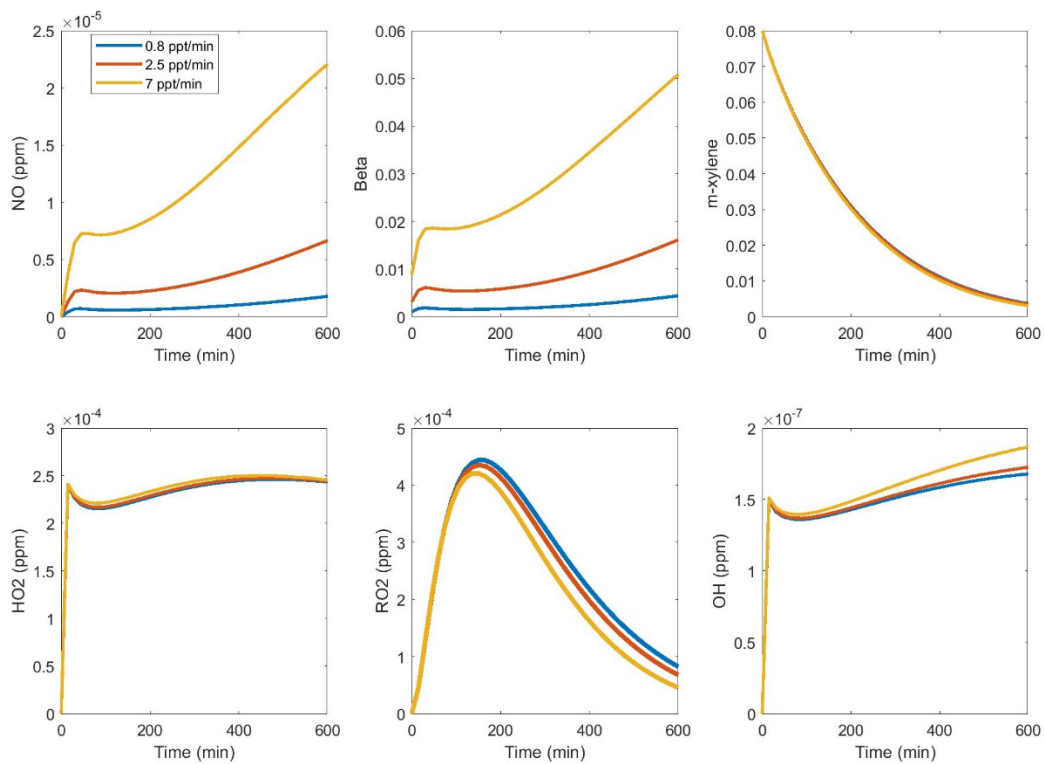


Figure 48. Gas-phase chemistry simulation of *m*-xylene+H₂O₂ with different NO_x offgassing rates

H₂O₂ effects.

A series of experiments was conducted with ~100 ppb initial *m*-xylene present with 0.4, 1, 2, and 4 ppm H₂O₂. SOA forms faster and the final formation increases as H₂O₂ concentration was increased (**Figure 49**). This indicates the concentration of H₂O₂ affects SOA formation with similar *m*-xylene present. While *m*-xylene consumption increases with H₂O₂ increase, due to the higher oxidant (OH) level, the final SOA yield (the ratio of final SOA formation to the final *m*-xylene consumption) shows an increase on SOA formation potential of *m*-xylene in the absence of NO_x. When plotting SOA formation and *m*-xylene consumption with H₂O₂ concentration (**Figure 50**), it shows the 29 experiments conducted in this study can be differentiated by H₂O₂ concentration and the H₂O₂ concentration in chamber increases SOA formation with the *m*-xylene consumption: with ~300 ug/m³ *m*-xylene consumption, SOA formation was about 50-70, ~90, and 110-130 ug/m³ with 1, 2, and 4 ppm H₂O₂ injected.

This shows that the amount of H₂O₂ increases the SOA formation potential the OH-initiated *m*-xylene oxidation system in absence of NO_x and explains the different yields of SOA formation from *m*-xylene without additional NO_x in this study and other studies. It is important to understand how H₂O₂ affect *m*-xylene oxidation system and this must be considered when studying SOA formation from *m*-xylene and possible other aromatic compounds in absence of NO_x.

The gas-phase chemistry while varying H₂O₂ concentration was modelled using SAPRC11 mechanism ⁴. Different than *m*-xylene + NO_x photo-oxidation system where both RO₂+NO and RO₂+HO₂ pathways need to be considered to form SOA, in *m*-xylene+H₂O₂ system, RO₂+HO₂ is the major pathway as its branching ratio is about 30 – 550 times higher (among the experiments

in this study) and its SOA formation potential is >4 times higher than RO₂+NO pathway. The hydroperoxide products from HO₂+RO₂ reactions are quite low in volatility and is a major component of SOA, especially in the scenarios in absence of NO_x. In addition, the self- and cross- reactions of RO₂ is very small in *m*-xylene + NO_x system due to that the its reaction constant is 1 to 2 order of magnitude lower than HO₂+NO and HO₂+RO₂ reactions. However, in *m*-xylene+H₂O₂ system where RO₂ concentrations are very high, RO₂+RO₂ pathway may also impact SOA formation⁵. The average vapor pressure of products from (RO₂ + RO₂ → ROH+RCHO+O₂) tend to be higher than the products from HO₂+RO₂ reactions; thus, forming less particles. However, the organic peroxides (ROOR) formed through RO₂+RO₂ reactions are like be in low volatility and may form more particles compared with HO₂+RO₂ reactions⁶. The SOA formation from RO₂+RO₂ is unclear and not well understood. In our study, we considered both HO₂+RO₂ and RO₂+RO₂ pathways and use the ratio of HO₂/RO₂ to indicate the contribution from HO₂+RO₂ pathway.

Figure 51 shows final SOA mass with HO₂/RO₂ ratio. For similar *m*-xylene consumption, at lower HO₂/RO₂, the SOA mass increases drastically and the fraction of RO₂ reacting with HO₂ increases as HO₂/RO₂ increases. As HO₂/RO₂ ratio further increases, SOA mass tend to level off and increasing HO₂/RO₂ does not increase HO₂+RO₂ reaction branching ratio since it is RO₂ limited. This indicates that HO₂+RO₂ pathway has higher SOA potential from *m*-xylene in the absence of NO_x than RO₂+RO₂ pathway and the SOA potential depends on the HO₂+RO₂ reactions and the ratio of HO₂/RO₂.

It was previously reported in the literature that a constant yield (36%) of non-volatile SOA from *m*-xylene occurs in the absence of NO_x and those results are currently used in SOA model (e.g. GEOS-Chem) to represent the SOA yield of HO₂ pathway^{1,7}. We present three different yield

curves of *m*-xylene at three different HO₂/RO₂ scenarios (0 to 0.75, 0.75 to 1.5, and >1.5) (**Figure 52**). The 36% yield reported by Ng et. al¹, is closest to SOA yield curve at HO₂/RO₂>1.5, where SOA yield levels off at 40%; however, the constant yield is not able to represent SOA potential at HO₂/RO₂<1.5 and about twice as the yield at HO₂/RO₂<0.75. This result shows SOA yield is not constant but varies with HO₂/RO₂ conditions and it is important to understand the HO₂/RO₂ condition to predict SOA formation from *m*-xylene. VBS parameters for three scenarios are presented in **Table 8**.

These SOA yield curves are obtained from experiments with only *m*-xylene present and did not consider the impacts from the presence of other VOCs. A reactive organic gas (ROG) surrogate mixture⁸ was used to simulate urban atmosphere as well as *m*-xylene and H₂O₂. Without surrogate mixture added, the average HO₂/RO₂ ratios varied from 0.5 to 5 with 25 to 100 ppb *m*-xylene and 1ppm H₂O₂. With 1 ppm surrogate, the ratios drop to a constant level (0.19 to 0.34), indicating that the presence of surrogate mixture controls the HO₂/RO₂ ratio to a relative constant level with varied initial *m*-xylene. SOA yield of runs with surrogate is presented in **Figure 52** and they all agree with SOA yield curve at HO₂/RO₂<0.75 scenario. This shows that our conclusion applies with *m*-xylene SOA formation in absence of NO_x in urban atmosphere with the presence of other VOCs.

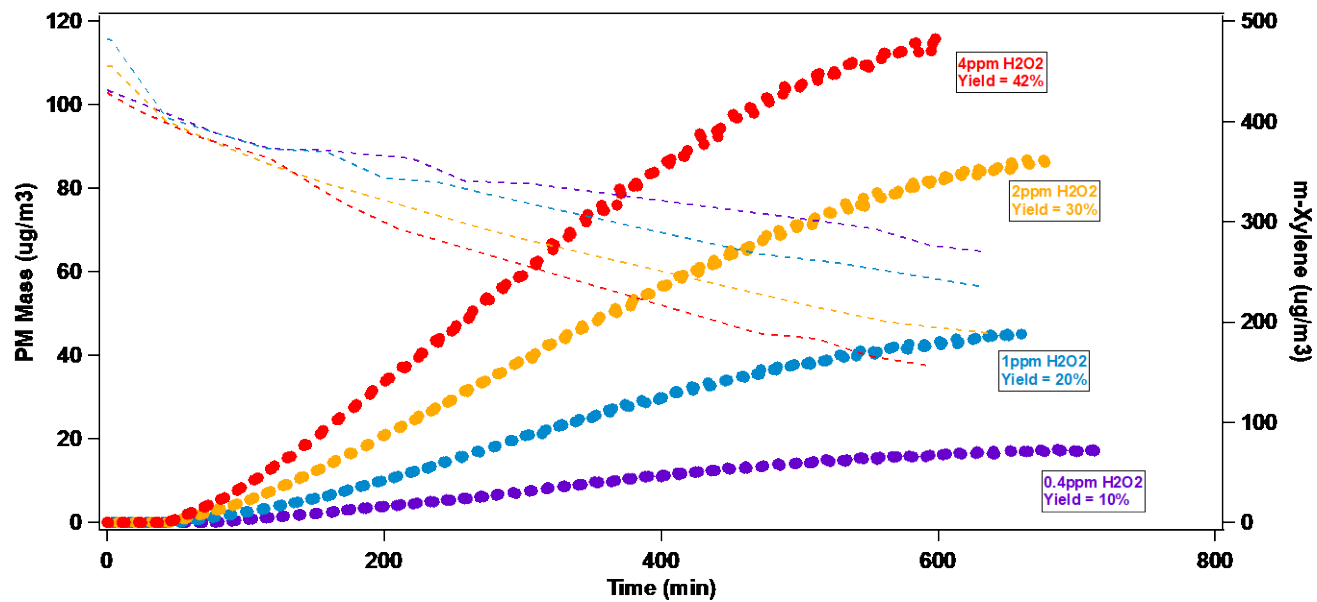


Figure 49. SOA formation and *m*-xylene concentration from *m*-xylene with different initial concentration of H₂O₂.

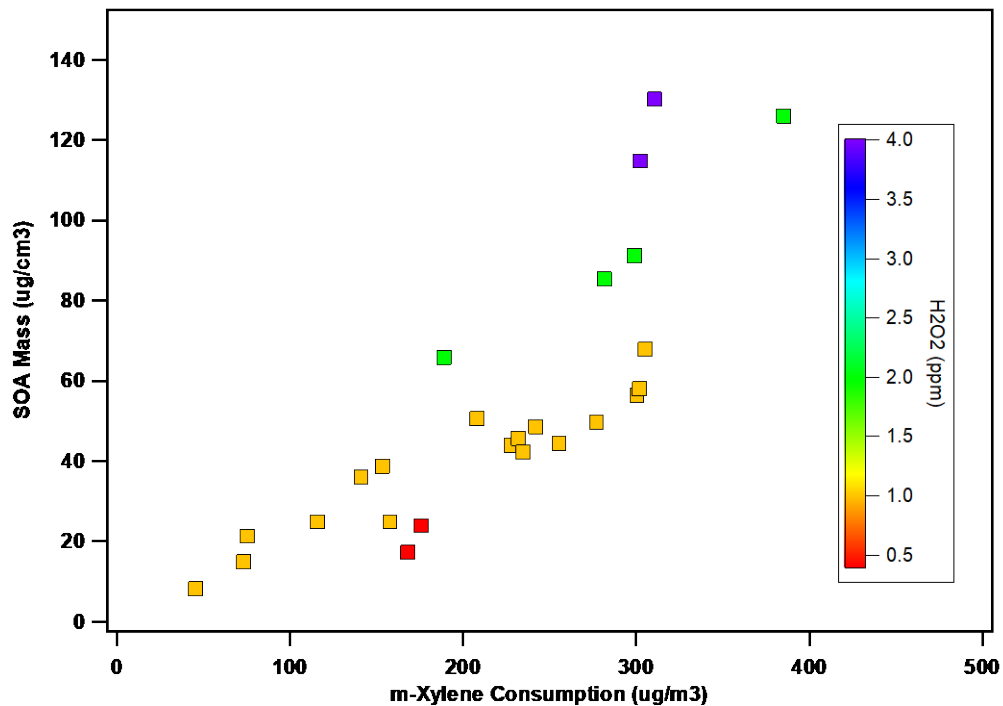


Figure 50. SOA yield from *m*-xylene experiments with no additional NO_x with different initial H_2O_2 .

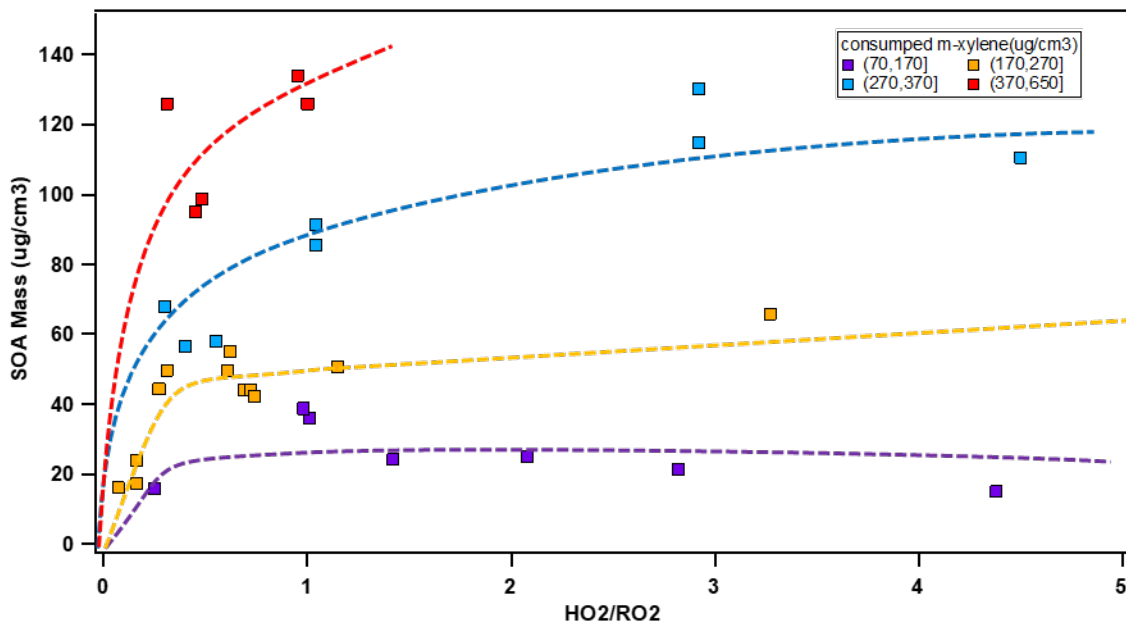


Figure 51. SOA formation with average HO_2/RO_2

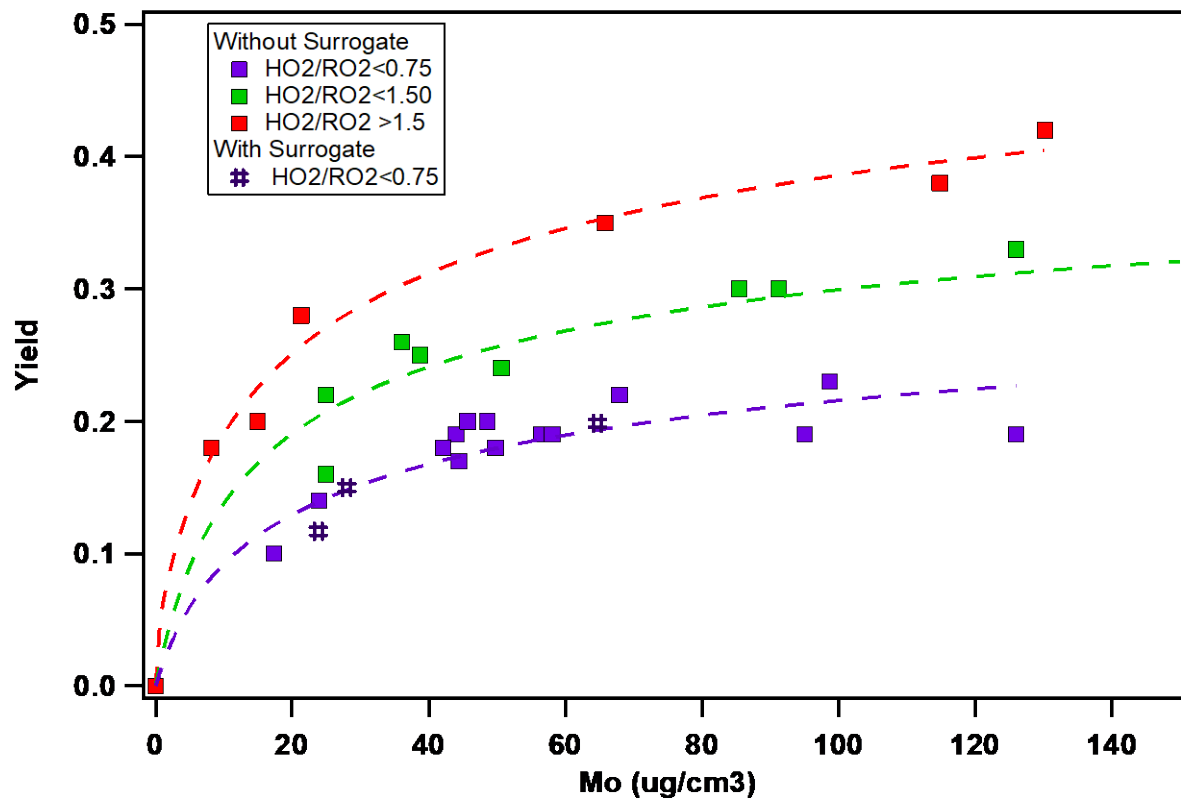


Figure 52. SOA yield from *m*-xylene experiments with no additional NO_x at different HO₂/RO₂.

Table 8. SOA yield VBS parameters at different HO₂/RO₂ conditions.

HO ₂ /RO ₂	c*=0.1	c*=1	c*=10	c*=100
<.75	0	0	0.1584	0.1436
<1.5	0	0	0.25	0.1441
>1.5	.0378	0	0.2681	0.2087

Therefore, we conclude that higher light intensity increases the SOA formation rate but does not change the SOA potential significantly. The NO_x offgasing rate from the chamber wall affects the branching ratio beta (RO₂+NO) but cannot explain the large SOA yield variance within the NO_x offgasing rate range of UCR/CECERT chamber. The SOA formation potential has a strong dependence on the additional H₂O₂ injected into the chamber. *When further investigating the radical change when using different amount of H₂O₂, HO₂/RO₂ is the one that plays an important role.* Three yield curves were observed at different HO₂/RO₂ scenarios. The yield is the highest when HO₂/RO₂ is larger than 1.5. Three corresponding VBS parameters were developed to predict SOA formation of *m*-xylene at low NO_x with different HO₂/RO₂ conditions. A reactive organic surrogate gas mixture was also added into several *m*-xylene+H₂O₂ experiments to simulate urban atmosphere and a great agreement was observed between the measured SOA and estimated SOA using the VBS parameters developed here.

8.0 A deeper look into NO_x chemistry in the α-pinene system

An additional set of α-pinene experiments were performed to further our understanding of the role of NO_x on SOA formation. For each experiment (except β = 1), 1 ppm H₂O₂ was injected into the UCR-CECERT chamber at the beginning of the experiment as an ·OH source. In both low and medium branching ratios conditions, 1 ppm of H₂O₂ was injected initially for 15 min into the chamber, while in case of high branching ratio (β = 1), “no” H₂O₂ was injected into the chamber. The branching ratios were simulated using SAPRC11 modeling for each condition.

Table 9: Experimental conditions for additional α -pinene experiments

Run Number	β	HC type	HC (ppb)	H ₂ O ₂	NO (ppm/sec)	
					NO (ppb)	Yield %
EPA2628	0.30	α -Pinene	19	1	0.8×10^{-6}	29.4
EPA2690	0.32	α -Pinene	17	1	0.85×10^{-6}	28.2
EPA2630	0	α -Pinene	18	1	0	29.1
EPA2709	0	α -Pinene	20.	1	0	27.5
EPA2632	0.30	α -Pinene	44	1	0.9×10^{-6}	23.0
		α -Pinene				
EPA2718	0.32		46	1	1.0×10^{-6}	24.3
EPA2707	0	α -Pinene	46	1	0	25.9
EPA2646	0.3	α -Pinene	80.	1	1.35×10^{-6}	27.4
EPA2642	0	α -Pinene	81	1	0	27.1
EPA2644	0.3	α -Pinene	102	1	1.5×10^{-6}	28.0
EPA2714	0	α -Pinene	103	1	0	24.2
EPA2641	0	α -Pinene	105	1	0	24.8
EPA2653	1	α -Pinene	19.6	0	0.8×10^{-6}	5.94
EPA2661	1	α -Pinene	20.3	0	1.15×10^{-6}	1.83
EPA2655	1	α -Pinene	21.3	0	1.5×10^{-6}	1.02
EPA2657	1	α -Pinene	40.6	0	1.5×10^{-6}	12.1

EPA2659	1	α-Pinene	40.8	0	$2.8 \cdot 10^{-6}$	5.88
EPA2663	1	α-Pinene	81.6	0	$4.7 \cdot 10^{-6}$	16.7
EPA2665	1	α-Pinene	80.	0	$9.4 \cdot 10^{-6}$	0.564
EPA2692	Classical	α-Pinene	21	1	26	18.1
EPA2694	Classical	α-Pinene	???	1	27	19.4
EPA2674	Classical	α-Pinene	80.	1	43	37.4
EPA2682	Classical	α-Pinene	100.	1	52	41.0
EPA2697	Classical	α-Pinene	39.4	1	40	38.3
EPA2687	Classical	α-Pinene	75.4	0	141	16.3
EPA2695	Classical	α-Pinene	23.5	0	40	1.9
EPA2698	Classical	α-Pinene	38.8	0	63	15.2
EPA2707	0	α-Pinene	46	1	0	25.9

The chamber experiments are designed using SAPC-11 simulations, and the β values are calculated by SAPRC-11 outputs, using equation 1. The averaged β values varies from 0 to 1, depending on the initial NO_x and VOC concentrations the latter indicating high NO_x conditions without H_2O_2 injection. For this study, the SOA yields were measured under averaged β equals to 0, 0.3, and 1. **Figure 53A** shows the SOA yields vs SOA mass formed ($\mu\text{g}/\text{m}^3$) under 20ppb, 40 ppb, 80 ppb, 100ppb VOC concentrations under low ($\beta=0.3$) and no ($\beta=0$) NO_x conditions. Despite, higher decay rate of SOA precursor at low NO_x conditions vs no NO_x injections, the SOA yields were roughly the same under both β values, ranging from 24% to

28%, indicating that the organic proxy radicals were mostly reacting with RO_2+HO_2 pathway for both low and no NO_x conditions. **Figure 53B**, shows the SOA mass formed (ug/m^3) versus delta HC consumed. As expected, the SOA mass increased with delta HC consumed for each experiment, with 100 ppb forming the highest SOA mass.

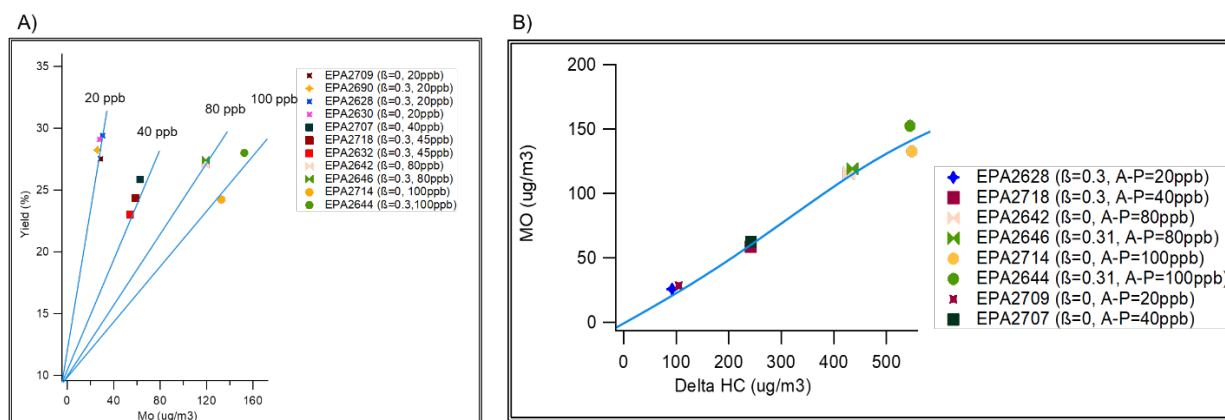


Figure 53. A) SOA yield versus SOA mass formed under no and low NO_x conditions. B) SOA mass formed versus Delta HC consumed at low and no- NO_x conditions.

The SOA yields were studied under high NO_x and extremely high NO_x conditions keeping both conditions at a constant β equals to 1. At extremely high NO_x conditions, NO injections were 2X higher compared to high NO_x conditions. As shown in **Figure 1** from Li et. al. the NO can either promote SOA formations (at <1 ppb levels) by enhancing $\cdot OH$ radical formation, which further enhances the RO_2 and HO_2 or suppress SOA formation by favoring RO_2+NO pathway forming higher volatile species. Comparing SOA formation under β equals to 1 vs 0, and 0.3 the SOA yields are much lower which is consistent with previous studies on NO_x effects using biogenic precursors (Ng *et al.*, 2007; Wu *et al.*, 2020; Zhao *et al.*, 2018).

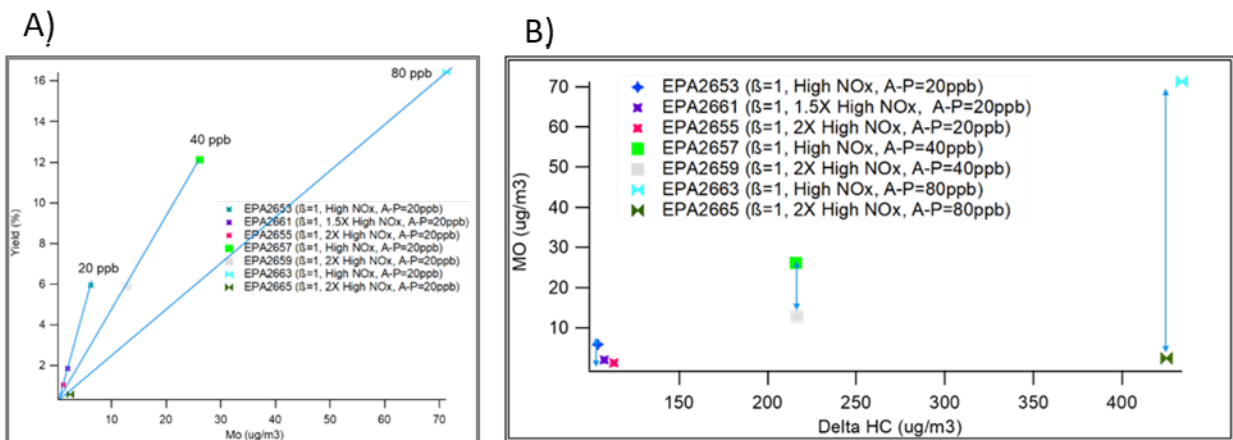


Figure 54. A) SOA yield versus SOA mass formed under high and 2X high NO_x conditions. B) SOA mass formed versus Delta HC consumed at under high and 2X high NO_x conditions.

As shown in **Figure 54A**, The SOA yields under extremely high NO_x conditions were lower compared to high NO_x conditions, both under β value of 1. The RO₂ lifetimes were investigated using SPRAC-11 simulation, interestingly the RO₂ lifetimes were longer under high NO_x conditions versus extremely high NO_x conditions, which can lead to autooxidations forming lower volatile species leading to higher SOA yields. **Figure 54B** shows the SOA mass formed (ug/m³) versus delta HC consumed (ug/m³). The lowest SOA mass formed from 100 ppb HC consumption is related to extremely high NO_x condition, which the RO₂ lifetime was the shortest among all **Figure 55**.

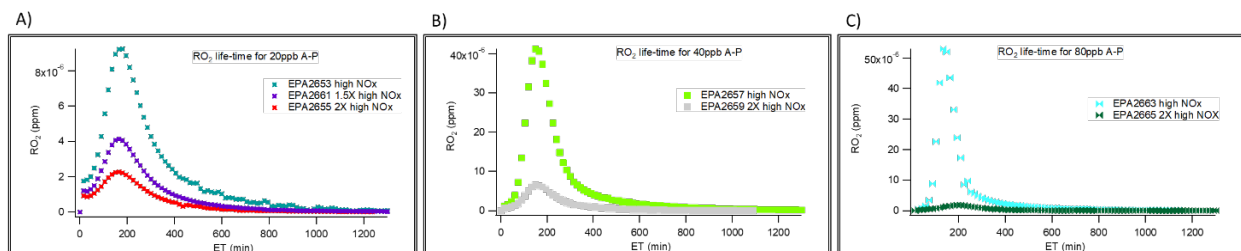


Figure 55: RO₂ lifetime simulated under high and 2X high NO_x conditions at A) 20 ppb, B) 40 ppb, C) 80 ppb.

Chamber experiments were performed for more than 20 hours, the goal was to have the particle volume plateau before the end of the experiment. **Figure 56** shows the volume evolution of the particles under different NO_x/VOC conditions. The SOA volumes formed under low NO_x conditions are higher compared to high NO_x conditions, indicating higher HO₂/RO₂ ratio with lower NO_x leading to lower volatile species. Moreover, it is observed that the SOA forms faster at low NO_x conditions compared to no NO_x conditions. The OH concentrations were simulated using SAPRC-11 and calculated based on HC decay rate generated by gas chromatography, both indicating the OH concentration to be roughly 5.12×10^6 (molecules cm⁻³) for all experimental conditions.

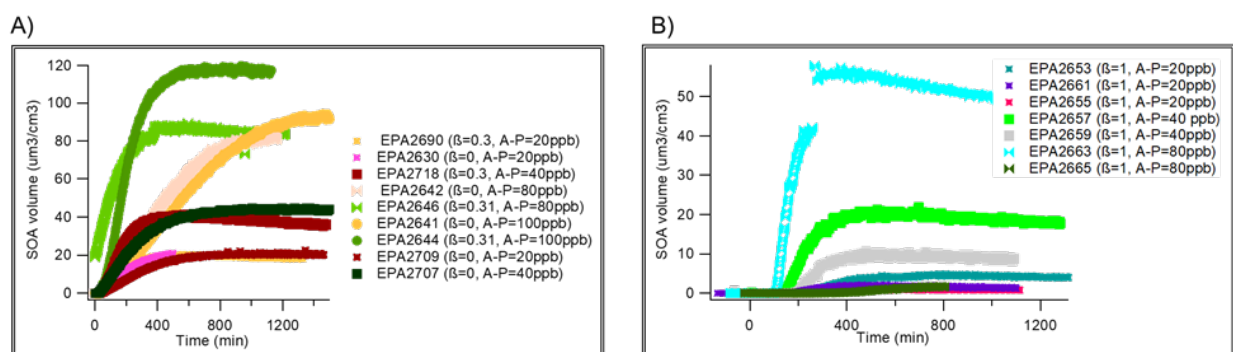


Figure 56. Volume of the particles formed over the course of experiment at A) low and no-NO_x conditions, B) at high NO_x conditions.

Classical experiments versus continuous NO_x injections:

The continuous experiments have been repeated using instantaneous NO_x injection where the NO is injected at the beginning of the experiment before the photooxidation process. The amount of NO injections are calculated based on the total amount of NO injected (ppm/second) until the RO_2 is completely consumed, which varies experiment by experiment (**Table 9**). **Figure 57A** shows the SOA yields versus SOA mass formed under 20, 40, 80 ppb HC initial concentrations. It is important to note that in the presence of NO_x the SOA yield increase as the HC initial concentrations increase. Moreover, the SOA formation potentials are suppressed at high NO_x conditions, due the formation of higher volatile oxidation products. **Figures 57B and 57C** shows the SOA yields from continuous NO injection method versus instantaneous injection method, it can be observed that the SOA yield was underestimated at low hydrocarbon (HC) concentration (20 ppb) and overestimated under high HC concentrations (40, 80 ppb).

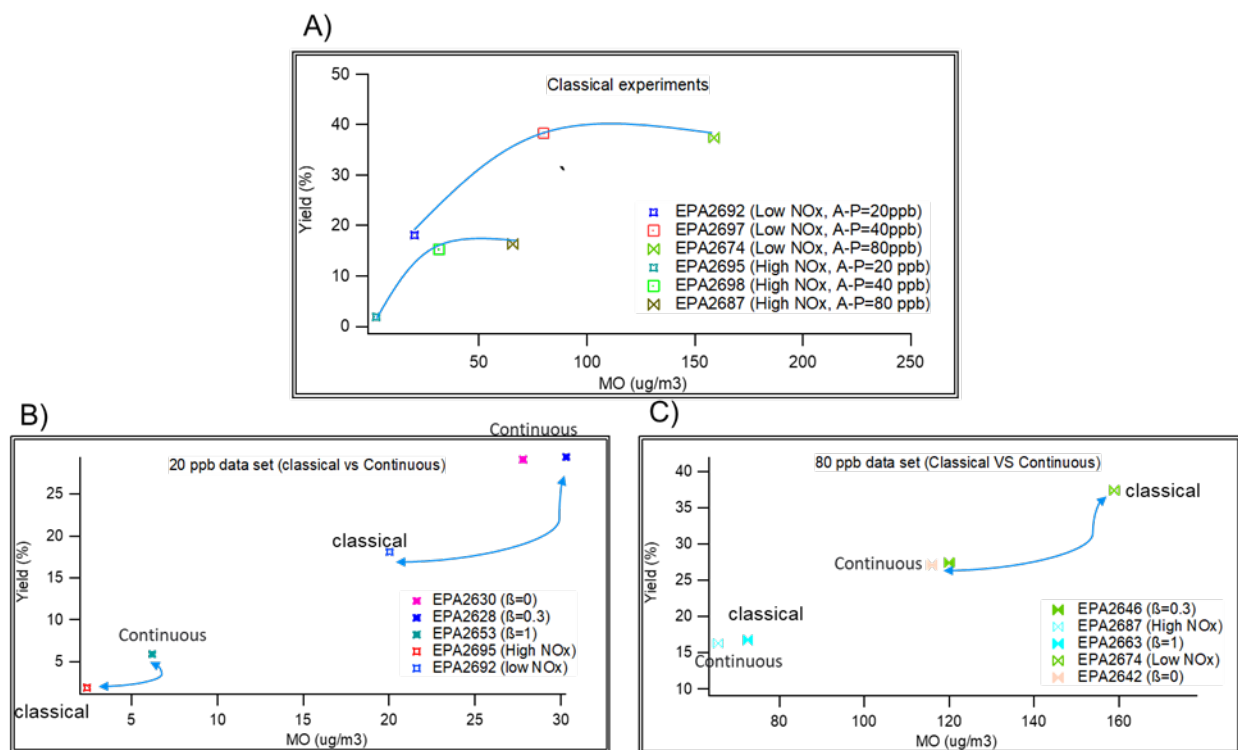


Figure 57. SOA yield versus SOA mass formed of Continuous NO injections versus instantaneous NO injections.

9.0 A deeper look into NO_x chemistry of Naphthalene system

The SOA formation potentials have also been analyzed using naphthalene, which enables us to compare SOA formation from a poly-cyclic aromatic hydrocarbon (PAH) under high, low, no NO_x conditions. **Figure 58** shows the preliminary data of the SOA yield versus SOA mass formed. It can be observed that the SOA formation is mostly affected by HO₂/NO conditions rather than HC initial concentrations. At high NO_x regime the SOA formations are suppressed compared to no-NO_x and low NO_x conditions. The yield is highest at low NO_x regime. In this regime, sufficient NO is available to cycle some HO₂ and RO₂ radicals and promote further oxidation (relative to no-NO_x case) of naphthalene and its oxidation products but still low enough to not suppress SOA formation by lowering RO₂ and HO₂ lifetimes to the extent observed for high-NO_x scenario. A similar effect has been observed by our research group for m-xylene and is detailed in Li et al., 2015. The SOA yield acquired under both high NO_x and no- NO_x conditions using 20 ppb and 100 ppb naphthalene are mostly identical, indicating that the initial HC injected does not affect SOA formation. This is just preliminary data/result on naphthalene, it is planned to perform different VOC/NO_x ratio, using continuous NO_x injection, to gain a better understanding on PAH SOA patterns under different atmospheric relevant conditions.

Table 10: Naphthalene experimental conditions

Run Number	β	HC type	HC (ppb)	H ₂ O ₂	NO (ppm/sec)	
					NO (ppb)	Yield %
EPA2720	0.3	Naphthalene	42.4	1	3.8×10^{-6}	38.1
EPA2721	1	Naphthalene	112.7	0	2.4×10^{-6}	4.1
EPA2727	0	Naphthalene	109.5	1	0	16.1
EPA2728	1	Naphthalene	34.4	0	1.5×10^{-5}	4.6
EPA2730	0	Naphthalene	28.4	1	0	16.9

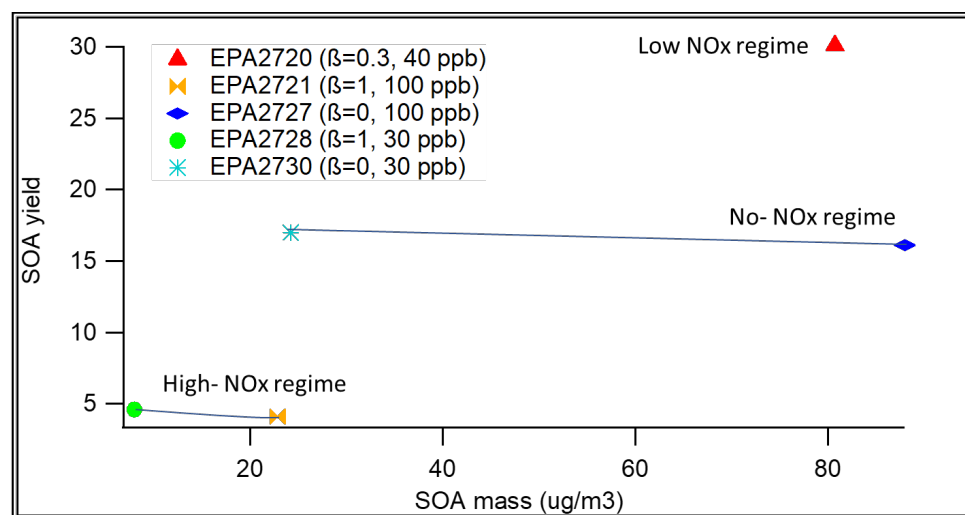


Figure 58. SOA yield versus OA mass formed under no-NO_x, low NO_x, and high NO_x experiments using Naphthalene as SOA precursor.

10.0 The elemental composition of SOA formed from α -pinene versus naphthalene

The elemental composition of SOA formed from α -pinene photooxidation is evaluated using Aerodyne high-resolution time-of-flight mass spectrometer data. Previous studies have reported the O/C between 0.3-0.43 for α -pinene ozonolysis, which correlates with type of compounds formed from α -pinene+O₃ pathway, such as pinonic acid, pinonaldehyde, pinic acid consisting of mostly 3 to 4 number of oxygen (Chhabra *et al.*, 2010; Kim *et al.*, 2014). As can be seen in **Figure 59** SOA formed from α -pinene photooxidation the O/C ratios range from 0.51 to 0.65, and the H/C ranges from 1.48 to 1.70. This indicates the products that have been formed after more than 20 hours of photooxidation have 5 to 6 oxygens and 14 to 17 of hydrogen numbers. It is important to note that the atomic ratios do not vary between different experimental conditions, and the range seems to be relatively constant for high vs low NO_x conditions. The average O/C range for Naphthalene is 0.69 to 0.89 and the average H/C range is 1.06 to 1.20. The O/C range is higher and the range of H/C is lower for Naphthalene versus α -pinene, which is consistent with their chemical structure.

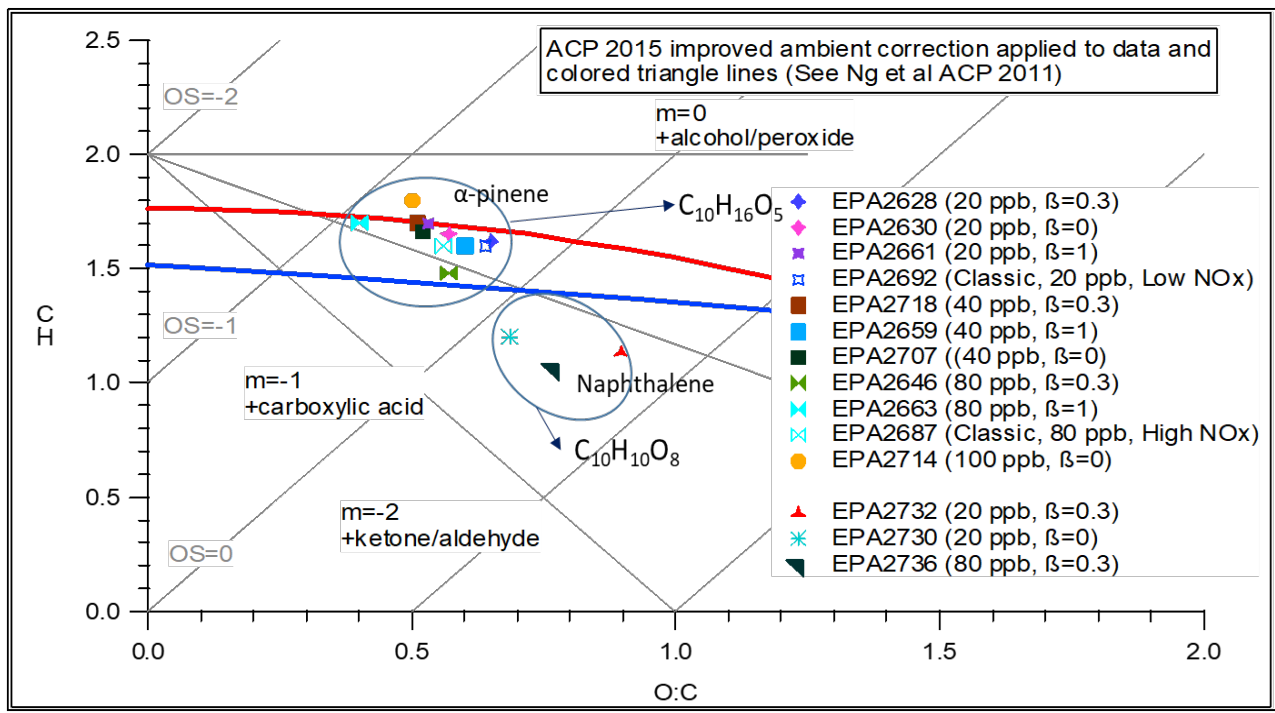


Figure 59: H:C and O:C ratios determined by HR-ToFMS for α -pinene and naphthalene

11.0 Conclusions and Future Work

This above work explored the SOA from select aromatic (*m*-xylene), poly-aromatic (naphthalene), and biogenic monoterpene (α -pinene) VOCs over a variety of atmospheric chemical regimes. The work explored new chamber experimental strategies to explore various NO_x in the atmosphere ultimately determining that a continuous NO injection throughout the course of the experiment was the most effective approach to investigation SOA formation processes under fixed NO_x regimes defined by β , the chemical branching ratio. Continuous VOC injections were determined to be less useful in this regard.

Thorough analysis of SOA formation yields as a function of β was then used to determine the impact of predicted SOA formation from large scale models such as GEOS-CHEM. It was determined that a linear extrapolation of β zero and β one experiments improved interpretation of traditional chamber data but did not completely predict SOA formation from intermediate β values. Further analysis of SOA formation from traditional environmental chamber SOA experiments was evaluated using SAPRC-11 predicted β values to interpret SOA prior SOA formation studies of *m*-xylene improving SOA predictions from prior work. Exploration of the β zero regime for *m*-xylene showed multiple SOA formation levels for the same β values. This ultimately was determined to be due to changes in HO_2/RO_2 ratios within the regime and has been published (Peng et al., 2022). A similar study at β one regime for α -pinene found similar ranges of SOA formation, which was attributed to the competition between RO_2 self-reaction (auto-oxidation) and reaction with NO. This work is the subject of another paper expected to be completed for peer review submission by end of December, 2022. The ability of β to be used to help predict SOA formation from current and future environments was established throughout the work.

This work clearly indicates the importance of accurate simulation of chemical conditions (such as NO_x chemistry) to appropriately estimate SOA formation. It is recommended that future research further improve simulation of chemical conditions in the chamber to more accurately predict SOA formation from

VOC precursors such as NO_x, RH, temperature, VOC and organic aerosol loading to best predict the atmosphere of tomorrow.

12.0 References

- Canagaratna, M. R., Jimenez, J. L., Kroll, J. H., Chen, Q., Kessler, S. H., Massoli, P., Hildebrandt Ruiz, L., Fortner, E., Williams, L. R., Wilson, K. R., Surratt, J. D., Donahue, N. M., Jayne, J. T., and Worsnop, D. R.: *Elemental ratio measurements of organic compounds using aerosol mass spectrometry: characterization, improved calibration, and implications*, Atmos. Chem. Phys., 15, 253–272, 2015
- Carter, W., Cocker, D., Fitz, D., Malkina, I, Bumiller, K., Sauer, C, Pisano, J., Bufalino, C., Song, C. (2005). *A New Environmental Chamber for Evaluation of Gas-Phase Chemical Mechanisms and Secondary Aerosol Formation*. Atmospheric Environment, 39 (4), 7768-7788.
- Carter, W.P.L. and G. Heo, *Development of revised SAPRC aromatics mechanisms*. Atmospheric Environment, 2013. 77: p. 404-414.
- Chen, C., Tang, P., Cocker, D. (2018), *SOA formation from naphthalene, 1-methylnaphthalene, and 2-methylnaphthalene photooxidation*, 180, 256-264.
- Chhabra, P.S., R.C. Flagan, and J.H. Seinfeld, *Elemental analysis of chamber organic aerosol using an aerodyne high-resolution aerosol mass spectrometer*. Atmospheric Chemistry and Physics, 2010. 10(9): p. 4111-4131.
- Cocker, D. R., Flagan, R. C. and Seinfeld, J. H.: *State-of-the-art chamber facility for studying atmospheric aerosol chemistry*, Environ. Sci. Technol., 35(12), 2594–2601, doi:10.1021/es0019169, 2001.
- DeCarlo, P., Kimmel, J., Trimborn, A., Northway, M., Jayne, J., Aiken, A.,, Jimenez, J. (2006). *Field-Deployable, High-Resolution, Time-of-Flight Aerosol Mass Spectrometer*, Analytical Chemistry, 78(24), 8281-8289.
- Deng, W., et al., *Primary emissions and secondary organic aerosol formation from in-use diesel vehicle exhaust: Comparison between idling and cruise mode*. Sci Total Environ, 2020. 699: p. 134357.
- Donahue, N., Robinson, A., Stanier, C., Pandis, S. (2006). *Coupled partitioning, dilution, and chemical aging of semivolatile organics*. Environmental Science and Technology, 40(8), 2635-2643.
- Farina, S.C., P.J. Adams, and S.N. Pandis, *Modeling global secondary organic aerosol formation and processing with the volatility basis set: Implications for anthropogenic secondary organic aerosol*. Journal of Geophysical Research, 2010. 115(D9).
- Guenther, A., et al., *A Global-Model of Natural Volatile Organic-Compound Emissions*. Journal of Geophysical Research-Atmospheres, 1995. 100(D5): p. 8873-8892.
- Jimenez, J.L., *Evolution of Organic Aerosols in the Atmosphere*. Science, 2009. 326 (5959): 1525-1529
- Kavouras, I.G., N. Mihalopoulos, and E.G. Stephanou, *Formation and gas/particle partitioning of monoterpenes photo-oxidation products over forests*. Geophysical Research Letters, 1999. 26(1): p. 55-58.

- Kim, H., et al., *Dependence of Real Refractive Indices on O:C, H:C and Mass Fragments of Secondary Organic Aerosol Generated from Ozonolysis and Photooxidation of Limonene and α -Pinene*. *Aerosol Science and Technology*, 2014. 48(5): p. 498-507.
- Li, L., Tang, P., Cocker, D. (2015). *Instantaneous nitric oxide effect on secondary organic aerosol formation from m-xylene photooxidation*. *Atmospheric Environment*, 119, 144-155.
- Li, L., Tang, P., Nakao, S., Cocker, D. (2016a). *Impact of Molecular structure on secondary organic aerosol formation from aromatic hydrocarbon photooxidation under low-NO_x conditions*. *Atmospheric Chemistry and Physics*, 16 (17), 10793-10808.
- Li, L., Tang, P., Nakao, S., Chen, C., Cocker, D. (2016b). *Role of Methyl Group Number on SOA Formation from Monocyclic Aromatic Hydrocarbons Photooxidation under Low-NO_x Conditions*. *Atmospheric Chemistry and Physics*, 16 (4), 2255-2272.
- Li, L., Tang, P., Nakao, S. (2016c). *Novel Approach for Evaluating Secondary Organic Aerosol From Aromatic Hydrocarbons: Unified Method for Predicting Aerosol Composition and Formation*. *Environmental Science and Technology* 50 (12), 6249-6256.
- Li, L., Li, Q., Cocker, D. (2017). *Contribution of Methyl Group to Secondary Organic Aerosol Formation from Aromatic Hydrocarbon Photooxidation*. *Atmospheric Environment*, 151, 133-139.
- Malloy, Q. G. J., Nakao, S., Qi, L., Austin, R., Stothers, C., Hagino, H., and Cocker III, D. R.: *Real-Time Aerosol Density Determination Utilizing a Modified Scanning Mobility Particle Sizer–Aerosol Particle Mass Analyzer System*, *Aerosol Sci. Technol.*, 43, 678, 2009.
- Ng, N.L., et al., *Effect of NO_x level on secondary organic aerosol (SOA) formation from the photooxidation of terpenes*. *Atmospheric Chemistry and Physics*, 2007. 7(19): p. 5159-5174.
- Peng, W., Le, C., Porter, W., Cocker, D. (2022) *Variability in Aromatic Aerosol Yields under Very Low NO_x Conditions at Different HO₂/RO₂ Regimes*. *Environmental Science and Technology*, 2022, 56, 2,750-760.
- Porter, W.C., J.L. Jimenez, and K.C. Barsanti, *Quantifying Atmospheric Parameter Ranges for Ambient Secondary Organic Aerosol Formation*. *Acs Earth and Space Chemistry*, 2021. 5(9): p. 2380-2397.
- Pye, H.O.T., et al., *Global modeling of organic aerosol: the importance of reactive nitrogen (NO_x and NO₃)*. *Atmospheric Chemistry and Physics*, 2010. 10(22): p. 11261-11276.
- Seinfeld, J. H., and Pandis, S. N. (2016). *Atmospheric Chemistry and Physics: From Air Pollution to Climate Change*. John Wiley & Sons, Hoboken, 3rd edition.
- Wu, K., et al., *Estimation of biogenic VOC emissions and their corresponding impact on ozone and secondary organic aerosol formation in China*. *Atmospheric Research*, 2020. 231.
- Zhang, S.-H.a.S., Martha and Seinfeld, John H. and Flagan, Richard C., *Photochemical aerosol formation from α -pinene- and β -pinene*. *Journal of Geophysical Research*, 1992, 97LD18, 20717-20729,
- Zhao, D.F., et al., *Effects of NO_x and SO₂ on the secondary organic aerosol formation from photooxidation of alpha-pinene and limonene*. *Atmospheric Chemistry and Physics*, 2018. 18(3): p. 1611-1628.

